Thesis for the Degree of Doctor of Philosophy

Starfish Routing to Maximize Lifetime of Sensor Networks with Mobile Sink

Registration No: 68/2019-2020

Department of Computer Science and Engineering
University of Dhaka
Dhaka, Bangladesh

January 2022

Starfish Routing to Maximize Lifetime of Sensor Networks with Mobile Sink

Md. Ahsan Habib

Department of Computer Science and Engineering
University of Dhaka
Dhaka, Bangladesh

January 2022

Starfish Routing to Maximize Lifetime of Sensor Networks with Mobile Sink

by

Md. Ahsan Habib

Registration No: 68/2019-2020

Supervised by

Prof. Md. Abdur Razzaque, Ph.D.

Prof. Md. Mamun-Or-Rashid, Ph.D.

Submitted to the Department of Computer Science and Engineering of the Faculty of the Engineering and Technology in University of Dhaka, Bangladesh for the partial fulfillment of the requirements of the degree of Doctor of Philosophy (Ph.D.)

As the candidate's supervisor, I have approved this dissertation for submission.

Name: Dr. Md. Abdur Razzaque

Signed: _____

Name: Dr. Md. Mamun-Or-Rashid

Signed: _____

Declaration of Authorship

We declare that this thesis titled **"Starfish Routing to Maximize Lifetime of Sensor Networks with Mobile Sink"** and the works presented in it are our own. We confirm that:

- The full part of the work is done during PhD research study in University of Dhaka, Bangladesh.
- This thesis or any portion of it has not been previously submitted for a degree or other qualification at this University or any other institution.
- We have cited the published works of others with appropriate references.
- This thesis work is done entirely by us and our contributions and enhancements from other works are clearly stated.

Signed:

Candidate

Countersigned:

Supervisor : Dr. Md. Abdur Razzaque

Co-supervisor : Dr. Md. Mamun-Or-Rashid

Abstract

Nowadays, the development of smart cities has become a dire necessity to improve the quality of human life. Wireless sensors and necessary information and communication technology (ICT) infrastructures are the fundamental building blocks of smart cities. The number of connected sensor nodes worldwide is jumping to 125 bn by 2030. We are continuously witnessing the rapid development of sensor networks for a vast range of real-time applications. It becomes challenging to collect data on time from these versatile sensor nodes. Moreover, the energy criticality of these autonomous nodes is a crucial constraint to maximize lifetime of sensor networks. Existing works in the literature suffer from imbalance energy consumption, reducing the network lifetime, and many of those don't explore efficient methods for on-time data collection from a network having obstacles.

In this dissertation, we aim to explore real-time data routing and collection strategies both for obstacle-free and obstructed networks. At first, we focus on developing a novel data routing backbone to maximize network lifetime in an obstacle-free sensor network. The first contribution of this thesis is introduction of a *Starfish routing (SFR) backbone* for sensor networks with a mobile sink that spreads the backbone nodes over the different regions of the network in such a manner that any source node can directly access at least one of the backbone nodes. The con-

struction of the *SFR backbone* is motivated by the water vascular system of a sea Starfish. Following this, the backbone nodes are placed on a central *ring-canal* that helps to alleviate the hot-spot problem around the network center, and on the *radial-canals* that facilitate faster data delivery towards the mobile sink from any corner of the network. These canals jointly help to distribute data routing loads and uniform energy consumption throughout the network, resulting in extending network lifetime.

The second contribution of this thesis is the development of a data collection strategy for a mobile sink in an *obstructed network* to reduce data delivery delay and to maximize network lifetime. Due to the presence of obstacles (e.g., building, forest, etc.) and heterogeneous data generation rates, the data collection strategies become more challenging and have not yet been well-studied. Therefore, it necessitates developing a data collection schedule to maximize network lifetime for real-time applications in an obstructed network. A high-speed data routing backbone and data collection schedule of a mobile sink in an obstructed network have been developed as a mixed-integer linear programming problem that maximizes network lifetime while meeting delay-deadline requirements of real-time applications. It finds an optimal travel plan of the mobile sink and corresponding sojourn durations at sojourn locations. The proposed *Starfish data collection schedule* also guarantees loop-free travel scheduling among the sojourn locations, ensuring balanced energy consumption throughout the network. Finally, the performances of these works have been carried out in Network Simulator-2, and significant improvements are observed for both obstacle-free and obstructed sensor networks in terms of network lifetime, end-to-end data delivery delay, throughput, etc. compared to the state-of-the-art works.

Table of Contents

List of Figures

List of Tables

Chapter 1
Introduction

In this chapter, we overview the key motivation to develop Starfish routing (SFR) backbone in real-time data collection with a mobile-sink aiming to maximize network lifetime.

1.1 Introduction

The world's urban population is proliferating with a projection to grow up to 68% by 2050 [5], [6]. Consequently, the development of smart cities has become a dire necessity to improve the quality of human life; where different smart utility services, efficient resource management, smart energy management, precision agriculture [7], [8], [1], smart home and building, smart transportation systems, etc. would be available with the help of sensors or Internet of Things (IoT) devices [9] and necessary information and communication technology (ICT) infrastructures. These are considered as the fundamental building blocks of smart cities [10], [11]. Usually, the wireless sensor nodes include sensing, processing, storing, transmitting, and strand-alone power capabilities. A number of sensors deployed in an area collectively form a sensor network. Due to the higher degree of deployment flexibility, we have witnessed a rapid growth of sensor networks based on a wide variety

of applications [12], [13], [2], [3], [14], [15], [4], due to their deployment flexibility.

Broadly, sensor network applications may be divided into two categories: monitoring and tracking. Monitoring applications include environmental observation such as precision agriculture [1], forest fire detection [12], flood detection, industrial process, nuclear power plant and structural monitoring [2], smart grid monitoring applications [3], emergency medical response [15], [16], military surveillance [17], e-health, embedded intelligent systems, etc. On the other hand, tracking applications include objects, animals, humans, vehicle tracking, etc.

Since the sensor networks are growing beyond simple connectivity for the applications, and it is projected that number of connected sensors or IoT devices worldwide are jumping at 125 billion by 2030 [9]; it becomes challenging to collect data from these multi-dimensional sensors within the required time limit [18], [19], [20]. Besides, the efficiency of real-time data collection in sensor networks highly depends on different strategies [21] within the bounded delay-deadline. The energy criticality of these autonomous sensor nodes is still a constraint to maximize lifetime [22] of sensor networks. Moreover, it is also challenging to determine efficient data routing that offers uniform energy consumption throughout the network to extend network lifetime and reduce end-to-end packet delivery delay for a real-time application. Furthermore, the presence of obstacles in the network and heterogeneous data generation rates of sensor nodes [23], the data collection strategies become more complicated that has not yet been well-explored in the literature. Therefore, to maximize network lifetime, it is necessary to develop an efficient data collection schedule for a real-time application in an obstructed network.

In the early stage of development, static-sink-based data collection strategies [24] seem to be quite reasonable since it is easy to develop, maintain, and, there-

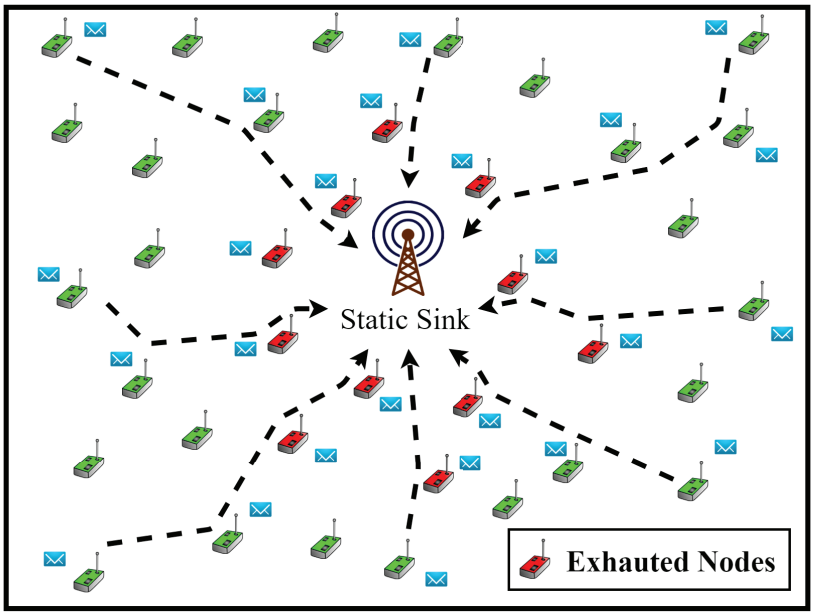

Figure 1.1: A sensor network with a static sink

fore, simplify design challenges of routing protocols in the networks. However, researchers have discovered a number of shortcomings in this type of architecture [25]. For example, the entire network's traffic is confined to a small number of sensor nodes because of the unique many-to-one converge-cast, as shown in Fig. 1.1. As a result of this impact, the nodes in close proximity to a static sink (e.g., red marked sensors in Fig 1.1) are exhausted with energy expenditure and become dead. Therefore, the static sink is inaccessible from the rest part of the network, and thus network is partitioned.

To prevent network partitioning problem, recent works have demonstrated the effectiveness of *mobile sink* based routing strategies in the network [26]. Typically, the mobile sink collects data traveling across the network, and this technique has already been proven not only to enhance the network lifetime but also to minimize

average end-to-end data collection latency to a great extent compared to its static counterpart [27]. These works have also demonstrated that sink mobility ensures data network connection under sparse and disconnected sensor networks.

In the state-of-the-art works, data collecting strategies employing a mobile sink fall into two major categories: *direct-contact based* and *rendezvous-node based*. In the direct-contact based strategy [18], [19], [28], the mobile sink visits each and every node in the network; and collects data directly. On the other hand, a mobile sink gathers data from a few designated nodes in a network using a rendezvous node-based data collection strategy [29], [30], [31], instead of visiting all sensor nodes in the network.

However, these strategies invite the problem of locating the destination sink, establishing source-sink routing path dynamically, extending network lifetime, or developing efficient data collection scheduling for various applications. Exhaustive visits via all rendezvous nodes on cluster heads or backbone nodes are likewise rendered infeasible for real-time applications due to application delay deadline violations. Even Nevertheless, there is still space to improve network longevity while satisfying delay deadlines for real-time applications. In addition, most of the existing state-of-the-art works focus on developing routing paths or data collection techniques in obstacle-free network environments. However, practical sensor network applications suffer from adopting these protocols due to the presence of obstacles (i.e., building, tree, pond, lake, forest, mountain, etc.) in the network. In the presence of obstacles and heterogeneous data generation rates, data collection strategies become more challenging to enhance network performances and lifetime of sensor networks that have not yet been well-explored in the literature. As a result, a real-time data collection strategy for an obstructed network should be

developed to maximize network lifetime. Therefore, in this dissertation, we concentrate on exploring an efficient data routing and data collection scheduling of a mobile sink to maximize lifetime of sensor networks for a real-time application.

The rest of the chapter is organized as follows. The effectiveness of a mobile sink in sensor networks is presented in section 1.2. An overview of data collection strategies with mobile sink, and lifetime of sensor networks are described in Section 1.3, and Section 1.4, respectively. Next, we discuss few real-time applications focusing on different challenges in Section 1.5. The motivation of this research work is presented in Section 1.6. To alleviate issues of the practical applications, Section 1.7 presents the problem statement and the solution methodologies. The contributions of the research effort are discussed in Section 1.8, and finally, Section 1.9 presents the organization of the dissertation.

1.2 Sensor Networks with Mobile Sink

Typically, a static sink receives data from different locations of a network, as shown in Fig. 1.1. In the literature, routing protocols with a static sink have been well studied. These include QoS aware [32], end-to-end data routing, interference aware, hop-by-hop data transmission, cross-layer protocols, multipath routing protocols, etc. While a static sink collects data, its nearby nodes are exhausted with energy expenditure, and therefore, the sink is inaccessible from the rest of the network. This phenomenon is known as the energy-hole problem that disrupts communication between source sensor nodes and the sink.

In order to alleviate the problem, a mobile sink travels and collects data across the network, as illustrated in Fig. 1.2. This technique has already been proven not only to enhance the network lifetime but also to minimize average end-to-end data

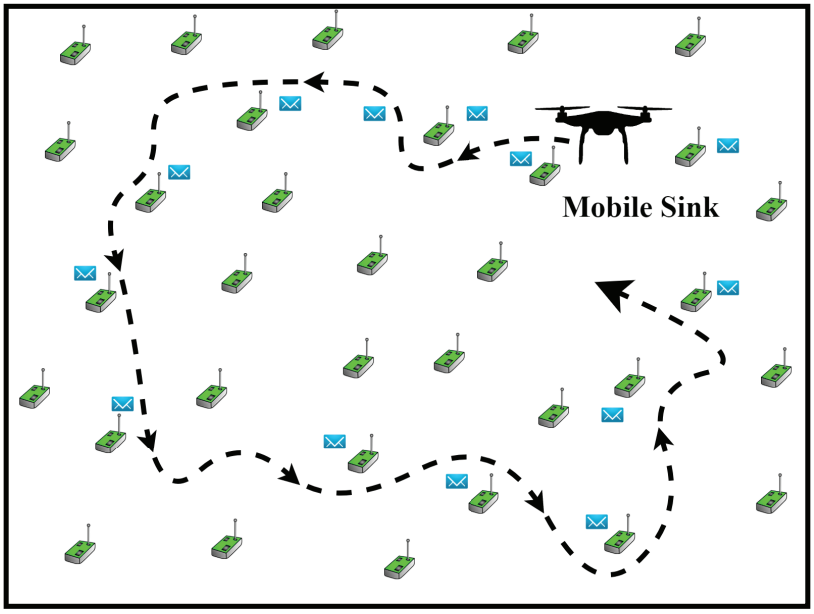

Figure 1.2: A sensor network with a mobile sink

collection latency to a great extent compared to its static counterpart [26], [27]. Introducing a mobile sink is very much effective for many applications. Therefore, a recent trend is to exploit sink mobility as a promising approach to develop an efficient data collection schedule and network connectivity in an obstructed network that extends network lifetime for real-time applications. However, sink mobility invites several research challenges: to localize the sink position and to establish source-sink routing path, link breakage, increased communication overheads, etc. Therefore, it is necessary to develop a mobile sink based data collection scheduling for a real time application.

1.3 Data Collection with Mobile Sink

Recently, a wide range of applications has significantly changed data collection strategies that can be divided into two major categories: *direct-contact based* [18], [19], and *rendezvous based* [30], [31], [29] data collection strategies. Using a mobile sink, all source nodes in the network can be reached using direct-contact based strategy. These solutions can fully eliminate message relay overhead, advertising the changing location of the sink, and so on. As a result, direct contact based data collection strategy can extend network lifetime. However, these are prone to exaggerated traveling path distance, buffer overflow, higher data delivery latency, and failures to satisfy the application's hard delay-deadline.

On the contrary, in *rendezvous-based* data collection strategies [29], [30], [31], a mobile sink visits and collects data from a few designated nodes, instead of visiting all sensor nodes. Though rendezvous-based strategies are suitable for real-time applications in sensor networks, determining an efficient data collection scheduling of a mobile sink is still challenging to maximize network lifetime. In addition, obstacles are considered an integral part of a practical network. Therefore, developing an efficient data collection strategy in an obstructed network over the rendezvous nodes becomes more complicated.

1.4 Lifetime of Sensor Networks

The lifetime of a sensor network is defined as the time interval between the start of operation and the death of the first node. In other words, network lifetime can be defined as the total duration of time that a network is capable of retaining full functionality and/or accomplishing specific goals during operation, as discussed in

[22] [33] [34] [35]. Typically, network lifetime is an important statistic for maintaining network quality of service (QoS). However, depending on the application, the concept of a lifespan may differ. In [34], lifetime is defined as the point in time when a particular number of nodes in a network are exhausted due to energy depletion or the point in time when the first data collecting failure occurs.

There are various approaches for extending the lifetime of a network. It is possible for each to have their own concept of what constitutes an objective function. According to the literature, the key strategies for extending network lifetime include data routing, sleep-wake scheduling, clustering, opportunistic transmission schemes, mobile relay, sink deployment, connectivity, coverage, energy harvesting, and so on.

Typically, the physical impediments in networks were generally neglected. However, obstacles are a necessary component (e.g., a building, pond, trees, forests, etc.) of the network in real-world circumstances and cannot be ignored. A few studies have been published recently that discuss the physical obstacles that exist in networks. Conventional routing protocols suffer from well-functioning in an obstructed network due to the low signal strength, longer travelling path, energy constraints of nodes, etc. Moreover, obstacle identification is also a significant challenge, particularly in random deployment. In comparison, mobile elements are more efficient in obstructed network scenarios due to lower energy constraints and their mobility. The newest trends in sensor networks indicate a strong swing toward overcoming hurdles of obstacles through the use of mobile sinks.

1.5 Applications of Sensor Networks with Mobile Sink

Sensor networks have become increasingly popular in recent years for a wide range of applications. The following sections go over a few real-time and sensitive applications.

1.5.1 Sensor networks in precision agriculture

Every industry, such as smart cities, smart health, smart grid, smart home, smart agriculture, or precision agriculture, is being transformed by technological breakthroughs based on wireless sensor nodes [1], [9]. Agricultural science diligence is more exact, precise, data-driven, and aggressive than it has ever been. Predicting natural conditions and reacting to them as quickly as feasible is critical to farming efficiency. Yield productivity varies due to the varied nature of climatic conditions in different parts of a country. Moreover, pests, insects, illnesses, birds, and animals impact global agricultural productivity, resulting in yield reductions ranging from 20% to 40% [1].

On the contrary, the world population is projected up to 10 billion by 2050, and we are moving towards food scarcity. Consequently, food production ability will bankrupt unless we establish and advance intelligent technologies in agriculture. Human-oriented traditional supervision and management of crop health are not enough.

Therefore, real-time monitoring by sensors greatly helps to boost agricultural yield while also reducing crop waste and the negative impact on the environment, as shown in Fig. 1.3. Agriculture consumes more than 70% of the world's water,

Figure 1.3: A sensor network application in precision agriculture [1]

despite the fact that people are running out of fresh drinking water. As a result, in the coming years, it will be worthwhile to implement effective irrigation and pesticide usage based on real-time and high-accuracy monitoring. It's worth noting that a mobile sink (or drone) equipped with hyperspectral and multispectral sensors can help identify the health of plant leaves, water stress levels, humidity, temperature, and soil nutrients in real-time, reducing risk and disaster loss.

1.5.2 Sensor networks for wildfire management

As technology advances, natural and artificial disasters have become increasingly common in recent years. Forests cover over 30 percent of the world's land area,

Figure 1.4: A real-time wildfire management using sensor networks

making it critical to protect natural resources. Because of the dense structure of the forest, fire spreads quickly across vast regions, disrupting the entire ecological system and putting wild animals in danger. Forest fires (also known as wildfires) have become more common in recent years as a result of global drought conditions, wreaking havoc on the environment. The Australian bushfires of 2019/2020, as shown in Fig. 1.4, were one of the worst in recent memory, destroying 4.6 million acres, destroying thousands of homes, and exposing countless numbers of animals. Since 2020, there have been 267 major fires in the Amazon, which have burned approximately 260 thousand acres in the Brazilian Amazon. According to [13], over 306 thousand large fires occurred in the United States over the last five years, burning over 4.92 million acres.

Figure 1.5: A real-time nuclear power plant monitoring using sensor networks [2]

In such a scenario, this is emerging to detect forest fire through sensor networks to avoid fire hazards, as illustrated in Fig. 1.4. The real-time monitoring system inherently interacts with smart sensors or IoT devices deployed in forests, estimate forest growth, monitor trees' health along with fire detection. Besides, different environmental factors, e.g., temperature, humidity, CO, CO_2, and wind speed, would help predict rapid action against wildfire and support predicting climate change to a great extent. Therefore, it is necessary to develop efficient data collection techniques from sensors that are deployed in the forest.

1.5.3 Sensor networks in nuclear power plant

A nuclear power plant (NPP) generates electricity in which heat energy is used to generate the steam to drive the turbine. In the NPP, the discharge of radioactive wastes causes hazardous impacts on the environment and, thus it affects normal

human lives, plants, animals, and sea creatures. Besides, it is challenging to keep the environment safe from harmful gases and liquids produced in an NPP. While any explosion occurs, a higher level of security is reinforced nationwide. To mitigate the issues, multidimensional sensors and many safety measures using sensors or IoT devices have already been installed to monitor the entire plant on a 24/7 basis from a remote location [2].

For example, the Rooppur nuclear power station, shown in Fig. 1.5, is located at Paksey, in the Ishwardi Upazila of Pabna district, on the bank of the Padma. It is Bangladesh's first nuclear power plant (NPP), with a capacity of 2.4 GWe. The nuclear power station is located near the historic Hardinge and Lalon Shah bridges, which are bordered by residential neighborhoods. The lifespan of two reactors is estimated to be 60 years (with a 20-year extension) at a cost of USD 12.65 billion. The safety of human life and ecological health around the Padma river and historical icons may be jeopardized if the nuclear facility fails catastrophically. In such a critical situation, it is necessary to monitor and control its sensitive valves, as well as to report any unusual incidents to the control station immediately, in order to ensure overall habitat and nuclear power plant safety.

Therefore, efficient data collection techniques from sensors or IoT devices are a burning issue. Data collection becomes more hazardous during the radioactive explosion and becomes more complicated passing through the power plant's existing obstacles. A sensor network with a mobile sink can alleviate real-time data collection deficiencies in such a critical and hazardous situation.

Figure 1.6: A sensor network to monitor solar panels with a mobile sink [3]

1.5.4 Sensor networks to monitor solar panels

Renewable energy sources are lucrative and clean technologies with zero carbon emissions that are continuously rising as one of the prominent sustainable energy sources in the world. However, several issues could affect the performance of solar panel monitoring, such as extensive data management, signal interference, long-range data transmission, and security. Recently, the monitoring system has been integrated with sensor networks to acquire performance data of various sensor nodes, as illustrated in Fig. 1.6.

The global energy market is going through substantial change with renewable energy sources. According to a study, the renewable energy source is anticipated to reach approximately 4391.18 GW by 2026 [3]. Integrating solar energy into

intelligent homes is becoming more popular as solar panels continue to reduce cost.

Consumers and companies may use the Internet of Things to track the use of solar energy at a much finer level, gaining a better understanding of which products and services are the most energy-efficient, how much electricity is being consumed, and when and how it is being utilized. At the company level, however, it is difficult to facilitate and maintain solar panels. Sensor-based monitoring systems are becoming increasingly popular for remote maintenance, as shown in Fig. 1.6, predictive analysis, which reduces costs even further. Deep visibility may help businesses reduce equipment stress, balance energy loads, and detect concerns like overheating before they become a problem. Furthermore, smart monitoring systems with a mobile sink are particularly useful in ensuring the safety of solar panels from physical theft or even vandalism.

1.5.5 Sensor based smart health-care management

Chronic diseases, such as diabetes, neurological disorders, cardiovascular disease, obesity, and so on, are becoming more widespread as the population of the elderly grows [15]. Healthcare monitoring systems at hospitals and health centers have increased significantly, and portable systems based on emerging technologies are now a major source of concern. The emergence of the sensors and Internet of Things (IoT) technologies, sensing, remote health monitoring, and, ultimately, identifying activities of daily living through wearable sensors has been a promising solution, as presented in Fig. 1.7(a). In the case of the COVID-19 pandemic [36], health care management becomes more challenging to collect patient health-related data from a contaminated environment Fig. 1.7(b). As a result, sensor-network-based intelligent healthcare management, which includes a heartbeat sensor, body

(a) Patient monitoring [15] (b) Hospital environment monitoring [36]

Figure 1.7: IoT based smart health-care management

temperature sensor, humidity sensors, CO and CO_2 gas level sensors, outdoor and room temperature sensors, and other devices, can significantly reduce casualty rate of emergency patients in a hospital.

1.5.6 Sensor networks in mass transit railway monitoring

The next generation smart transportation systems aim to explore wireless sensors over a large rail network infrastructure for automatic ticketing systems, scheduling, safety management, capacity handling, digital display, smart metering, integrated security, real-time decision-making, predictive maintenance, asset management, and so on. Since the global smart mass transit railway market is estimated to grow up to USD 20.58 bn by 2021, 200-300% passenger mobility and 150-250% freight activity by 2050 [4]. Due to this trend, this is obvious to monitor different elements of mass transit railway on a 24/7 basis. For instance, the Dhaka mass transit railway (MTR) in Bangladesh has been developing soon, as depicted its route plan in Fig. 1.8(a). Therefore, the regular operation is performed using the

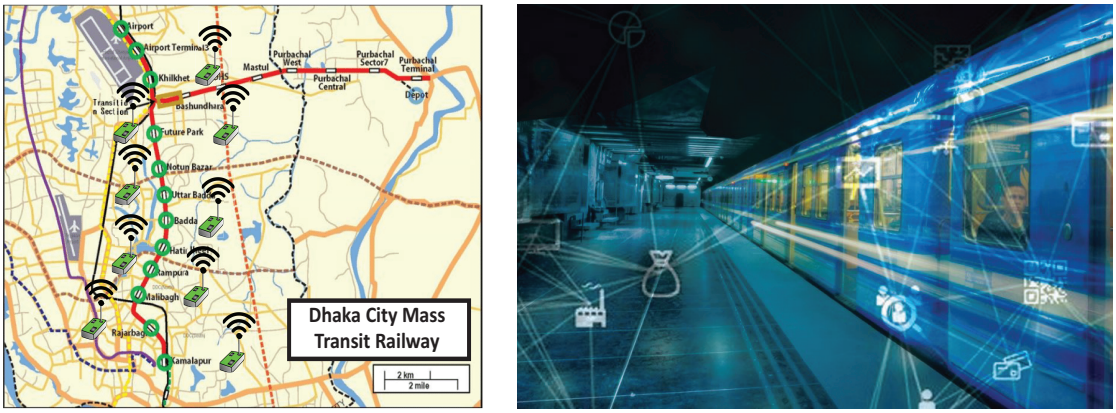

(a) Dhaka MTR routes

(b) Smart MTR management

Figure 1.8: A real-time mass transit railway monitoring system [4]

precise location of the train, its speed, weight, vibration sensors, weather reports, power connections, and so on, as shown in Fig. 1.8(b). This is why implementing sensor networks, and seamless high data rate connectivity is essential to collect data from various sensors or IoT devices.

1.6 Motivation of the Research Work

We can see from the examples above that sensor networks are critical for data collection in a wide variety of real-time applications. However, the efficiency of these applications depends on network lifetime and data collection within a bounded delay deadline. When a number of sensor nodes are deployed in a large network area, it is preferable that a mobile sink collects data traveling across the network. Since the typical sensors are battery powered and stand alone in a large network, energy depletion of these sensors is minimized through collecting data by a mobile sink. This technique has already been proven not only to enhance the network lifetime

but also to minimize average end-to-end data collection latency to a great extent compared to its static counterpart [26], [27]. Therefore, we consider a mobile sink in the network for data collection.

In the literature, we have found a good number of data collection strategies for sensor networks with a mobile sink, i.e., *direct contact based* [18], [19], [28], and *rendezvous-based* [37], [38], [39] and *backbone-based* [40], [41], etc. In the *rendezvous-based* approaches, few rendezvous nodes are designated to collect data either over rectangular region [37], central vertical region [38], or hexagonal regions [39] in the network.

However, these protocols suffer from imbalance energy consumption on a few rendezvous nodes in the network that restricts network lifetime. There is, nevertheless, opportunity for further optimization of the network lifetime while preserving real-time application deadlines. Determining an optimal set of rendezvous nodes for a time-constrained application, maximizing network lifetime is still challenging. Moreover, collecting data in the presence of obstacles in a network becomes more complicated for the real-time applications.

Therefore, in an obstructed network, it necessitates developing an efficient schedule of a mobile sink to maximize network lifetime. These issues motivate us to develop a novel routing backbone to maximize network lifetime for real-time applications with a mobile sink, and after that to find a set of optimal rendezvous nodes over a backbone architecture in an obstructed network.

1.7 Problem Description and Solution Methods

In this section, we briefly discuss the problem addressed in the dissertation and the solution methodologies.

1.7.1 Problem description

Though individual sensor node's energy consumption is a crucial issue for a longer network lifetime, a well-balanced energy consumption across all sensor nodes throughout the network is also highly expected. Traditionally, sensor nodes are scattered throughout the sensing field, and when they detect an event of interest, they communicate it back to any sink via multi-hop or single-hop communication. Data collection strategies based on mobile sinks not only ensure that nodes consume rational amount of energy, but also they cover disconnected parts of the network. However, in an obstructed-network, these strategies exhibit higher end-to-end delay due to sink's longer traveling path over a viable circular path [42], [43] or cluster heads [44], [45], [46] to collect data. These works may also violate the delay-deadline of real-time applications and increase energy consumption among the sensor nodes significantly. Therefore, it necessitates developing efficient data collection scheduling of a mobile sink in sensor networks to satisfy real-time delay deadline requirements.

In an obstructed network, mobile-sink-based sensor network applications are lucrative. However, few works considered sojourn duration, different data arrival rates at nodes, and application delay-deadline in selecting rendezvous nodes. Consequently, strategies for optimal rendezvous nodes and sojourn durations at individual nodes in an obstructed network have been left unexplored. Motivated by the above challenges, in this dissertation, we have answered the following research questions:

- What routing strategy can minimize hotspot problem through implementing balanced energy consumption of nodes across the whole network?
- How to formulate an optimization framework for maximizing lifetime in an

obstructed sensor network?

- What travel plan of a mobile sink can guarantee sub-loop free movement while maintaining the application's quality of services (QoS) and delay deadline during data collection?
- How to derive a statistical analysis or mathematical model to find end-to-end packet delivery delay?
- What performance improvement can we achieve due to introducing the Starfish routing (SFR) backbone and an optimal data collection strategy of a mobile sink?

The following subsection highlights the key concepts for addressing the above research questions in our thesis work.

1.7.2 Solution methodologies

To mitigate the above issues, in this dissertation, we follow the solution methodologies as presented in a block diagram in Fig. 1.9. At first, we study the state-of-the-art works in Chapter 2, and then focus to develop a solution mechanism to maximize network lifetime in an obstacle-free sensor network through developing a novel data routing backbone that offers balanced energy consumption throughout the network, as explained in Chapter 3. The construction of the proposed *Starfish routing (SFR) backbone* is motivated by the water vascular system of Starfish [47]. The key philosophy of designing the proposed Starfish routing (SFR) backbone is to spread the backbone nodes over the different regions of the network in such a way that a source node can access at least one of the backbone nodes directly. Following Starfish's water vascular system, the backbone nodes are placed on a central

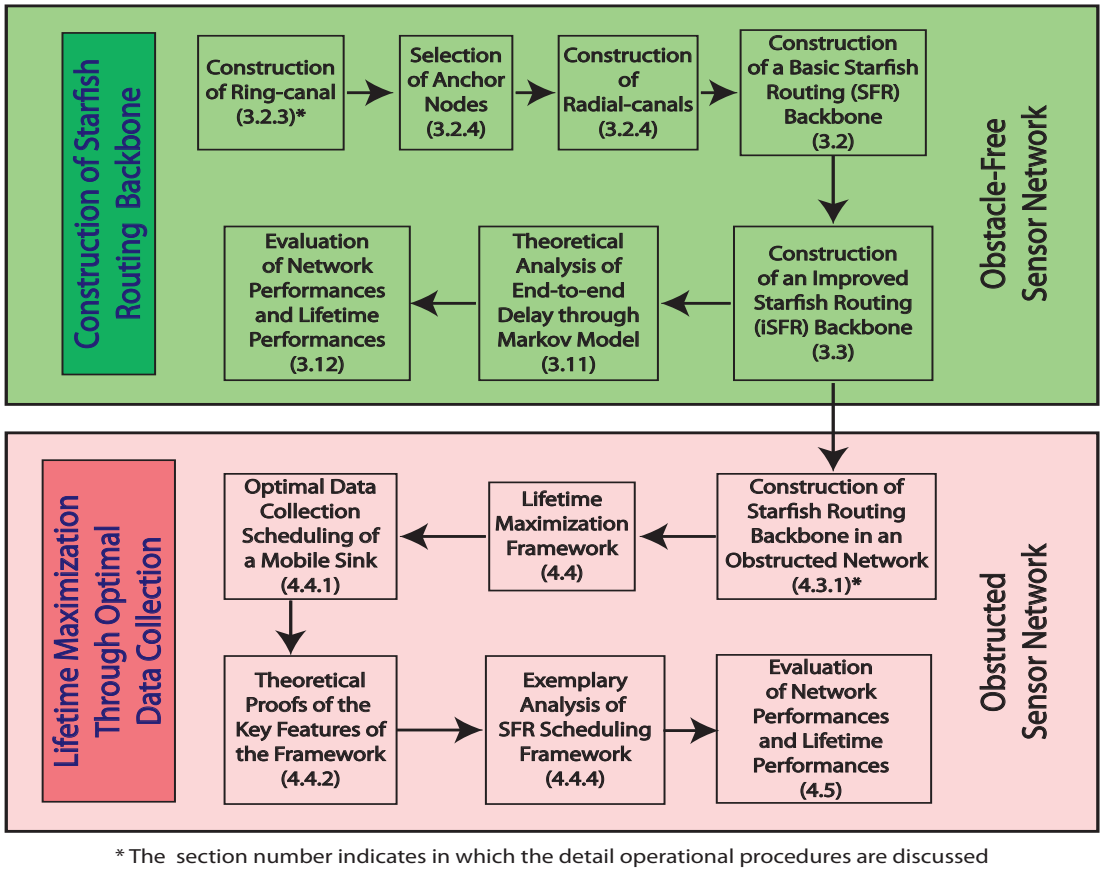

Figure 1.9: A block diagram showing different components of the proposed solution

ring-canal that resolves the hotspot issue in the vicinity of the network center, and on the *radial-canals* that facilitate faster data delivery towards the mobile sink from any corner of the network. The existence of a central ring-canal along with a number of radial-canals jointly helps to distribute data routing loads to many nodes instead of over a few designated nodes in the network.

Since obstacles are considered as an integral part of a network, as presented in the bottom part of the block diagram in Fig. 1.9, we reconstruct the SFR backbone in an obstructed network. After that, we develop a data collection strategy of a

mobile sink, as discussed in Chapter 4, in such a way that it maximizes lifetime while meeting quality of service (QoS) requirements of a delay sensitive application. The proposed data collection schedule determines a set of optimal rendezvous nodes on the SFR backbone and sojourn durations through a MILP formulation for a time-constraint application. In brief, jointly, both the proposed data routing backbone and mobile sink's data collection schedule have significant impacts to maximize the lifetime of an obstructed sensor network, for a real-time application, that is discussed elaborately in the following chapters.

1.8 Contributions of the Thesis

In this thesis work, we have explored real-time data routing and collection strategies for obstacle-free and obstructed networks. The first contribution of this thesis is to introduce mobile sink based *Starfish routing (SFR)* backbone architecture for sensor networks with a mobile sink that spreads the backbone nodes over the different regions of the network in such a manner so that any source node can directly access at least one of the backbone nodes. It inherently offers uniform energy consumption throughout the network, resulting in extending network lifetime and reducing end-to-end data delivery delay for a real-time application. The *ring-canal* and *radial-canals* of the proposed Starfish routing backbone are mathematically modeled based on *transmission range* of sensor nodes and the size of *network area*. The key concept of getting single-hop accessibility to one of the backbone nodes from any source node has significant contribution to minimize end-to-end delay and maximize network lifetime. This high-speed routing backbone can simultaneously optimize end-to-end data delivery delay, energy consumption, network lifetime for a delay-constrained applications.

The second significant contribution of this work is the formulation of a mixed-integer linear programming (MILP) problem to maximize lifetime of an obstructed network. Moreover, it determines an optimal data collection scheduling of a mobile sink for visiting a set of sojourn locations, and sojourn durations at those. The planned data collection schedule meets application's QoS requirements. It also ensures loop-free travel scheduling across RNs, resulting in reduced end-to-end data delivery delay and optimal network lifetime. Finally, the performances of the proposed works have been carried out in Network Simulator (e.g., NS-2) [48], and significant improvements are observed for both obstacle-free and obstructed sensor networks in terms of network lifetime, data delivery delay, throughput, etc.

1.9 Organization of the Dissertation

In this dissertation, the rest of the chapters of this dissertation are organized as follows. Chapter 2 discusses the state-of-the-art works elaborately focusing on maximizing the lifetime of sensor networks in real-time data collection with a mobile sink. In Chapter 3, we construct the proposed Starfish routing (SFR) backbones to achieve an extended network lifetime while maintaining delay-deadlines of real-time applications. Furthermore, in Chapter 4, we develop an optimal data collection scheduling of a mobile sink over a set of sojourn locations in an obstructed network to maximize the lifetime of sensor networks. Finally, we conclude the dissertation in Chapter 5 by summarizing the research findings, along with the future extensions of this work.

Chapter 2
Literature Review

In this chapter, we overview necessary background studies for data routing strategies with a mobile sink in sensor networks. We also discuss real-time data collection strategies aiming to maximize network lifetime in obstructed networks.

2.1 Introduction

Routing protocols in sensor networks with static sink(s) have been well studied in the literature which include end-to-end and hop-by-hop single path routing; node-disjoint, quality-of-service (QoS) aware [49], interference aware, cross-layer protocols, multipath or geographic routing protocols [50], etc. However, these protocols suffer from reduced network lifetime due to quicker depleting batteries of the nodes near the sink, resulting in the premature death of sensor networks. It is observed that when the network is dead, the residual energy of the nodes in the far-sink area is up to 80% [51]. In order to alleviate this problem, routing protocols that consider sensor networks with a mobile sink are emerging, and these are proven to achieve load-balancing and uniform energy consumption across the network. In the meantime, data collection from different IoT and sensor devices has been dramatically increasing due to the development of 5G and edge network

[52], cloud and fog computing [53], big data analysis, etc. Therefore, in the era of fourth industrial revolution [11], it necessitates to form a high-speed backbone (HSB) paths in sensor networks [40], [41], [51], [54], [55], [56], [57], [58], to satisfy the QoS requirements of real-time applications that facilitate timely and energy-efficient data gathering from source node to a mobile sink.

The primary goal of routing protocols in sensor networks is to efficiently transmit sensed data to the sink. While a routing protocol is developed for a sensor network, energy consumption becomes the primary concern that is directly related to neighborhood discovery, communication, and computation, etc. However, developing routing protocols for sensor networks is very challenging due to lack of global addressing, many-to-one data convergence, redundant traffic, and tightly constrained by battery power, storage and processing capacity, etc. [34], [59]. Moreover, while establishing a routing path in a large sensor network, the flooding technique is followed that broadcasts each received packet to all of its neighbors. However, it suffers from energy wastage in the network due to implosion, overlap, and resource blindness, etc. [22], [60]. Therefore, it necessitates to develop a data routing backbone that not only prevents energy wastage but also guarantees balanced energy consumption throughout the network.

In the state-of-the-art works, routing protocols are typically categorized as data-centric, hierarchical, and location-based [61]. Data-centric protocols are mostly query-based that help to eliminate redundant packets. On the contrary, hierarchical protocols focus on determining cluster heads for data aggregation to preserve energy. In contrast, location-based protocols utilize the position information to find the shortest route to the sink. These protocols mainly focus on energy consumption while constructing routes in the network. Therefore, these protocols lack

to satisfy certain requirements of real-time applications or multimedia communication, such as end-to-end packet delivery, network lifetime, delay, correctness, fault tolerance, stability, jitter, scalability [62], etc. Energy consumption is one of the most critical performance metrics in sensor networks, but it is not the only one. Moreover, in some cases, the delay may be even more significant than energy consumption. Therefore, it necessitates developing an energy-efficient and quality-of-service (QoS) aware data routing path along with an efficient data collection strategy of a mobile sink that guarantees high-speed end-to-end packet delivery for real-time and multimedia applications.

Moreover, practical sensor network applications may contain many obstacles [23], [63], (i.e., building, tree, pond, lake, forest, mountain, etc.) that restrict the free movement of the mobile sink and to adopt state-of-the-art protocols in sensor network to collect data. Furthermore, in the presence of obstacles throughout the network and heterogeneous data generation rates, data collection strategies become more challenging that have not yet been well-studied in the literature. Therefore, it necessitates to develop a mobile sink based data collection schedule in an obstructed network to maximize lifetime of sensor network [64]. Therefore, in this dissertation, we concentrate on exploring a high-speed data routing backbone for real time applications, and mobile sink based data collection scheduling in an obstructed network to maximize lifetime of network.

The performance of sensor networks with a mobile sink greatly depends on efficient data routing strategies, data collection strategies of a mobile sink, network lifetime issues, etc. Therefore, the rest of the chapter is organized as follows. An overview of data routing strategies with a static sink, and mobile sink is presented in Section 2.2, and Section 2.3, respectively. After that, different data collection

strategies in obstacle-free and obstructed networks are described in Section 2.4. Next, we discuss various techniques of maximizing network lifetime, and QoS requirements in real-time data collection in Section 2.5, and Section 2.6, respectively. After that, a comparative study among the state-of-the-art works is presented in Section 2.7. We discuss limitations of the existing studies in Section 2.8, and finally, we conclude the Chapter in Section 2.9.

2.2 Routing Strategies with a Static Sink

In the early days, a typical sensor network was composed of static sensor nodes and a static sink deployed in an observed region. In the state-of-the-art works, routing strategies with a static sink can be distinguished into proactive [65], [66], [67]; reactive [68], [69]; and hybrid [70], [71], [72], etc. approaches. The proactive strategy, also referred to as table-driven, relies on the periodic dissemination of routing information to maintain consistent and accurate routing tables across all nodes of the network. On the other hand, reactive routing strategies establish routes to the sink on demand. A hybrid routing strategy can be adopted whereby proactive routing is used within a cluster, and reactive routing is used across clusters.

In the literature, sensor protocols for information via negotiation (SPIN) (e.g., SPIN-PP, SPIN-EC, SPIN-BC, SPIN-RL, etc.) is a family of negotiation-based, data-centric, and time-driven flooding protocols [73], [74], [75]. However, compared to classic flooding, SPIN nodes rely on two key techniques to overcome the deficiencies of flooding. Directed diffusion [76] is another data-centric data dissemination protocol that is also application-aware in that data generated by sensor nodes is named by attribute-value pairs. Directed diffusion does not rely on globally valid node identifiers but instead it uses attribute-value pairs to describe a sensing task

and steer the routing process. Directed diffusion differs from SPIN in that queries (interests) are issued on demand by the sinks and not advertised by the sources as in SPIN.

Another variant of the directed diffusion is Gradient-Based Routing (GBR) [77], where a gradient is determined based on the number of hops to the sink. Similar to directed diffusion, GBR uses interests to capture a sinks desire to receive certain types of information. During the flooding of these interests, gradients are established on each node.

The Destination-Sequenced Distance Vector (DSDV) routing protocol [65], [66] is a modified version of the classic Distributed Bellman-Ford algorithm in which every node maintains a list of distances. The DSDV uses two types of packets (e.g., full dump and incremental packets) to share its routing table content. Another example of a proactive protocol is the Optimized Link State Routing (OLSR) protocol [67] that is based on the link-state algorithm. In this approach, nodes periodically broadcast topological information updates to all other nodes in the network, obtaining a complete topological map of the network and immediately determining paths to any destination in the network.

In the literature, an example of an on-demand or reactive protocol is the Adhoc On-Demand Distance Vector (AODV) protocol [68]. Unlike OLSR, nodes neither maintain any routing information nor participate in periodic routing table exchanges. AODV relies on a broadcast route discovery mechanism. Moreover, the Dynamic Source Routing (DSR) protocol [69] employs route discovery and route maintenance procedures similar to AODV. In DSR, each node maintains a route cache with continuously updated entries as a node learns new routes.

Hierarchical routing protocols are based on the grouping of nodes into clusters

Table 2.1: Comparative characteristics of the static sink based protocols

Protocols	**Characteristics**
DSDV [65]	Flat topology with proactive route discovery
OLSR [67]	Flat topology with proactive route discovery
AODV [68]	Flat topology with reactive route discovery
DSR [69]	Flat topology with reactive route discovery
LEACH [70]	Hierarchical, support of MAC layer
GAF [71]	Location based, unicast
GEAR [72]	Location based, geocast
SPIN [73]	Flat topology, data centric, query based, negotiation
Directed diffusion [76]	Flat topology, data centric, query based, negotiation
GBR [77]	Flat topology, data centric, query based
PEGASIS [78]	Hierarchical
SPEED [79]	Location based with QoS (real time)
MMSPEED [80]	Location based with QoS (real time, reliability)
DARA [81]	Location based with QoS (real time, reliability)

to address some weaknesses of flat routing protocols. The Low-Energy Adaptive Clustering Hierarchy (LEACH) protocol [70] combines a clustering approach with MAC-layer techniques. The main idea of the Power-Efficient Gathering in Sensor Information Systems (PEGASIS) protocol [78], [82] is for each node to exchange packets with close neighbors and take turns in being responsible for relaying packets to the base station.

Location-based or geographic routing [72], [81] can be used in networks where sensor nodes can determine their position using a variety of localization systems

and algorithms. In the Geographic and Energy Aware Routing (GEAR) protocol [72], packets are forwarded to all nodes within a specific target region.

Although most routing and data dissemination protocols aim for some kind of Quality-of-Service (QoS), some protocols proposed for sensor networks explicitly address one or more QoS routing metrics. The goal of these protocols [79], [80], [81] is to find feasible paths between the source and sink, while satisfying one or more QoS metrics (latency, energy, bandwidth, reliability), but also optimizing the use of the scarce network resources. These protocols are summarized along with their key characteristics in Table 2.1.

While routing, in general, is a crucial component of any multi-hop network, routing is particularly challenging in the static sink-based sensor networks due to their characteristics such as stringent resource constraints and unreliability of links and nodes. Specifically, while transmitting data from different locations to the static sink, nearby nodes are exhausted with energy expenditure and become dead due to many-to-one data convergence. Therefore, the static sink is inaccessible from the rest of the network, and thus the network is partitioned. Consequently, the static sink-based routing strategies must balance energy consumption through limited processing, communication, and overheads. Mobile sink-based routing strategies are getting popular in different sensor-based applications to mitigate those problems.

2.3 Routing Strategies with a Mobile Sink

In the literature, we have found a good number of data routing strategies for sensor networks with a mobile sink, and those can largely be categorized into two groups: *region-based* and *backbone-based*. In the *region-based* strategies [37], [38], [39], [83],

a set of nodes in a region collects data from source nodes, stores it, and later forwards to the mobile sink upon request, as shown in Fig. 2.1. On the contrary, in *backbone-based* strategies [40], [41], [51], a routing backbone is formed, where each source sensor node acquires the updated sink position from the backbone and/or forwards data to the mobile sink over backbone nodes in multi-hop fashion, as shown in Fig. 2.2. These strategies are discussed elaborately in the following subsections.

2.3.1 Region-based data routing

In region-based data routing strategy, railroad [37], line [38] or hexagon [39], [83] like regions are constructed in the network, as shown in Fig. 2.1. In Railroad routing [37], a rectangular region is constructed in the network, as shown in Fig. 2.1(a), to store metadata of the source node. When a source senses data, stores it locally, and sends metadata to the railroad. While the mobile sink requires data, it sends a unicast query to the railroad. Upon receiving this query, the railroad acquires data from the source and transmits it to the sink through the unicast path. This protocol suffers from higher latency due to traveling longer paths using unicast queries and data loss for node failure.

To mitigate data loss problem from a source node in [37], a vertical strip of nodes is created to store data in Line-based Data Dissemination protocol (LBDD) [38], as shown in Fig. 2.1(b). The vertical region in [38] splits the network into two equal portions. When a source senses data, it immediately sends it to the inline nodes of the vertical region. Later, while the sink queries data, the inline nodes broadcast the query in the rendezvous region, and the corresponding inline node sends back the required data in the reverse path.

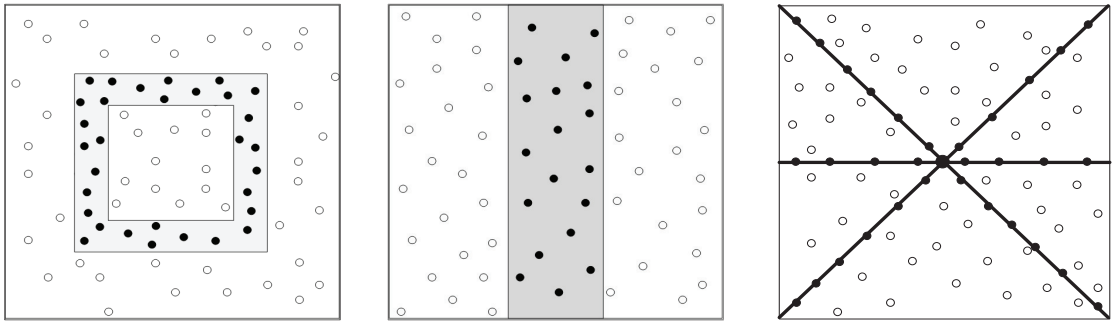

(a) Railroad [37] (b) LBDD [38] (c) HexDD [39]

Figure 2.1: Region-based routing strategies with a mobile sink

However, this protocol suffers from higher latency for boundary nodes in a large network with a single central zone. Besides, regular broadcasting in the central zone decreases the network lifetime and data throughput significantly due to high network collisions. One key difference between Railroad [37], and LBDD [38] protocols is that the queries issued by the sink in the Railroad travel by unicast transmission rather than broadcast. However, the expected data delivery delay in Railroad protocol is higher than that in LBDD [38] since the queries travel longer paths in Railroad [37].

These problems are further addressed in HexDD (Honeycomb architecture and Hexagonal Tiling based Data dissemination) protocol [39] to enhance the network performances by creating six rendezvous regions along three principal diagonals in the network passing through the center cell, as shown in Fig. 2.1(c). These regions replicate and store data while sending toward the central intersection node over the closest principal diagonal lines. To retrieve data, the sink queries over the rendezvous region. If requested data exists in any rendezvous node, it sends data back to the sink through the reverse path of the sink's query forwarding.

Moreover, HexDD protocol suffers from hotspot problem, especially in the central zone, because all data and queries are transmitted through the central node. Besides, the fixed six rendezvous regions, irrespective of network size, cause imbalance energy consumption on a few rendezvous nodes in the network. Recently, some other variants of region based protocols [83], [84], [85], [86], have been proposed; but a few of those are suitable for real-time applications.

2.3.2 Backbone-based data routing

Typically, source nodes in the network suffer from establishing a routing path to the mobile sink due to its random, unpredictable, or controlled mobility. For real-time applications, it is challenging to get a new sink position to transmit data instantly. In *backbone-based* strategy, a backbone is developed to acquire the fresh sink position and/or to transmit data over the backbone nodes toward a mobile sink [40], [41], [51], [55], [58], [87], [88].

In Ring routing [40], a closed loop of nodes is constructed that encapsulates a globally predetermined network center, as shown in Fig. 2.2(a). As soon as the mobile sink changes its position, it advertises an updated location to the ring-backbone by forwarding packets towards the network center. Thus the source nodes can acquire the sink's new position from the ring. Later, the source nodes send data directly to the sink in a multihop fashion. Though this routing backbone offers quicker localization of the sink, its scalability is questionable for large networks. Moreover, progressive flooding toward the ring-backbone significantly undermines the network lifetime and throughput due to high network collisions. Furthermore, it has not explored appropriate ring radius with respect to network size or communication range of sensors. Experimental results show that if the ring radius is

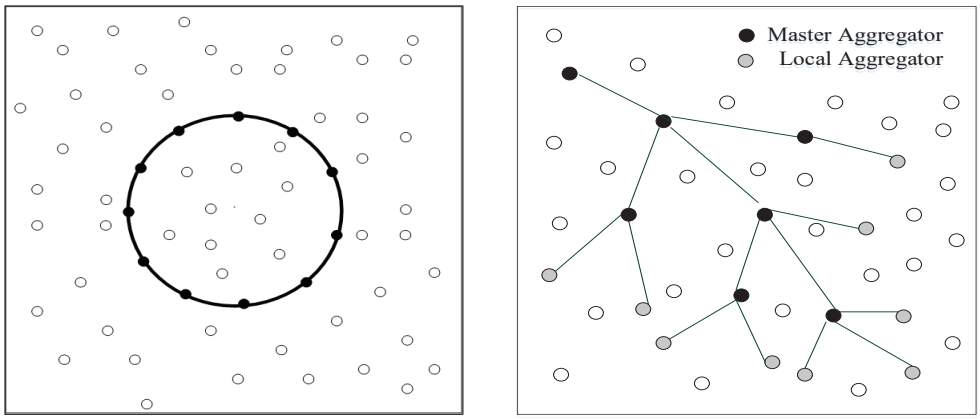

(a) Ring routing backbone [40] (b) Fishbone routing backbone [41]

Figure 2.2: Backbone-based routing strategies with a mobile sink

too small, the sink localization time is greatly increased for network border nodes. The same problem occurs for central nodes when a large ring radius is chosen. The backbone is effective not only for faster localization of the sink but also to provide energy-efficient data delivery to the sink.

On the contrary, the Fishbone routing backbone, as developed in [41], is constructed using different levels of aggregators (e.g., master and local aggregators), as shown in Fig. 2.2(b). The source nodes transmit data over the backbone in multihop forwarding. Though these routing backbones provide better communication infrastructures, the offered end-to-end data delivery latency is higher due to either lack of choosing optimal ring-radius in [40] or multi-level aggregation in [41]. In [88], wireless high-speed routing (WHISPER) protocol is developed to ensure guaranteed data delivery to a high-speed mobile sink. The sink initially injects a query along with its current location, direction, speed, etc., so that packets are routed to the estimated latest location of the high-speed mobile sink. However, the protocol lacks unchanged speed, and the trajectory remains after the query that is

not realistic for most real-time applications or obstructed sensor networks.

Motivated by the above challenges of routing data packets from source nodes to the mobile sink in sensor networks, in this thesis, we aim to introduce a high-speed routing backbone in a sensor network. Recently, bio-inspired systems have been attracted to develop routing paths or to determine the mobile sink's trajectory in a network. Therefore, the water vascular system of a seafish Starfish [47], as illustrated in Fig. 3.2, motivates us to develop a Starfish-like routing backbone in a sensor network.

The key philosophy of the proposed work is to distribute data routing loads to many nodes throughout the network. Such a policy has multidimensional benefits, including extended network lifetime, faster data delivery to the mobile sink, reduced operational overhead, and increased throughput. The construction details of the proposed Starfish routing backbone in discussed in Chapter 3. Besides, the proposed work significantly eliminates redundant data report that helps to minimize wastage of energy, time, computing overhead, data collision, excessive transmission, etc., in the network.

2.4 Data Collection Strategies with a Mobile Sink

In the era of information age, the key responsibility of sensor networks is to collect data from the IoT devices, and to transmit successfully to the sink. Diverse advancements in sensor networks and their applications have recently substantially changed data collection strategies. Developing an effective data collecting system is critical for boosting network lifetime and lowering end-to-end data collection la-

tency. Mobile sink-based data collection strategies have been categorized into two distinct subcategories in state-of-the-art works: *direct-contact based* [18], [19], [89], and *rendezvous-node based* [30], [43], [44], [90], [91]. These strategies are discussed in the following subsections.

2.4.1 Direct-contact based data collection

In the direct-contact based strategies [18], [19], [28], [89], a mobile sink visits to sensor nodes on a regular basis and collects data directly from each one of them. Typically, a mobile sink travels in the field of interest, and traveling path is specified by popular traveling salesman problem (TSP) solution methodologies. In addition to the TSP-based solutions, Hilbert- [18], Moore- [19], and Z-curves [89] are used in a network to determine traveling pathways of a mobile sink to collect data via one-hop communication.

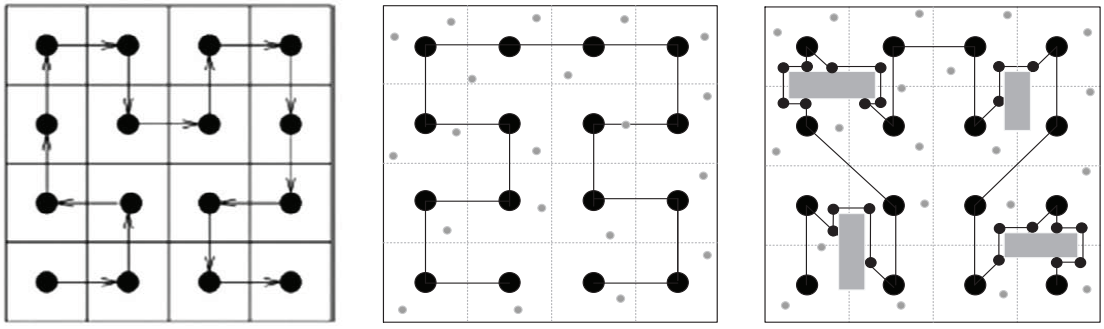

(a) Hilbert-curve [18] (b) Moore-curve [19] (c) Z-curve [89]

Figure 2.3: Direct-contact based data collection strategies

A mobile sink visits along a *Hilbert-curve* [18], a continuous fractal space-filling curve, to collect data from the sensors directly, Fig. 2.3(a). However, a

mobile sink cannot return to the starting location along Hilbert-curve. Therefore, a *Moore-curve* [19] is developed as the loop version of the Hilbert curve, as shown in Fig. 2.3(b). Data collection schedule along both Hilbert- and Moore-curves is easy to develop with similar recursive constructions for a large network.

However, the path length of a mobile sink shows polynomial growth for the larger networks. Besides, their constructions become more complicated, while the network contains either path-restricted or location-restricted obstacles in the network. *Z-curve* [89], [92], tried to minimize data collection time through bypassing obstacles in the network, as depicted in Fig. 2.3(c).

Since a mobile sink collects data from each sensor directly; these approaches can completely avoid message relay overhead, broadcasting sink's fresh location, etc. Thus, direct-contact-based data collection strategies essentially increase network lifetime. However, they suffer from exaggerated traveling path distance, higher data delivery latency, buffer overflow that violates in meeting real-time application's delay-deadline. Therefore, direct-contact-based strategies are not suitable for time-constraint or multimedia applications.

2.4.2 Rendezvous-based data collection

To alleviate the problems of direct contact based data collection strategies, rendezvous-node-based data collection strategies [29], [30], [31], have been introduced. In this strategy, rather than visiting every sensor node in the network, a mobile sink visits and collects data from a few rendezvous nodes via a designated tree-like backbone [90], cluster-heads [91], [93], or routing-backbones (e.g., Fish-bone [41], Honeycomb [83], etc.). Ordinary sensors deliver their packets to a few rendezvous nodes in advance, minimizing the sink's moving path length and

data collection delay. The challenge of choosing rendezvous nodes over a particular routing backbone has been addressed in [20], [30], [94], [95]. The key philosophy of these works is to develop an energy-efficient data collection path avoiding multi-hop communication, to minimize end-to-end data collection latency, or to reduce computational complexity for determining mobile sink's path.

In the literature, rendezvous-node-based strategies have been developed for two varieties of networks: *obstacle-free* and *obstructed-networks*. In the former type, a mobile sink can travel to any rendezvous node along a straight-line direction without any interruption. On the contrary, an *obstructed-network* area may contain a building, tree, pond, lake, forest, mountain, etc., opposing free movement of the mobile sink along the straight-line direction between two rendezvous nodes. Rendezvous-based data collection strategies developed for both obstacle-free and obstructed sensor networks are presented in the following subsections.

2.4.3 Data collection in obstacle-free networks

In an *obstacle-free-network*, a set of rendezvous nodes (RNs) constructs a one-time stationary path for data collection based on residual energy of sensors to maximize network lifetime [29], [30], [94], [95], [96], [97]. In [29], weighted rendezvous planning (WRP) selects RNs, and avoid hotspot problems in sensor networks through adopting the shortest path tree and traveling salespersons for path construction. Though it works efficiently for a smaller network, it has higher computational complexity for larger networks. Meanwhile, the expected sojourn time to the corresponding RN is optimized to enhance network lifetime in different works [30], [94]. The sojourn time of a mobile sink in [94] is determined over each grid of a network. This work suffers from buffer overflow, increased data loss, and energy hole

problems while collecting data. To further improve the network lifetime, Basagni et al. [30] determine an optimal tour over rendezvous-nodes so as to maximize network lifetime. Sensor nodes, located within the transmission range of RNs, can send data directly to the mobile sink, while others send data through multihop communication to the mobile sink.

However, these works lack from applying in a non-grid network or an irregular node distribution in the network. Recently, In [95], Gharaei et al. proposed a collaborative approach (namely, CMS2TO) to balance the energy consumption of the cluster heads (CHs) in the network. Since it focuses on the lifetime of CHs, hotspot regions are created around the CHs. Wen et al. [96] proposed energy-aware path construction (EAPC) scheme by selecting RNs on the spanning tree and constructing a data collection path using a convex polygon algorithm. Since the path is not the shortest and the mobile sink traverses more network distance, the deadline for application is violated. In [97], the authors proposed an efficient path planning for reliable data gathering (EARTH) that determined RPs based on distance and hop-count. Like the CMS2TO, the nearby nodes to the RPs die quickly in the EARTH approach for large-scale wireless sensor networks (WSNs). To enhance the reliable data collection, trust-based energy-efficient data collection techniques have been proposed in [98], [99].

Since any practical network contains obstacles, these data collection strategies are likely to prejudice to maximize network lifetime or maintain delay-deadline requirements of real-time applications. Therefore, we focus on data collection strategies in obstructed sensor networks that are discussed elaborately in the following subsection.

2.4.4 Data collection in obstructed networks

Based on the aforementioned literature review, we observe that the works optimize network performances in terms of energy consumption, data delivery delay, network lifetime, data throughout, sojourn time [100], [101], etc. for obstacle-free networks. However, obstacles are an integrated part in a practical network environment, and aforementioned cluster-head and tree-based routing protocols become complicated to construct sink's tour. Moreover, a few work addresses data collection schedule in an obstructed network [43], [44], [45], [46], [102], to maximize network lifetime or to minimize latency.

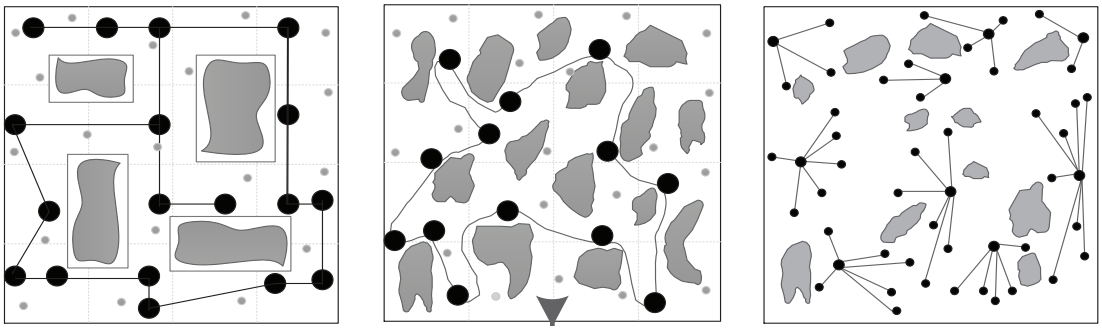

(a) Spanning-graph [42] (b) VPS [43] (c) LAS [44]

Figure 2.4: Data collection strategies in obstructed network

In this consequence, to overcome the complexity of the data collection schedule within a network containing obstacles, Xie and Pan introduced spanning graph-based data collection schedule [42] of a mobile sink. In this work, they developed a heuristic path planning algorithm to skirt obstacles, as shown in Fig. 2.4(a). In [43], the authors developed the shortest viable path scheduling (VPS) for a mobile sink based on a road-map, as shown in Fig. 2.4(b), which aimed to construct a tree-like graph (or similar to a convex-hull) using dynamic

programming for a unicycle robot or mobile sink. Though this approach reduces data collection time significantly, it suffers from a higher data traffic load. Besides, it is inappropriate for larger networks since its computational complexity is $\mathcal{O}(\mathbb{N}^3)$, where $\mathbb{N}$ is the number of all sensor nodes. In another work, Redhu and Hegde proposed the landmark-assisted scheduling (LAS) [44] for a mobile sink, as shown in Fig. 2.4(c). The key philosophy of the work is to identify the optimal clusters and associated landmark nodes to minimize energy consumption. Since this approach uses random walks over a network, and then it performs matrix multiplication operations over its Markov model, its computational complexity is also $\mathcal{O}(\mathbb{N}^3)$, similar to VPS.

Recently, rendezvous node selection and data collection approaches have been developed for obstructed networks using artificial intelligence [45], fuzzy logic [46], and machine learning algorithms. In [45], Ghabel et al. proposed a DGOB algorithm for data collection over an obstructed network. The DGOB executed into two phases, cluster- and tour- constructions. This approach exploited hierarchical agglomerative clustering, ant colony optimization, and genetic algorithms to construct clusters in the presence of obstacles. In [46], Verma et al. developed fuzzy-logic based effective clustering (FLEC) that used three-tier communication-based approaches: nodes to cluster heads (CHs), CHs to supercluster heads (SCH), and then SCH to mobile sink. Both works [45], [46] exhibit higher computational complexity to select efficient rendezvous nodes in a large scale network.

Moreover, most of above works for obstructed-networks exhibit higher end-to-end data collection latency using a mobile sink due to scheduling periodically over

a large circular-path [43] or cluster heads [44], [45], [46] to collect data. These works also violate the delay-deadline of real-time and multimedia applications and minimize network lifetime significantly. Therefore, it necessitates developing an efficient data collection scheduling of a mobile sink in an obstructed sensor network to satisfy real-time delay deadline requirements. Furthermore, few works in the literature considered sojourn duration and heterogeneous data rate at different nodes. Consequently, strategies for optimal rendezvous nodes and sojourn duration at individual nodes have been left unexplored for obstructed networks.

Motivated by the above challenges of real-time data collection, in this thesis, we aim to develop an efficient data collection schedule of a mobile sink determining an optimal set of rendezvous nodes in an obstructed network together with sojourn duration at each rendezvous node so as to maximize the lifetime of sensor networks.

2.5 Maximizing Lifetime of Sensor Networks

Lifetime generally refers to the time when the first node in the network dies. However, network lifetime is suitably defined in the context of different applications that can be based on the number (or percentage) of alive nodes, network connectivity or coverage status, etc. [33], [34]. Depending on application requirements, lifetime may be defined as the time until the network no longer provides an acceptable event detection ratio. However, this definition becomes irrelevant when connectivity is not guaranteed toward the mobile sink. Therefore, it must consider connectivity and coverage while aiming to maximize network lifetime along with high-speed routing backbone in the network.

The problem of maximizing the lifetime of sensor networks has been well studied in the literature [92], [103]. The primitive strategies follow optimal coverage

and connectivity [104], opportunistic transmission schemes, dynamic beam-forming [105], [106], etc. Further improvement of network lifetime is achieved through greedy energy-efficient routing, clustering techniques, and machine learning approaches [107]. Though the strategies can achieve an extended network lifetime, they lack to maintain delay deadline for real-time applications. A set of recent studies has been found to further minimize energy consumption by designing an efficient traveling path of a mobile sink while collecting sensed data from different regions in the network [59], [108]. These are achieved through predictable path planning or dynamic cluster-based data collection strategies [109].

In sensor networks, the problem of maximizing lifetime is still challenging mainly due to the stringent QoS requirements of real-time applications, heterogeneity of sensor devices, distinct application characteristics, etc. The problem is further complicated when the network contains many obstacles. In maximizing network lifetime, existing literature either addresses issues of application delay-deadline or the presence of obstacles. Therefore, it necessitates formulating a mobile sink's optimal data collection schedule in an obstructed network that ensures balanced energy consumption among the nodes to maximize network lifetime.

2.6 QoS Requirements in Real-time Data Collection

Mobile-sink-based data collection in a sensor network is challenging for real-time applications. The image, audio, and video data collection capabilities of sensors enable broader and enhanced surveillance applications. Therefore, it necessitates maintaining minimum QoS requirements while designing real-time multimedia data

collection with a mobile sink. The QoS issues are data delivery throughput, end-to-end delivery delay, packet delivery rate, network lifetime, operational overheads, etc.

Data throughput refers to the amount of data successfully received by the mobile sink per unit time. This QoS metric is highly dependent on packet delivery rate. The higher values of throughput and PDR are expected during real-time data collection in sensor networks. On the other hand, average end-to-end (e2e) packet delivery delay is the key QoS performance metric that determines whether the protocol is feasible for real-time data collection or not. A lower value of e2e delay is expected. Operational overhead is another QoS metric that reflects the control packets required for successful packet transmission.

The predicted network lifetime is the primary consideration when installing the routing protocol in sensor networks because a limited battery powers sensor nodes. The time interval between the deployment of a network and the moment at which the first node has spent its energy to transmit data packets in the network is referred to as network lifespan. The standard deviation of residual energy while the network is dead can assess how efficient the routing protocol is in lifespan management. This is supposed to be a significant metric that indicates the network's overall energy consumption. The performance of state-of-the-art works will be assessed in order to determine the most efficient routing protocol in terms of these QoS measures.

Table 2.2: Comparative characteristics of mobile sink based protocols

Protocols	**Backbone**	**Environment**	**Delay**	**Lifetime**	**Overhead**	**Data generation**
Hilbert [18]	Grid	Obstacle-free	×	✓	✓	Homogeneous
Moore [19]	Grid	Obstacle-free	×	✓	✓	Homogeneous
Railroad [37]	Rectangular	Obstacle-free	×	✓	×	Homogeneous
LBDD [38]	Vertical	Obstacle-free	✓	×	×	Homogeneous
HexDD [39]	Hexagonal	Obstacle-free	✓	✓	×	Heterogeneous
Ring [40]	Circular	Obstacle-free	×	✓	✓	Homogeneous
Fishbone [41]	Tree	Obstacle-free	×	✓	×	Heterogeneous
VPS [43]	Tree	Obstructed	✓	✓	×	Heterogeneous
LAS [44]	Cluster	Obstructed	✓	✓	×	Heterogeneous
Z-curve [89]	Grid	Obstructed	×	×	✓	Heterogeneous
Starfish [110], [111]	Starfish	Obstacle-free, and Obstructed	✓	✓	✓	Heterogeneous

2.7 Comparative Characteristics of the State-of-the-art Works

The key characteristics of mobile-sink baed state-of-the-art works are summarized in Table 2.2. Most of the works focus on developing various virtual backbone structures, e.g., rectangular, vertical, hexagonal, circular, tree, clusters, etc., to forward data to the mobile sink in the networks. We also observe that the most of the protocols are developed for obstacle-free network environments, and very few are developed to adopt with practical obstructed network environment. The key performance metrics, e.g., delay, overhead, lifetime, etc. that are summarized in Table 2.2 that the protocols concentrate to optimize in the state-of-the-art works.

In a practical network scenario, the data generation rate varies depending on the applications. We observe that the most of the protocols consider homogeneous data generation rate that are not practical for different types of IoT and sensor based applications. Therefore, in this thesis, we consider both obstacle-free and obstructed network with heterogeneous rates of data generation in the network.

2.8 Limitations of the Existing Studies

In the state-of-the-art works, the railroad routing [37] acquires data from the source and transmits it to the sink through the unicast path. Therefore, this protocol suffers from higher latency due to traveling longer paths using unicast queries and data loss for node failure. On the other hand, due to the vertical region in [38], the protocol suffers from higher latency for boundary nodes in a large network with a single central zone. Besides, regular broadcasting in the central zone decreases the

network lifetime and data throughput significantly due to high network collisions. Moreover, HexDD protocol [39] suffers from the hot-spot problem, especially in the central zone, because all data and queries are transmitted through the central node. Besides, the fixed six rendezvous regions cause imbalanced energy consumption on a few rendezvous nodes in the network irrespective of network size. The backbone is effective not only for faster localization of the sink but also to provide energy-efficient data delivery to the sink.

In Ring routing [40], progressive flooding toward the ring-backbone significantly undermines the network lifetime and throughput due to high network collisions. Furthermore, it has not explored appropriate ring radius with respect to network size or communication range of sensors. Experimental results show that if the ring radius is too small, the sink localization time is greatly increased for network border nodes. The same problem occurs for central nodes when a large ring radius is chosen.

In direct-contact based data collection strategies [18], [19], [89], since a mobile sink periodically travels to all source sensor nodes, they exhibit high lifetime among the studies works. However, they suffer from exaggerated traveling path distances that exhibit higher delays during data collection. On the other hand, in an obstructed network, the overhear is high due to finding an efficient routing path or sink's traveling path in the network. Finally, few works consider heterogeneous data generation rates while developing a data collection framework with a mobile sink.

Therefore, in this thesis, we develop a high-speed routing backbone aiming to ensure faster data collection and to maximize network lifetime for a delay-constrained application, and then formulate a mixed-integer linear programming (MILP) prob-

lem to find an optimal travel plan of a mobile sink for data collection by visiting a set of rendezvous nodes along with corresponding sojourn durations.

2.9 Summary

This chapter provides a detailed discussion on existing strategies for real-time data collection using a mobile sink, and after that, network lifetime maximization techniques in obstacle-free and obstructed networks have been explored. In the following chapters, we develop a novel data routing backbone and an efficient data collection strategy for real-time applications to maximize network lifetime that can diminish the challenges of state-of-the-art works.

Chapter 3
Starfish Routing Backbone

In this chapter, we introduce Starfish routing (SFR) backbone in a sensor network, motivating from the water vascular system of a sea Starfish. We also describe the detail construction procedure of the Starfish routing backbone to ensure balanced energy consumption throughout the network so that network lifetime is maximized.

3.1 Introduction

In recent years, the rapid advancement in sensor networks has enabled smart environments to provide ubiquitous real-time applications in various fields such as industry, smart city, transport, health, and the Internet of Things (IoT). The extraordinary computing and communication features of sensors are continuously helping to expand sensor networks from small scale applications [7] to large scale infrastructure, emergency medical response, military surveillance, agricultural monitoring [8], and sensor-data cloud applications [17], [112], [113]. To gather sensed data into the applications, mobile sink-based routing strategies outperform static sink-based techniques in terms of data delivery performances and network lifetime. It has been proven that sink mobility ensures better network connectivity under sparse and disconnected sensor networks. However, the sink mobility invites the

problem of locating the destination sink in real-time and to establish a source-sink routing path.

Typically, flooding and broadcasting data forwarding techniques are followed to establish a routing path from a source node to the mobile sink, which is an inherently energy-hungry strategy. Consequently, forming a routing backbone over a sensor network proactively facilitates timely and energy-efficient data collection from source nodes to the mobile sink. In the literature, a routing backbone is formed in the network either to acquire the updated position of the mobile sink or to forward data to the sink in multi-hop fashion [40], [41]. However, these protocols are criticized for their lack in reduced network lifetime, higher data delivery delays, and scalability. Therefore, it necessitates to develop an efficient routing backbone in the network that reduces not only the end-to-end data delivery delay but also extends the network lifetime to a great extent. For this reason, we introduce a data routing backbone for a sensor network, namely *Starfish routing backbone (SFR)*, that offers uniform energy consumption throughout the network to extend network lifetime as well as to reduce end-to-end packet delivery delay for a real-time application.

In this chapter, we develop a Starfish routing (SFR) backbone motivating from the water vascular system of a *Starfish* [47]. The key philosophy of designing the proposed SFR backbone is to spread the backbone nodes over the different regions of the network in such a way that a source node can access at least one of the backbone nodes directly. This strategy inherently gets advantages of uniform energy consumption as well as on data collection, instead of over a few numbers of localized backbone nodes, as developed in the state-of-the-art-works. Following the water vascular system of a Starfish, in the proposed *SFR*-architecture, the back-

bone nodes are selected in such a manner that they are distributed throughout the network to ensure single-hop accessibility from any source node in the network. The backbone nodes are placed on a central *ring-canal* that helps to alleviate the hotspot problems around the network center, and on the *radial-canals* that facilitate faster data delivery towards the mobile sink from any corner of the network. We elaborately discuss the construction of the Starfish routing (SFR) backbone, theoretical analysis, and performance analysis through exhaustive simulation studies.

The key contributions of the proposed *Starfish routing (SFR) backbone*, to be discussed in this chapter, are summarized as follows:

- We construct a *Starfish*-like routing backbone to spread the backbone nodes over the different regions of the network in such a manner so that any source node can directly access at least one of the backbone nodes. It inherently offers uniform energy consumption throughout the network, resulting in extending network lifetime and reducing end-to-end packet delivery delay for a real-time application.

- The construction of *ring-* and *radial-canals* of the proposed *Starfish routing (SFR) backbone* framework is mathematically modeled, and thus, it is extendable for rectangular-, square-, and circular-shaped networks.

- A statistical analysis for expected end-to-end packet delivery delay in *SFR* backbone has been carried out considering both hop distance to the sink and number of retransmission attempts.

- The performances of the proposed *SFR-backbone* have been carried out in Network Simulator (e.g., NS-2) [48] and significant performance improve-

ments are observed for both event-driven and periodic data reporting applications.

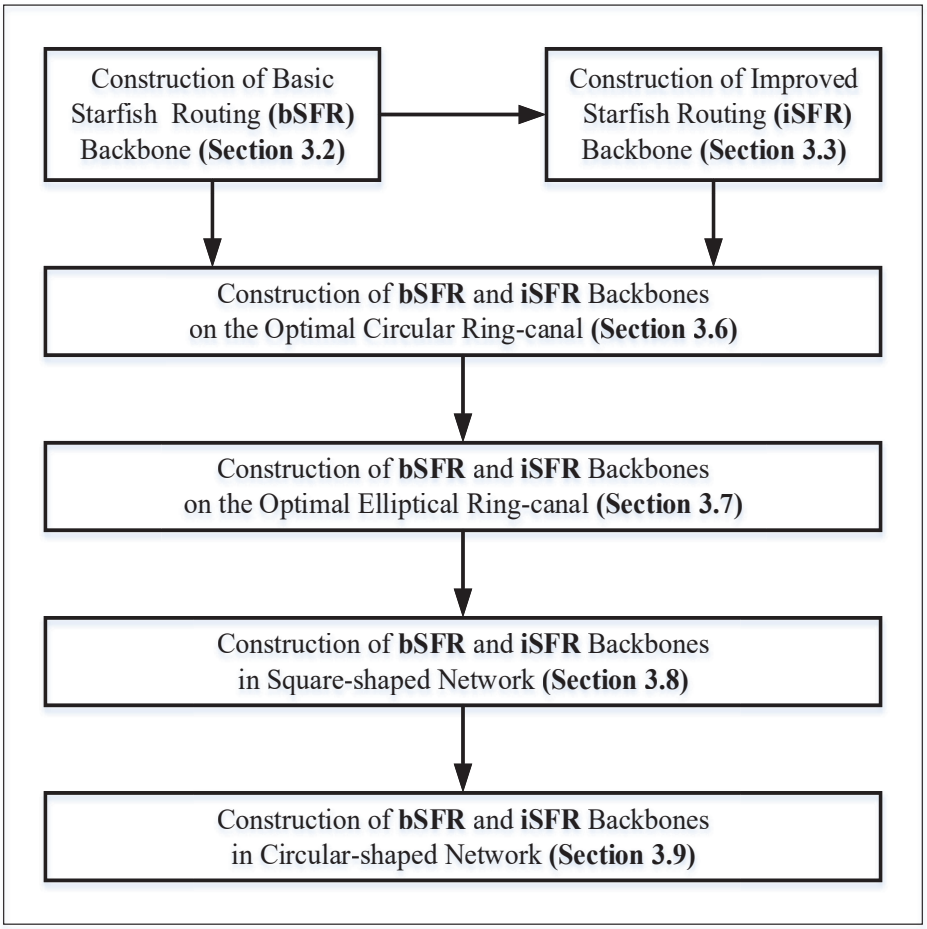

Figure 3.1: Construction of Starfish routing backbones and its variants

Fig. 3.1 presents the construction phases of Starfish routing backbones along with its variants that are organized in the rest of the chapter. In Section 3.2, we describe the construction and operational details of the proposed basic Starfish routing (bSFR) backbone architecture, motivating from the water vascular system

of a sea Starfish. Then we develop an improved version of the Starfish routing (iSFR) backbone in Section 3.3. We provide a theoretical prove to validate single-hop accessibility of SFR backbone architectures (e.g., bSFR and iSFR) from any sensor in Section 3.4. Next, in Section 3.5, it is discussed the techniques to update the mobile sink's location and data routing over the Starfish routing backbone. To improve the network and lifetime performances, we determine an optimal circular ring-canal and elliptical ring-canal for SFR backbone in Section 3.6, and Section 3.7, respectively. To ensure the scalability, the SFR**s**, and SFR**c** backbone architectures are constructed in square-shaped, and circular-shaped network in Section 3.8, and Section 3.9, respectively. After that Section 3.10 provides the comparative discussions on various SFR backbone architectures. An analytical model using the Markov chain is developed to investigate the average end-to-end packet delivery delay in Section 3.11, and the Section 3.12 discusses on the performance evaluation results. Finally, we conclude the Chapter in Section 3.13.

3.2 Construction of Basic Starfish Routing (bSFR) Routing Backbone

In this section, the construction and operational details of *basic Starfish routing backbone* are presented, followed by the assumed network model. Since its construction is motivated from a sea Starfish, therefore, at first, we provide a brief introduction to the water vascular system of a starfish.

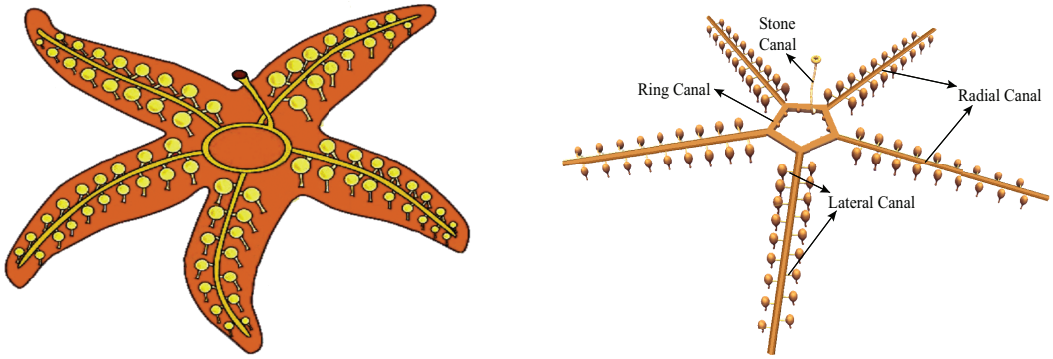

(a) A sea Starfish (b) Water vascular system of a Starfish

Figure 3.2: Sea Starfish and its water vascular system

3.2.1 Water vascular system of a Starfish

The water vascular system of a sea Starfish [47] is a hydraulic system that is made up of a network of fluid-filled canals, as shown in Fig. 3.2(a). Starfishes have a very unusual circulatory system over a complex water vascular system to keep things moving. To circulate water in different parts of its body, there are different types of canals, for example, ring-canal, radial-canals, lateral-canals, stone-canals, etc., as indicated in Fig. 3.2(b).

The ring-canal is a wide pentagonal ring-like vessel lying around the mouth-opening in the middle of its body. From the outer surface of the ring-canal, it gives off five radial canals, one entering each arm. The set of radial-canals run-up to the tip of Starfish's arm. In each arm, the radial-canal gives out two series of short, narrow, transverse branches that are called lateral-canals. In brief, the Starfish's water vascular system provides pressure to move water into the ring-canal, then into the radial-canals, and finally to the lateral-canals. These canals are like a network of water pipes.

Since bio-inspired systems have been attracted to develop and optimize the data routing path or mobile sink's trajectory in a network, the water vascular system of a Starfish motivates us to develop Starfish routing backbone. In Starfish, the central ring-canal and the radial-canals, as shown in Fig. 3.2(b), jointly take responsibility to transport water throughout its body. Therefore, we develop a Starfish routing backbone in a sensor network containing a central ring-canal and few radial-canals. Any source node can access and transmit data over the backbone nodes on the different canals within 1-hop distance. The following sections explain the construction details of the proposed Starfish routing backbone followed by the assumed network model.

3.2.2 Network model

We assume a wireless sensor network where homogeneous sensor nodes are randomly distributed in a rectangular network size of $\mathbf{2a} \times \mathbf{2b}$, as shown in Fig. 3.3, where $\mathbf{a}$ and $\mathbf{b}$ ($\mathbf{a} \geq \mathbf{b}$) are the half of the length and width of the rectangle, respectively, and (u, v) is the center of the network. Each sensor node i has an initial energy E_0 and has the same transmission range r. We also assume that each sensor node knows its own coordinate point (x_i, y_i) using GPS or any localization method.

All sensor nodes are considered as stationary after deployment, while the sink is mobile. Since the key objective of this work is to construct a routing backbone along with a mobile sink, in this Chapter 3, we consider the mobile sink moves randomly in the network and collects data from backbone nodes. However, in Chapter 4, we develop an efficient data collection schedule of the mobile sink over the routing backbone, rather than random way-point, so that overall network QoS performance and lifetime performance can be improved.

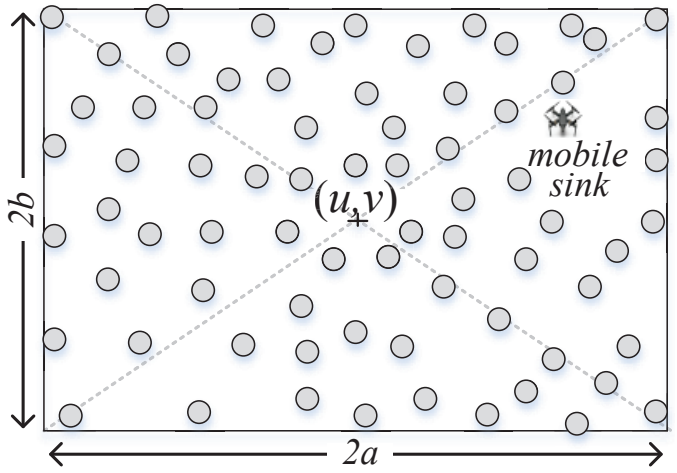

Figure 3.3: An obstacle-free sensor network model with a mobile sink

While a source node sense data, it immediately forward to any nearest backbone node. Then sensed data packets are forwarded to the mobile sink over the backbone nodes in multihop fashion. While forwarding data to the mobile sink, it follows selective greedy forwarding algorithm over the routing backbone nodes [81].

The proposed *Starfish routing backbone* consists of a central *ring-canal* and a number of *radial-canals* prolonged across the network. The nodes on the routing backbone are divided into three categories: a set of *anchor nodes* at the network edge, $Z_a = \{a_1, a_2, \ldots, a_{16}\}$; a set of *radial-canal nodes*, $Z_b = \{b_1, b_2, b_3, \ldots\}$; a set of nodes on the *ring-canal*, $Z_c = \{c_1, c_2, \ldots, c_6\}$; $Z = \{Z_a \cup Z_b \cup Z_c\}$ represents the set of all nodes, and a set of distinguished *radial-canals*, Z_d on the *Starfish routing (SFR) backbone architecture*.

In *Starfish routing backbone*, the *ring-canal* is constructed based on the transmission range r of the sensor nodes and several *radial-canals* are formed depending on both network size and transmission range r. During construction of *Starfish routing backbone*, the backbone nodes are selected based on the node's initial en-

ergy E_0, residual energy E_{res}, and energy threshold E_{th} for successful transmission of the nodes. The main responsibility of backbone nodes on the *ring-canal* and *radial-canals* is to collect data from the source sensor devices within 1-hop and forward those toward the *mobile sink node*.

The detail construction procedure of the Starfish routing backbones (e.g., bSFR and iSFR) is presented in the flowchart in Fig. 3.4, and explained in the following subsections. All the backbone nodes on the ring-canal, radial-canal, and anchor nodes are connected to form the Starfish routing backbone in the network. In the case of early death of a backbone node due to disconnection, energy depletion or obstructed condition, a node may change its role between backbone node and ordinary node in the network. In such case, a local repair policy is adopted from Ring routing protocol [40]. The notations used in this chapter are summarized in Table 3.1.

In order to achieve high-speed data routing in a sensor network, Starfish routing (SFR) backbone is proposed. If the network is large with respect to sensor's transmission range and has a number of nodes, the construction of the central ring-canal is initialized by the mobile sink or central controller. Thereafter, radial-canals of the proposed Starfish routing backbone are developed in the network based on its variants. The construction methodologies of basic Starfish routing (bSFR) and improved Starfish routing (iSFR) backbones are presented in Fig. 3.4 through a flowchart.

After the construction phase, the network steps into the data collection through the mobile sink that is carried out in rounds. In each round, the mobile sink halts

Table 3.1: List of notations for SFR backbone architecture

Symbols	Description
$2a \times 2b$	Area of the network
r	Transmission range of a sensor node
Z	Set of all backbone sensor nodes
Z_a	Set of anchor nodes on network edge
Z_b	Set of radial-canal nodes
Z_c	Set of ring-canal nodes
Z_d	Set of radial-canals on SFR backbone
R	Radius of the ring-canal
ϕ	Control variable for ring-canal radius
θ_1, θ_2	Incident angles of radial-canals on principal-axes
E_0	Initial energy of a sensor node
E_{res}	Residual energy of a sensor node
E_{th}	Energy threshold for backbone nodes

on few sojourn locations based on data availability and few constraints that are explained elaborately in Chapter 4.

3.2.3 Construction of ring-canal

A central *ring-canal* is a closed loop of nodes circularly located around the center of the wireless sensor network, as shown in Fig. 3.5. The primary objective of *ring-canal* is to alleviate the hot-spot problem, especially in the network center, due to the convergence of backbone nodes at the center. If the *ring-canal* size becomes

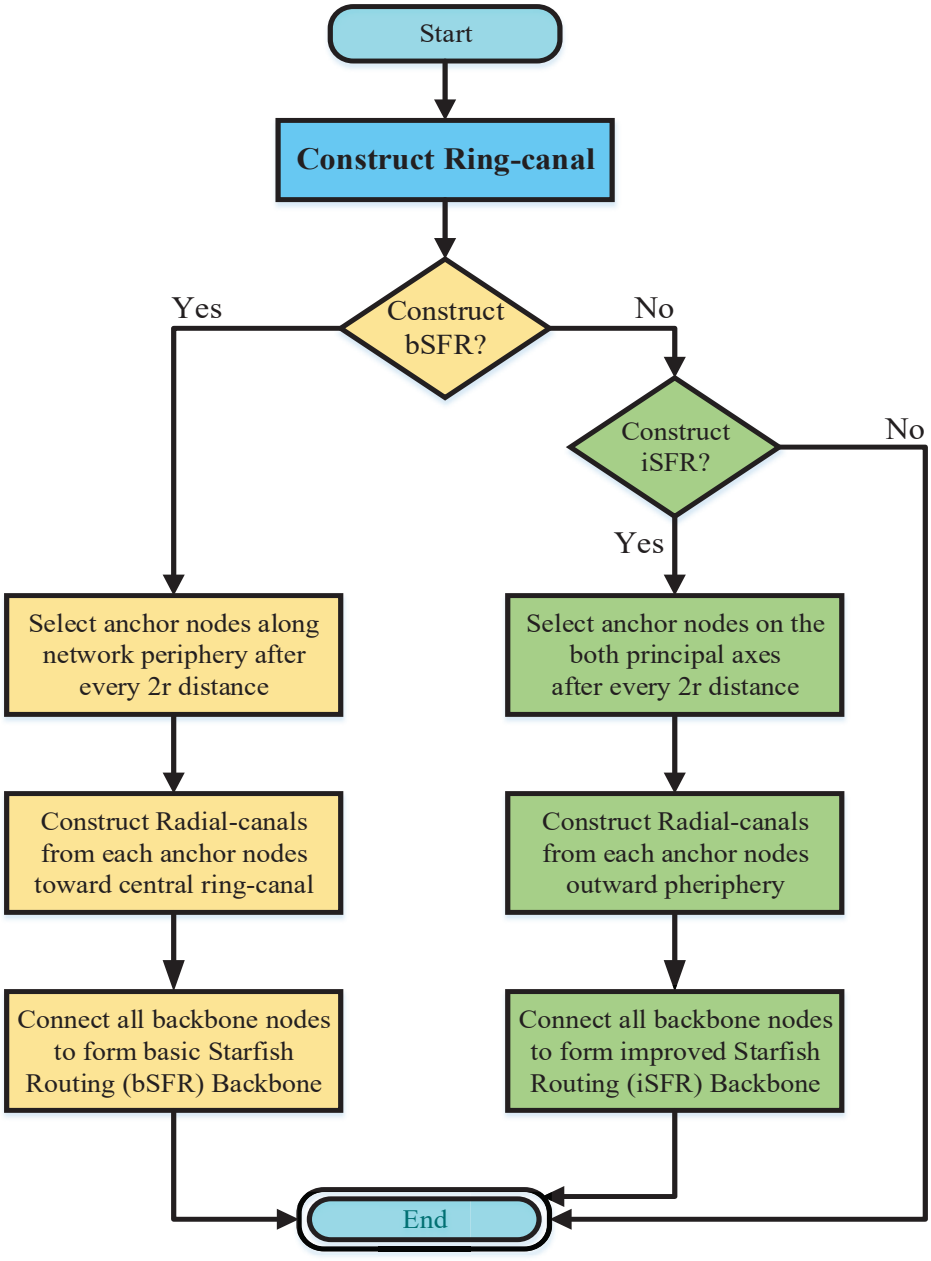

Figure 3.4: Construction methodologies of bSFR and iSFR backbones

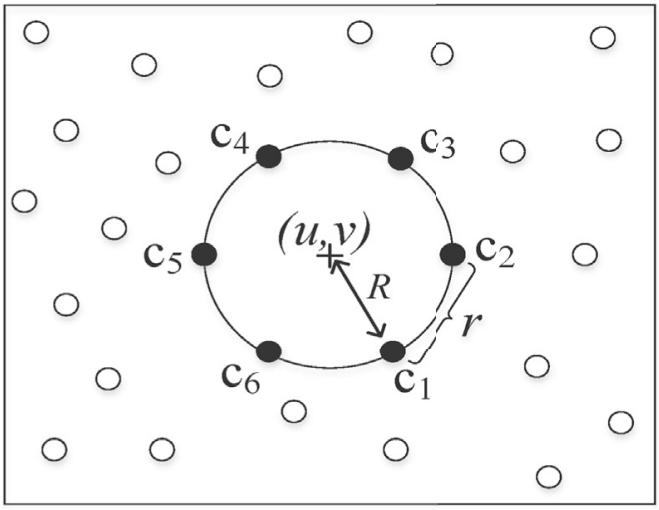

Figure 3.5: Construction of the central ring-canal

extraordinarily large with respect to the network size, the source nodes inside the *ring-canal* cannot access its backbone node directly. Meanwhile, if the *ring-canal* size is very small with respect to transmission range, it increases more interference and collision during transmissions from many nodes near to network center. This happens due to existence and convergence of more *radial-canals* onto the *ring-canal* of the *Starfish routing backbone*. We define the radius of a *ring-canal* as follows,

$$R = \phi \times r, \tag{3.1}$$

where, $0 < \phi \leq b$, is a control variable that determines the amount of expansion of the radius of *ring-canal* from the transmission range of a sensor. The control variable ϕ acts as an expansion factor that defines the ring-canal size with respect to the sensors' transmission range. The center of the *ring-canal* is fixed at the network center, *(u,v)*, and thus a set of nodes, $Z_c = \{c_1, c_2, \ldots, c_6\}$, located at any (x, y) position (or at very nearby) encapsulate the network center, as shown in

Fig. 3.5, to preserve its circular property as follows,

$$(x-u)^2 + (y-v)^2 = R^2. \tag{3.2}$$

Now, in order to construct the *ring-canal* of the proposed *Starfish routing backbone*, at first, the central controller determines the network center *(u,v)*, *ring-canal* radius R using Eq. (3.1) and sketch a reference circle using Eq. (3.2). The controller then picks a sensor node randomly on or somewhat inside reference-circle as the starting node (i.e., c_1) of the *ring-canal*, as shown in Fig. 3.5. Later, the next nodes are selected (i.e., c_2 to c_6) every after the distance equal to transmission range r (or somewhat less than r) lying on or inside the reference-circle maintaining the property stated in Eq. (3.2) and minimum energy threshold (E_{th}), i.e., $E_{res} \geq E_{th}$, where, E_{res} is the residual energy of a sensor node. Initially, (E_{th}) is determined in such a way that the backbone nodes are connected for few rounds during data collection by the mobile sink. Therefore, it is measured based on the total energy requirements for few rounds that is discussed in Section 4.4.

This selection process of *ring-canal* backbone nodes continues until the starting node of the *ring-canal* is reached. These backbone nodes on the *ring-canal* in Z_c (i.e., c_1 to c_6), form a complete loop of connected nodes, as shown in Fig. 3.5. The shape of the *ring-canal* need not to be a proper circle but it must be a connected closed loop of nodes.

3.2.3.1 Motivation to determine the optimal size of ring-canal

We have studied the behavior of the control variable, ϕ, to investigate its impact on network performances. As an initial study, we have investigated the impact of varying size of the *ring-canal* on average data throughput and end-to-end data delivery delay in the network, and have published the results in our earlier works

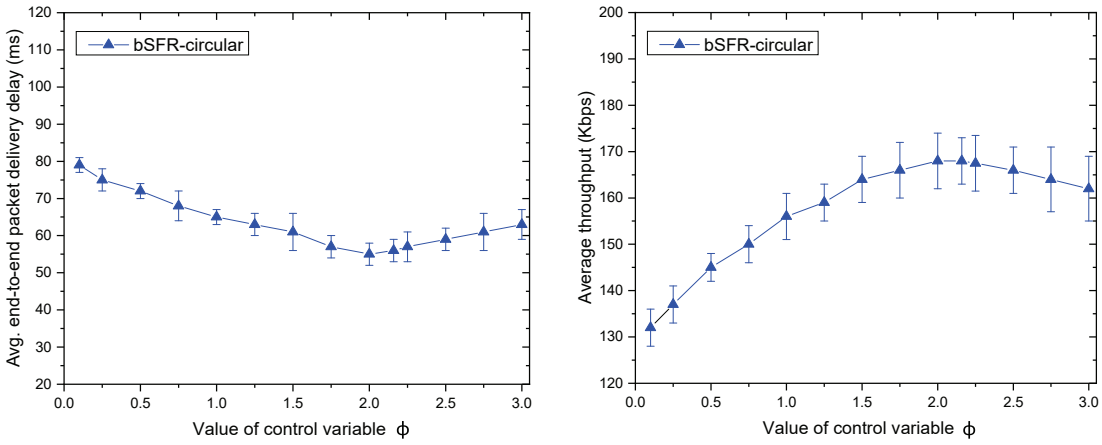

(a) End-to-end delay

(b) Throughput

Figure 3.6: Impacts of varying values of ring-canal control variable, ϕ

[110], [114]. In the experiment, we have varied the value of control variable, ϕ, between 0.1 to 3.0 and have shown experimental results in Fig. 3.6. Interestingly, we observe that the end-to-end data delivery delay decreases as the control value, ϕ, increases, as shown in Fig. 3.6(a). Later, it starts increasing delay for larger value of ϕ (i.e., larger size of the ring-canal).

On the other hand, data throughput initially increases for the incremental values of ϕ, as shown in Fig. 3.6(b). Later, data throughput decreases for larger value of ϕ (or larger size of the ring-canal). The detail of these simulation results are explained in performance evaluation Section 3.12.

These results are so interesting that insist further investigation on optimal values of ϕ that is an important concern for the suitable values of ϕ for various sizes of network. Therefore, we are motivated to determine the optimal size of the ring-canal (in terms of ϕ) in sensor networks. The detail theoretical study to determine the optimal value of ϕ is described in Section 3.6 through Section 3.9; and later

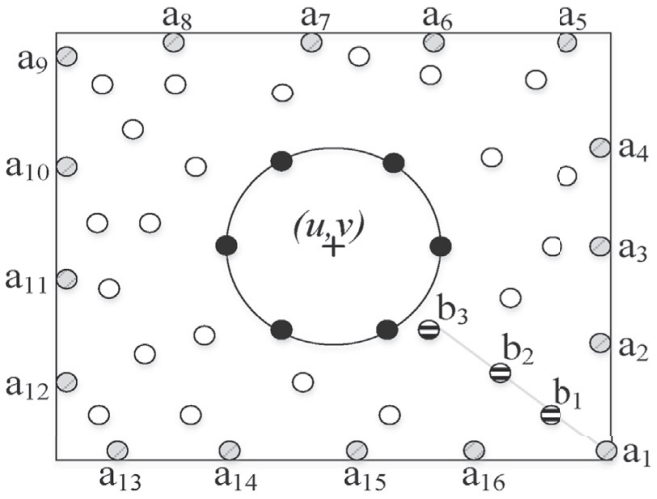

Figure 3.7: Construction of the radial-canals from anchor nodes

the exhausted simulation results are explained in Section 3.12.

3.2.4 Construction of radial-canals

In *Starfish routing backbone*, the *radial-canals* are prolonged toward the edge of the network from the *ring-canal*. The primary objective of constructing *radial-canals* is to spread the backbone nodes across the network so that the source nodes from all areas of the network can access at least one of the backbone nodes on *radial-canals*. If the backbone nodes are located far away from a particular source node, it takes higher time to localize the mobile sink, and the packets have to travel more hops to reach the sink. In such a case, the probabilities of packet loss, collision, and transmission overheads also increase significantly.

To construct the *radial-canals*, at first, a set of *anchor nodes*, $Z_a = \{a_1, a_2, \ldots, a_{16}\}$, is selected starting from the right-bottom half of the main diagonal keeping $2r$ (or somewhat less) distance interval along the periphery of the

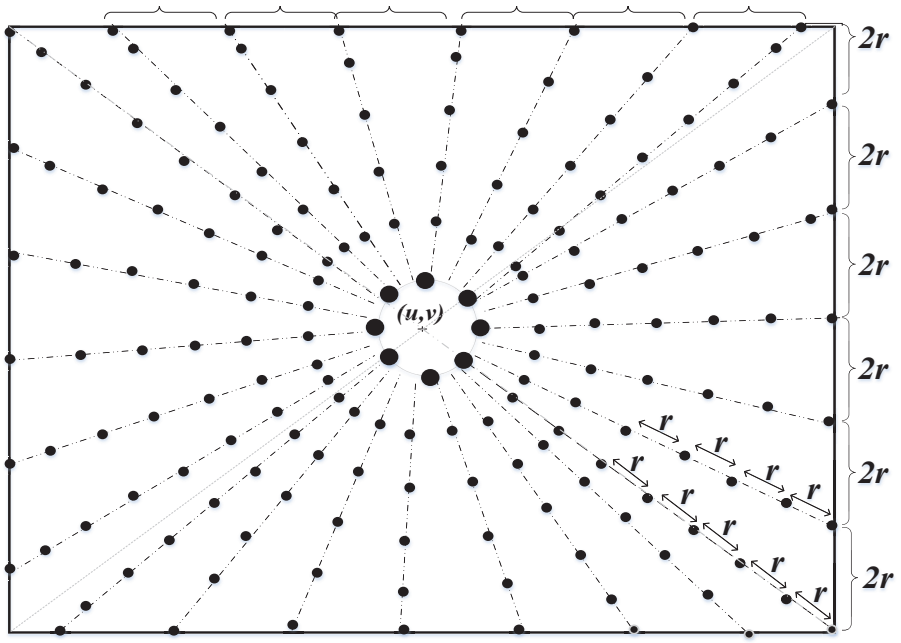

Figure 3.8: Construction of the basic Starfish routing (bSFR) backbone

network, as shown in Fig. 3.7. When the length of an edge is not exactly multiple of $2r$, we measure the total distance along the perimeter equal to $2r$ for selecting the next anchor node. Then, we draw reference lines from each of the *anchor nodes* j, located at (x_j, y_j), to the center of the network, as follows,

$$y = \frac{y_j - v}{x_j - u}\, x, \quad 1 \leq j \leq |Z_a|. \tag{3.3}$$

Now, for each of the reference lines, we construct a *radial-canal* backbone by choosing nodes (i.e., $b_1, b_2, \dots$) after every r (or somewhat less) distance, as shown in Fig. 3.8. The central controller selects the backbone nodes on a *radial-canal* maintaining the property stated in Eq. (3.3) and minimum energy threshold (E_{th}), i.e., $E_{res} \geq E_{th}$. The selection process of backbone nodes, Z_b (i.e., $b_1, b_2, b_3, \dots$), on

radial-canals starts from an *anchor node* and continues until one of the *ring-canal* nodes, Z_c (i.e., c_1 to c_6), is reached, as shown in Fig. 3.7. Thus, the *ring-canal, anchor* and *radial-canal* nodes altogether form a connected *basic Starfish routing (bSFR) backbone* for the network, as shown in Fig. 3.8. All source sensor nodes send their sensed data toward the sink node using this backbone. Furthermore, this development facilitates 1-hop availability of at least one backbone node from any source node within the network. What follows next, we investigate the construction of an improved *Starfish routing backbone* that can further enhance the network lifetime and decrease the end-to-end packet delivery delay.

3.3 Construction of Improved Starfish Routing (iSFR) Backbone

The main philosophy of the improved backbone structure is to avoid the convergence of all *radial-canals* onto the central *ring canal*.

3.3.1 Construction of ring-canal for iSFR

Since the key philosophy of iSFR backbone is based on different architecture of the radial-canal, the construction procedure of the *ring-canal* for the iSFR backbone remains the same as it is described in Section 3.2.3.

3.3.2 Construction of radial-canals for iSFR

Radial-canals in the iSFR backbone are parallel to the principal diagonals of the network. To construct the *radial-canals* of the *improved Starfish (iSFR) routing*

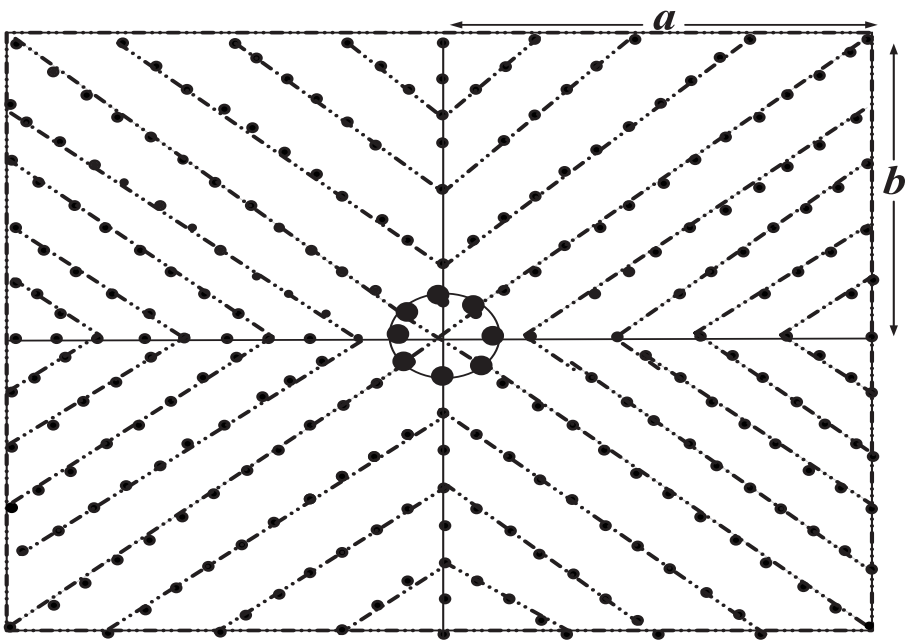

Figure 3.9: Construction of the improved Starfish routing (iSFR) backbone

backbone, at first, we draw the principal-axes and the principal-diagonals of the network passing through the network center. Now, for each of the reference axes and diagonals, we construct a *radial-canal* by choosing nodes every after r (or somewhat less) distance from network edge up to one of the nodes on the central *ring-canal*.

Now, for the first *anchor* node on the principal-axes just outside the *ring-canal*, we construct *radial-canals* parallel to both the principal-diagonals toward the edge of the network, as shown in Fig. 3.9. Similarly, for the next *anchor* node located on the principal-axes at approximately $2r$ distance from the previous one, we construct the remaining *radial-canals*. This procedure repeats for all other principal axes to form the complete *improved Starfish routing (iSFR) backbone* in the network.

3.4 SFR Backbones on the Single-hop Accessibility

The key philosophy of designing the proposed Starfish routing (SFR) backbone architectures is to spread the backbone nodes over the different regions of the network in such a way that a source node can access at least one of the backbone nodes directly. Following Starfish's water vascular system, the backbone nodes are placed on a central *ring-canal* that resolves the hotspot issue in the vicinity of the network center, and on the *radial-canals* that facilitate faster data delivery towards the mobile sink from any corner of the network. The existence of a central ring-canal along with a number of radial-canals jointly helps to distribute data routing loads to many nodes instead of over a few designated nodes in the network. Therefore, we provide the following *Lemma 1* to prove that a source node can access at least one of the backbone nodes on SFR backbones directly.

Lemma 1. *The Starfish routing backbone guarantees that every source sensor node in the network gets single-hop access to at least one node on the backbone, given that the principal diagonals of the network producing vertical angle not greater than* 120° *at network center.*

Proof. Following the principle of constructing *Starfish routing backbone* described in Section 3.2.3 and 3.2.4, all nodes in the network get guaranteed single-hop access to at least one of the backbone nodes since the farthest distance between two *anchor-nodes* at the network edge is kept equal to $2r$, and thus it is trivially true. In the case of improved Starfish routing backbone, the Lamma 1 is proved with an example of a worst case, as shown in Fig. 3.10(b).

In the case of *improved Starfish routing backbone*, the *radial-canals* stem out

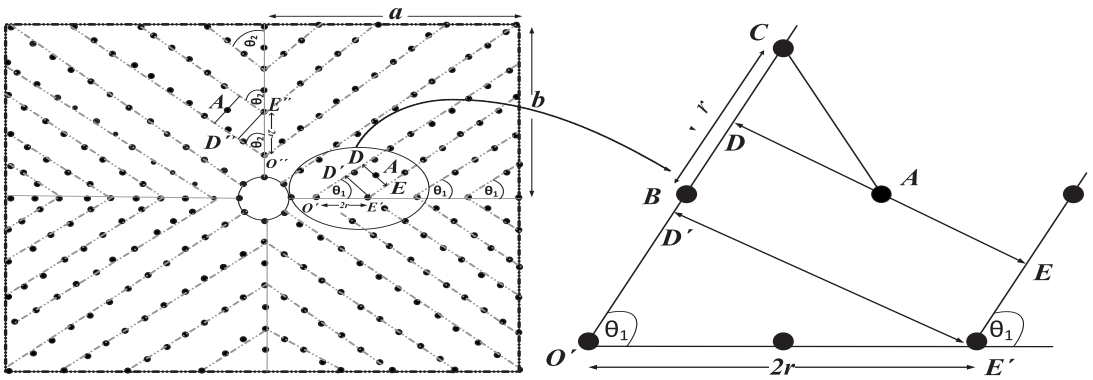

(a) Improved Starfish routing (iSFR) backbone (b) A worst case scenario on the iSFR

Figure 3.10: Improved Starfish routing backbone and a worst case

from the backbone nodes on the principal-axes located every after $2r$ intervals. The distance between two consecutive parallel *radial-canals* depends on their angles incident on the principal-axes. We prove here that if the principal-diagonals of a network don't produce vertical angles greater than 120° at the network center, then all nodes will have access to at least one backbone node irrespective of their positions.

Suppose a source A is located on a bisection-perpendicular line drawn from the middle point of two consecutive backbone nodes B and C on a *radial-canal*, as shown in Fig. 3.10(a). The node A will be at the farthest position from any backbone node when it is in the middle of the bisection-perpendicular line in between two parallel *radial-canals*. Therefore, proving that the node A is guaranteed to get access to at least one backbone node is enough and sufficient condition for the *Lemma 1*. In such a scenario, as depicted in Fig. 3.10(b), the right-angle triangle $\triangle ADC$ satisfies,

$$AC^2 = AD^2 + CD^2. \tag{3.4}$$

Since the distance between two consecutive backbone nodes B and C on a *radial-canal* is r, and the source node A must offer guaranteed access to the *radial-canal* backbone node C; putting $CD = r/2$ and $AC = r$ in Eq. (3.4), we obtain the maximum allowable value of $AD = \frac{\sqrt{3}}{2} \times r$, *i.e.*, $DE = \sqrt{3} \times r$.

Now, let us calculate the value of DE and determine whether the above condition satisfies or not. Note that the parallel *radial-canals* produce the same incident angle at the network center and subsequent points on the corresponding principal axes. We assume a line $D'E'$ parallel to DE, then the right-angle triangles $\triangle\ O'D'E'$ and $\triangle\ O''D''E''$ support,

$$D'E' = DE = 2r \times sin\theta_1 \quad \text{and} \quad D''E'' = 2r \times sin\theta_2, \tag{3.5}$$

respectively, where, for all values of $\theta_1, \theta_2 \leq 60°$, the value of DE (or $D''E''$) maintains the required condition, $DE \leq \sqrt{3} \times r$. That is, the maximum allowable vertical angle produced by principal-diagonals at network center is $60° \times 2 = 120°$. Therefore, *Lemma 1* is proved. □

Finally, we develop the Starfish routing (SFR) backbone architectures, e.g., bSFR, and iSFR, as depicted in Fig. 3.11(a), and Fig. 3.11(b), respectively.

The operational detail to update the location of the mobile sink and backbone repairing is described in the following Section 3.5. Hereafter, as a part of study to determine the optimal size of the ring-canal, we compute the value of expansion control variable, ϕ, for a few variants of bSFR- and iSFR-backbone architectures in Section 3.6 through Section 3.9. These strategies determine the optimal radius of the circular ring-canal along with the optimal minor-axes and major axes of the elliptical ring-canals.

3.5 Updating Location of the Mobile Sink

The nodes on the proposed *Starfish routing backbone* architectures, e.g., iSFR and bSFR backbones, as shown in Fig. 3.11, maintain an up-to-date position of the mobile sink. Since the backbones are constructed to be accessed from any location with a 1-hop distance within the network, the mobile sink can update its position instantly to the *Starfish routing backbone*. The sink periodically broadcasts its location, and as soon as one of the backbone nodes of *Starfish routing backbone* becomes aware of the change of sink location, it shares further to inform the updated sink location to all other backbone nodes over *ring-* and *radial-canals*. This is why it reduces the overhead of routing path creation and can deliver sensed data immediately over the backbone nodes.

Though the SFR backbone architectures aim to ensure uniform energy consumption throughout the network; the backbone nodes are susceptible to consuming more energy due to handling more traffic than regular nodes. To mitigate the issue, backbone nodes may switch their roles among neighboring nodes to preserve the SFR-backbone connectivity constraint in the network, as proposed in [40].

3.6 Optimal Circular Ring-canal on SFR Backbone

While constructing the Starfish routing backbone, in both variants of bSFR and iSFR backbones, there is a central circular ring-canal those radii are equivalent to the sensor's transmission range, as shown in Fig. 3.11(a), and Fig. 3.11(b). Since all the radial canals converge to the central ring-canal, they suffer from more

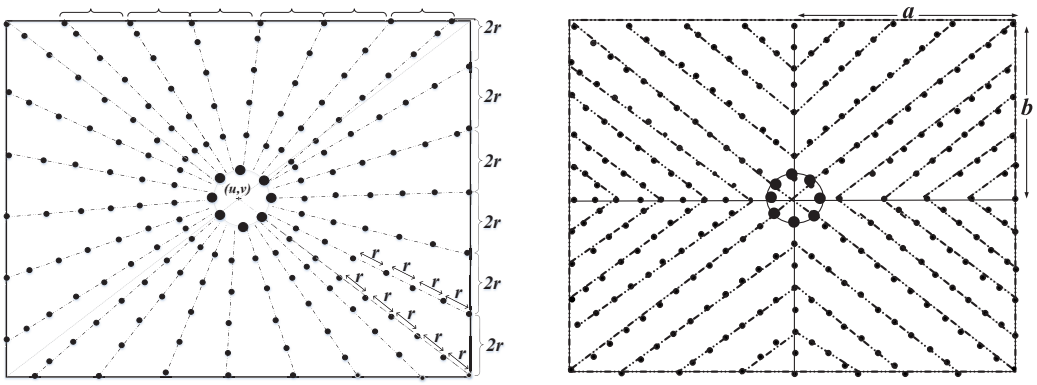

(a) Basic SFR (bSFR) backbone (b) Improved SFR (iSFR) backbone

Figure 3.11: The primitive Starfish routing (SFR) backbone structures

congestion, interference, forming a hotspot zone near the network center. It also affects QoS and network lifetime in sensor networks. To mitigate these issues for SFR-backbones, it necessitates determining an optimal radius of the circular ring-canal for both variants of SFR-backbones. The key objective for finding the optimal radius of the ring-canal is to converge each radial-canal onto one ring-canal node of the Starfish routing backbone. In this consequence, we recall that the *SFR-backbones* consist of three different sets of backbone nodes. The set of anchor nodes, radial-canal nodes, circular ring-canal nodes, number of radial-canals, and the radius of ring-canal are Z_a, Z_b, Z_c, Z_d, and R, respectively. Now, we estimate an optimal value of expansion control variable (for ring-canal) with respect to sensor's transmission range (r) and network size ($2a \times 2b$).

Therefore, in this section, we develop a mixed-integer linear program (MILP) that determines the optimal radius of a reference circle to construct the ring-canal in the network [114].

3.6.1 bSFR-circular backbone architecture

In the proposed *basic Starfish routing backbone* (bSFR-circular), a set of *anchor nodes*, Z_a, is selected along the network periphery every after $2r$ distance, as indicated in Fig. 3.12. Therefore, the number of anchor-nodes, $|Z_a|$, is approximated by the following Eq. (3.6).

$$|Z_a| = \frac{2 \times (2a + 2b)}{2r} = \frac{2 \times (a + b)}{r} \tag{3.6}$$

Since each anchor node initiates only one corresponding radial-canal in the basic SFR (bSFR) backbone architecture, the number of *radial-canals*, as assumed $|Z_d|$, is approximated as follows:

$$|Z_d| = \frac{2 \times (a + b)}{r} \tag{3.7}$$

Now, we formulate a mixed-integer-linear program (MILP) for an optimal radius of the circular ring-canal. In other words, we find an optimal value of the control variable, ϕ, through the following MILP formulation. It is noteworthy that the radius of the ring-canal should be large enough so that each radial-canal can converge to the only corresponding ring-canal node on the optimal Starfish routing backbone *(bSFR-circlular)*, as shown in Fig. 3.12. This strategy significantly mitigates collision as well as interference among the sensor nodes in the network.

$$Maximize: \quad R, \tag{3.8}$$

subject to,

$$0 < R \leq \phi r, \tag{3.9}$$

$$0 < |Z_d| \leq \frac{2 \times (a + b)}{r}, \tag{3.10}$$

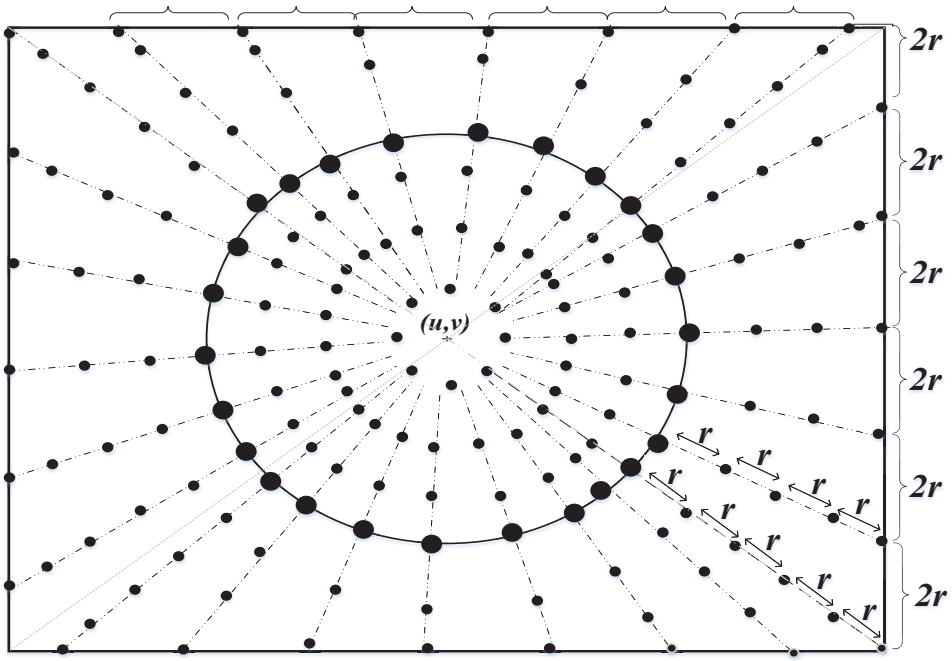

Figure 3.12: Construction of bSFR-circular backbone

$$0 < |Z_c| \leq \frac{2\pi R}{r}, \tag{3.11}$$

$$0 < |Z_c| \leq |Z_d|, \tag{3.12}$$

$$\phi > 0. \tag{3.13}$$

The above MILP formulation finds the optimal value of control variable, as stated in the following Eq. (3.14), in respect of transmission range of sensor node (r), and network size ($i.e., a, b$).

$$\phi = \frac{a+b}{\pi r} \tag{3.14}$$

Therefore, the optimal radius of the ring-canal is determined as follows,

$$R = \frac{a+b}{\pi} \tag{3.15}$$

Based on the above MILP, *Lemma 2* is presented that determines an optimal radius of the ring-canal in the network for a given network and sensor's transmission range.

Lemma 2. *Given that a and b $(a \geq b > r)$ are the halves of two sides, respectively, of a rectangular network, the optimal radius of the ring-canal of a Starfish routing backbone is estimated as $R \cong (a+b)/\pi$, if and only if the number of radial-canals has a linear relationship with the number of backbone nodes on the ring-canal.*

Proof. Since the backbone nodes on the ring-canal are positioned approximately every r distance away, the number is measured for the central ring-canal with radius R as $2\pi R/r$. Meanwhile, the number of radial-canals of the Starfish routing backbone is estimated for the given network as $(2a+2b)/2r$, since the radial-canals are rayed out approximately every $2r$ distance away along both principal-axes. If and only if the number of backbone nodes on the ring-canal and that of radial-canals has a linear relationship, or equal proportion (i.e., $2\pi R/r \cong (a+b)/r$), the Starfish routing backbone contains the optimal radius of the ring-canal that is estimated as $R \cong (a+b)/\pi$, and thus the *Lemma 2* is proved. □

Now, for *bSFR-circular* backbone, as shown in Fig. 3.12, based on the optimal reference-circle, $(x-u)^2 + (y-v)^2 = R^2$, the central controller selects backbone nodes on it, and continues until the closed-loop optimal circular ring-canal is formed.

3.6.2 iSFR-circular backbone architecture

Since the Starfish routing backbone has one of its variants, namely, iSFR-backbone, it necessitates finding an optimal radius of the ring-canal for iSFR. In this regard,

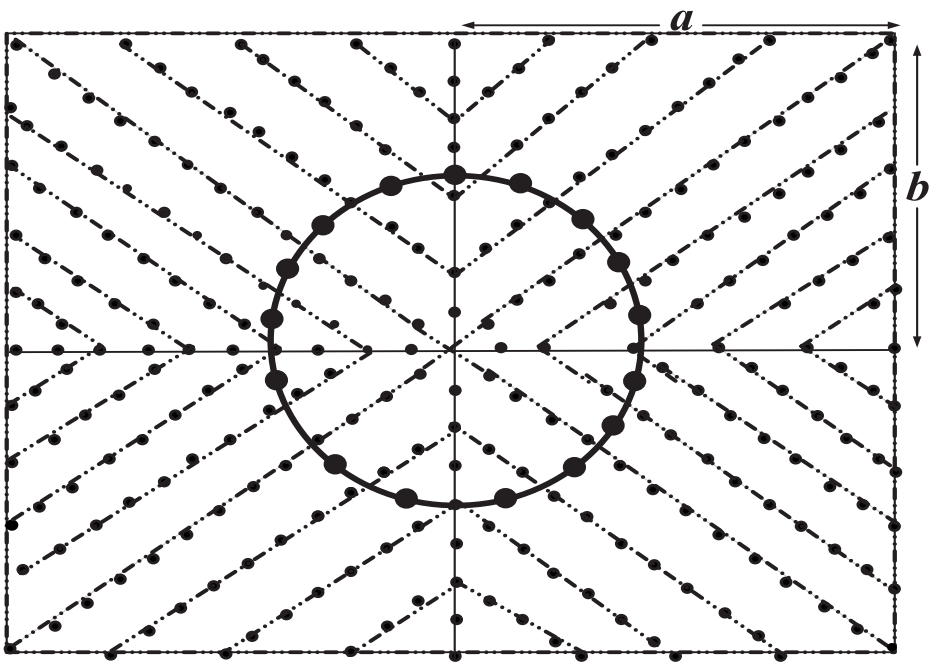

Figure 3.13: Construction of iSFR-circular backbone

we follow the similar MILP framework as formulated for the bSFR-circular and described in the previous Section 3.6.1.

The key idea of iSFR-circular backbone is to avoid the convergence of all radial-canals onto the central ring canal as determined for the bSFR-circular backbone in the previous section. In the iSFR-circular backbone architecture, as presented in Fig. 3.13, the radial canals are constructed parallel to the principal diagonals of the network. At first, we choose anchor nodes on the principal axes every after $2r$ distance, and then construct radial-canals parallel to both of the principal diagonals from each anchor node toward the edge of the network, as explained earlier in Section 3.4

Since the anchor nodes initiate radial-canals, it determines the maximum num-

ber of radial-canals in iSFR-circular. For a network area of $2a \times 2b$, the total number of anchor nodes can be a maximum of $(2a + 2b)/2r$ on the principal-axes. In iSFR-circular backbone architecture, each anchor node on the principal axes initiates two radial-canals parallel to the principal diagonals. Therefore, total number of radial-canals for iSFR-circular can be estimated as $2 \times ((a + b)/r)$. On the contrary, according to the principle of ring-canal construction, the number of backbone nodes on it is estimated as $2\pi\ R/r$.

Therefore, in the light of the MILP framework in *Lemma 2*, we find out the value of control variable (ϕ), and the optimal radius (R) of the ring-canal for iSFR-circular, respectively, as presented in Eq. (3.16), and Eq. (3.17), respectively.

$$\phi \leq \frac{a+b}{\pi r} \tag{3.16}$$

$$R \cong \frac{(a+b)}{\pi} \tag{3.17}$$

Finally, we construct iSFR-circular backbone that is illustrated in Fig. 3.13.

3.6.3 iSFR-optimized-circular backbone architecture

Though the above MILP framework computes the optimal radius of the ring-canal for both bSFR-circular and iSFR-circular, the ring-canal size for iSFR-circular would be further optimized. In the MILP framework, the value of the control variable, ϕ, depends on the number of radial canals initiated by the anchor nodes in the network. It is noteworthy that anchor nodes are selected every $2r$ distance on the principal axes. According to the basic construction principle of iSFR or iSFR-circular, the total number of radial canals are determined by the estimated anchor nodes on the principal axes. However, in a practical case, we would not

expect the ring-canal to be converged through the radial-canals initiated from the terminal anchor nodes on the principal axes. This scenario exhibits the ring-canal to be too large in the network. To mitigate this problem, we do further optimize the radius of the ring canal for iSFR.

Therefore, the total number of anchor nodes, excluding the terminal nodes on both side of the principal axes, can be re-estimated as $2 \times ((a + b - 2r)/r)$. Thus, in the light of *Lemma 2*, we find out the optimal radius of the ring-canal for the further optimized iSFR-circular backbone architecture, as illustrated in Fig. 3.13. Therefore, the optimal value of the control variable (ϕ), and the optimal radius of the ring-canal are presented in Eq. (3.18), and Eq. (3.19), respectively.

$$\phi = (a + b - 2r)/\pi r \tag{3.18}$$

$$R = \frac{a + b - 2r}{\pi} \tag{3.19}$$

Finally, the central controller picks backbone nodes on the ring-canal after every r-distance. This step continues until a closed loop of optimal ring-canal is constructed.

3.7 Optimal Elliptical Ring-canal on SFR Backbone

The above MILP formulation determines the optimal radius of the circular ring-canal for both bSFR-circular and iSFR-circular backbone architectures, irrespective of network area, either square- or rectangle-shaped. In the case of square size, circular ring-canal could be a good choice that would not be equally expected or as much as appropriate for a rectangular-shaped network.

In this consequence, the construction of optimal elliptical ring-canal for a rectangular-shaped network is still unexplored to maximize network lifetime and maintain QoS requirements of real-time applications. Therefore, we concentrate to develop bSFR-elliptical, and iSFR-elliptical backbones with an optimal elliptical ring-canal on the proposed SFR backbone architectures, as illustrated in Fig. 3.14, and Fig. 3.15. Similar to the above MILP framework, the optimal radius of the ring-canal in terms of the expansion factor of the ring-canal, ϕ, is determined based on network size and sensor's transmission range r. It is also expected that a significant reduction in end-to-end latency and extending network lifetime can be achieved for real-time data collection with a mobile sink. The following subsections unfold the optimal size of the elliptical ring-canal in terms of the control variable, ϕ.

3.7.1 bSFR-elliptical with optimal elliptical ring-canal

In basic SFR-backbone architecture, as discussed in Section 3.2, a set of *anchor nodes*, Z_a, is chosen along the network periphery after every $2r$. Since each anchor node initiates to construct a corresponding radial-canal, the number of *radial-canals*, $|Z_a|$, is estimated following Eq. (3.20).

$$|Z_a| = \frac{2 \times (2a + 2b)}{2r} = \frac{2 \times (a + b)}{r} \tag{3.20}$$

From the experimental results, it is observed that *bSFR* backbone may suffer from the extreme size of *ring-canals* in the network, e.g., extraordinarily large or very small. Therefore, we aim to find bSFR-elliptical backbone, as illustrated in Fig. 3.14, that contains an optimal elliptical ring-canal in the network. We assume, m and n are the major-radius and minor-radius of the ellipse, respectively. The

value of m and n are to be determined by a tuning parameter, ϕ, for varying size of networks, using Eq. (3.21) and Eq. (3.22).

$$m = \phi\ a \tag{3.21}$$

$$n = \phi\ b \tag{3.22}$$

The key motivation for finding the optimal major-radius and minor-radius is to converge each radial-canal onto one backbone node over the elliptical ring-canal. Thus, both m and n should be large enough so that each radial-canal can converge to the only corresponding elliptical ring-canal of the Starfish routing backbone. Since the ring-canal backbone nodes are placed on the reference-ellipse every after r distance, the total number of ring-canal backbone nodes Z_c depends on its perimeter $2\pi\sqrt{(m^2+n^2)/2}$. Thus, $|Z_c|$ can be estimated as follows,

$$|Z_c| = \frac{2\pi\sqrt{\Big((m^2+n^2)/2\Big)}}{r} \tag{3.23}$$

In the case of efficient converge of each radial-canal exactly onto a ring-canal backbone node, we find the optimal reference-ellipse, if and only if, $|Z_c| \cong |Z_a|$. Therefore, we get,

$$\frac{2\pi\sqrt{((m^2+n^2)/2)}}{r} \cong \frac{2\times(a+b)}{r} \tag{3.24}$$

$$\Rightarrow m^2+n^2 \cong 2\times\Big(\frac{a+b}{\pi}\Big)^2 \tag{3.25}$$

Now, putting the values of m, and n into Eq. (3.25) from Eq. (3.21) and Eq. (3.22), respectively, we get,

$$\phi^2\Big(a^2+b^2\Big) = 2\Big(\frac{a+b}{\pi}\Big)^2 \tag{3.26}$$

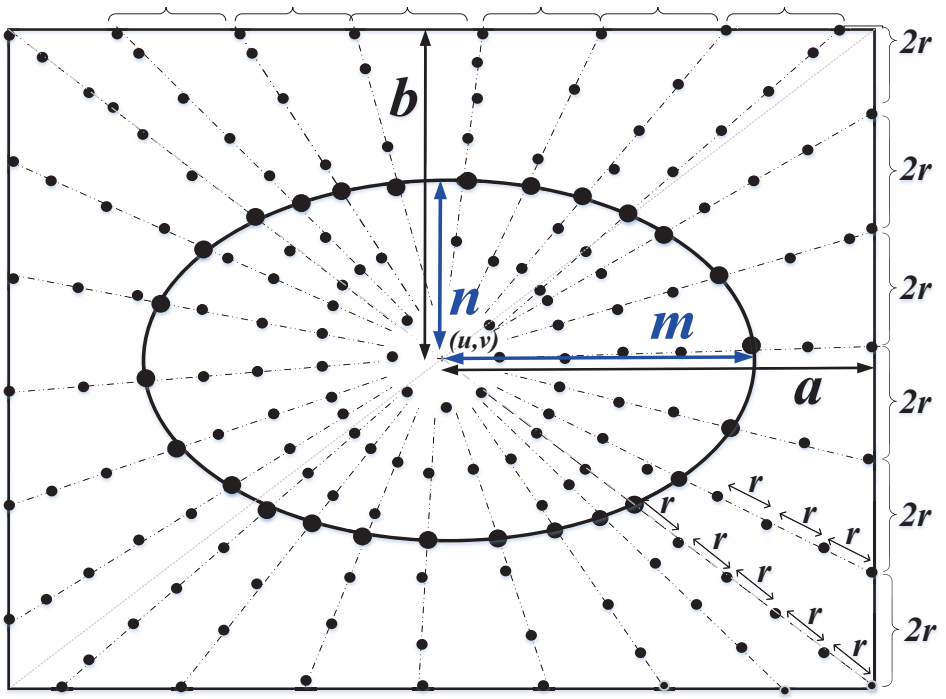

Figure 3.14: Construction of bSFR-elliptical backbone

After that, we compute the control variable, ϕ, for determining the optimal size of reference-ellipse in terms of m and n. Solving the quadratic Eq. (3.26), we find the value of ϕ as follows,

$$\phi = \frac{\sqrt{2}}{\pi}\,(a+b)\,\sqrt{\left(\frac{1}{a^2+b^2}\right)} \tag{3.27}$$

Therefore, we determine the optimal size of the ring-canal on bSFR-elliptical in terms of m and n, using the following equations.

$$m = \frac{\sqrt{2}a}{\pi}\,(a+b)\,\sqrt{\left(\frac{1}{a^2+b^2}\right)} \tag{3.28}$$

$$n = \frac{\sqrt{2}b}{\pi}\ (a+b)\ \sqrt{\left(\frac{1}{a^2+b^2}\right)} \tag{3.29}$$

Finally, based on the optimal major-radius (m) and minor-radius (n), we draw a reference-ellipse in the network using Eq. (3.30), as presented as follows,

$$\left(\frac{x-u}{m}\right)^2 + \left(\frac{y-v}{n}\right)^2 = 1 \tag{3.30}$$

Finally, we construct the proposed bSFR-elliptical backbone with optimal elliptical ring-canal in the network, as shown in Fig. 3.14. Then, the central controller picks backbone nodes on the reference-ellipse after every r-distance. This step continues until a closed loop of optimal bSFR-elliptical ring-canal is constructed. Now, in the next section, we construct the iSFR-elliptical backbone with an optimal elliptical ring-canal.

3.7.2 iSFR-elliptical with optimal elliptical ring-canal

Finding the optimal radius for iSFR-elliptical follows a similar approach, as described for the bSFR-elliptical backbone architecture in Section 3.7.1, except computing the number of radial-canals on the principal axes. Since anchor nodes initiate radial-canals, we determine the maximum number of radial-canals for iSFR-elliptical backbone architecture, as illustrated in Fig. 3.15 . For a network area of $2a \times 2b$, the total number of anchor nodes, Z_a, can be a maximum of $((a+b-2r)/r)$ on the principal axes excluding the terminal nodes for both sides. Since each anchor node initiates two radial-canals parallel to the principal diagonals, the total number of radial-canals, Z_d, for iSFR-elliptical can be estimated as $2 \times ((a+b-2r)/r)$.

For an efficient convergence of each radial-canal onto an elliptical ring-canal node, we find the optimal reference-ellipse, if and only if, it follows Eq. (3.31),

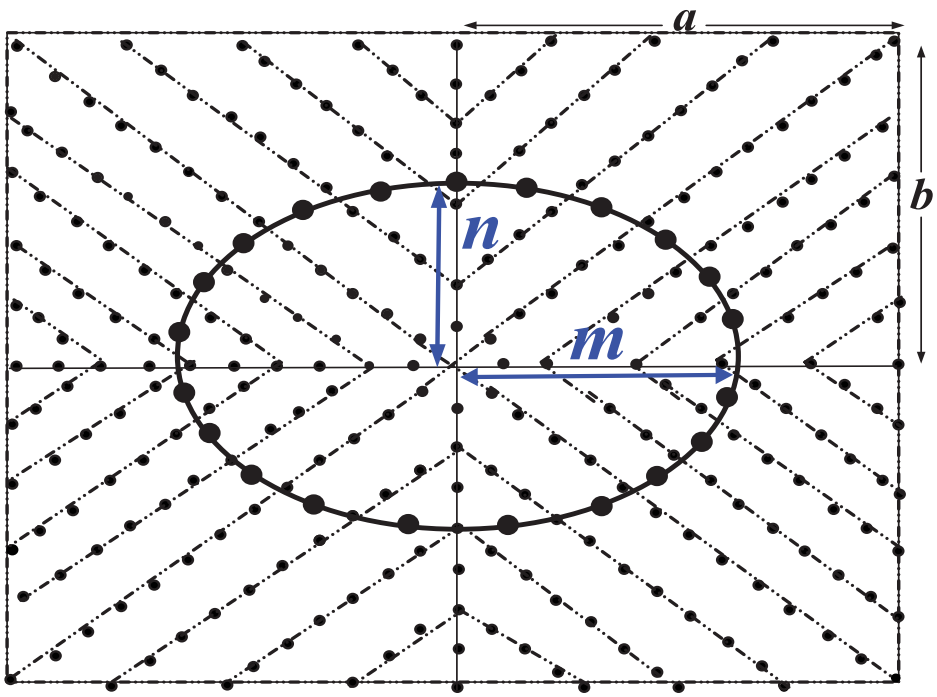

Figure 3.15: Construction of iSFR-elliptical backbone

maintaining Lemma 2.

$$\frac{2\pi\sqrt{((m^2+n^2)/2)}}{r} \cong \frac{2\times(a+b-2r)}{r} \tag{3.31}$$

Now, we get the value of control-variable (ϕ) for iSFR-elliptical, as presented in Eq. (3.32), by substituting the values of m and n, as stated in Eq. (3.21) and Eq. (3.22), respectively.

$$\phi = \frac{\sqrt{2}}{\pi}\,(a+b-2r)\,\sqrt{\left(\frac{1}{a^2+b^2}\right)} \tag{3.32}$$

Therefore, we determine optimal size of the ring-canal on iSFR-elliptical in

terms of m and n, using Eq. (3.33) and Eq. (3.34), as follows,

$$m = \frac{\sqrt{2}a}{\pi}\ (a + b - 2r)\ \sqrt{\left(\frac{1}{a^2 + b^2}\right)} \tag{3.33}$$

$$n = \frac{\sqrt{2}b}{\pi}\ (a + b - 2r)\ \sqrt{\left(\frac{1}{a^2 + b^2}\right)} \tag{3.34}$$

Now, based on the optimal major-radius (m) and minor-radius (n), we sketch a reference-ellipse in the network using Eq. (3.30). After that, we construct the proposed iSFR-elliptical backbone with optimal ring-canal in the network, as shown in Fig. 3.15. Then, the central controller picks backbone nodes on the reference-ellipse after every r-distance. This step continues until a closed loop of optimal iSFR-elliptical ring-canal is constructed.

Finally, for both bSFR-elliptical and iSFR-elliptical architectures, all backbone nodes on the elliptical ring-canal and radial-canals are connected to construct SFR-elliptical architectures.

As a planned study to construct Starfish routing (SFR) backbones, we consider a rectangular-shaped sensor network with a mobile sink. In this consequence, we computed the optimal sizes of circular and elliptical ring-canals in the rectangle-shaped network. However, in some practical applications, the network size may vary from square to circular.

Therefore, it necessitates constructing SFR backbones in square and circular-shaped networks. In the subsequent sections, we construct different variants of SFRs within square-shaped and circular-shaped sensor networks. Since the construction of the radial-canals is similar for all variants of Starfish routing (SFR) backbones, we concentrate on determining the optimal radius of the ring-canal for

the assumed square-shaped and circular-shaped sensor networks in the subsequent Sections 3.8, and 3.9, respectively.

3.8 SFR Backbones in a Square-shaped Network

To construct bSFR and iSFR backbones in a square-shaped network, we assume a square network of $\mathbf{2a} \times \mathbf{2a}$, as shown in Fig. 3.16 and Fig. 3.17, where $\mathbf{a}$ is the half of a side of square network, and sensor's transmission range is (r). Now, again we recall that Z_a, Z_b, Z_c, Z_d and R are the set of anchor nodes, radial-canal nodes, ring-canal nodes, the number of radial-canals, and the optimal radius of the ring-canal, respectively.

To simplify constructing bSFR and iSFR backbones in a square-shaped network, we refer the Section 3.6 where the optimal radius of the ring-canal has been determined for a rectangular-shaped network. We may consider that the square-shaped network is a special type of network where $b = a$, in Eq. (3.6) through Eq. (3.13), as described in Section 3.6.

While developing different variants of SFR backbones in the network, it mainly varies determining the optimal size ring-canal in the network. Therefore, apart from describing the detailed construction procedure of SFR backbones, we focus on determining the optimal size ring-canal in the square-shaped network.

3.8.1 bSFRs backbone in square-shaped network

Typically, the optimal radius (R) of the ring-canal is determined in terms of control variable, (ϕ). Therefore, at first, we determine the value of (ϕ) with respect to network size $(2a)^2$ and sensor's transmission range (r), based on the the discussion

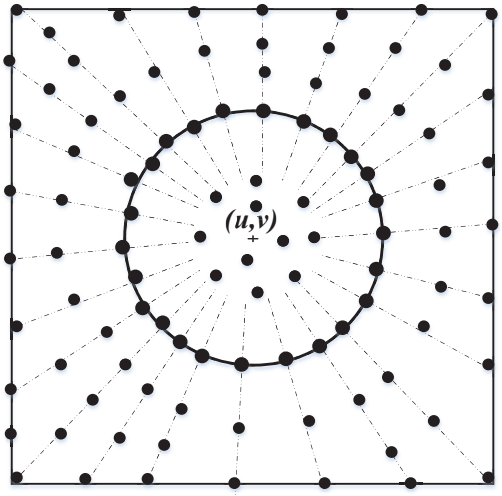

Figure 3.16: bSFRs backbone in square-shaped network

in Section 3.6. Considering square-shaped network as a special type of network environment, where $b = a$, in Eq. (3.6) through Eq. (3.13), we find the value of control variable (ϕ), and the optimal radius (R) of the ring-canal using the following Eq. (3.35) and Eq. (3.36), respectively.

$$\phi = 2a/\pi r \tag{3.35}$$

$$R = \frac{2a}{\pi} \tag{3.36}$$

Now, the proposed bSFRs-circular backbone in square-shaped network is illustrated in Fig. 3.16 based on the above optimal radius of the ring-canal, R. Now, in the following subsection, we determine the required values of the control variable (ϕ), and the optimal radius (R) of the ring-canal for the iSFRs-circular backbone architecture in a square-shaped network.

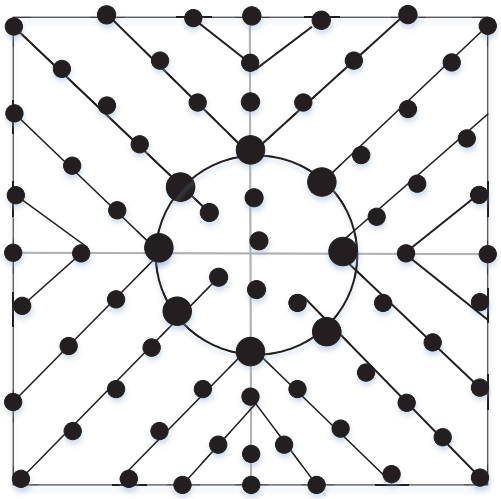

Figure 3.17: iSFRs backbone in square-shaped network

3.8.2 iSFRs in square-shaped network

Similar to the above Section 3.6, we determine the control variable (ϕ), and the optimal radius (R) of the ring-canal for the iSFRs backbone in square-shaped network, where $b = a$. The optimal values are determined using Eq. (3.37), and Eq. (3.38), respectively.

$$\phi = \frac{2(a-r)}{\pi r} \tag{3.37}$$

$$R = \frac{2(a-r)}{\pi} \tag{3.38}$$

The proposed iSFRs backbone in square-shaped network is depicted in Fig. 3.17 based on the above optimal values.

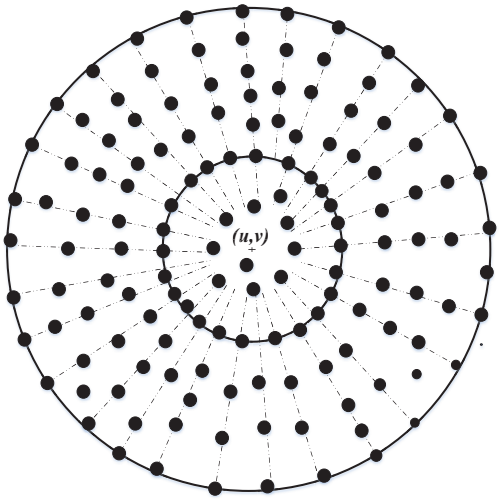

Figure 3.18: bSFRc backbone in circular-shaped network

3.9 SFR Backbones in Circular-shaped Network

To construct bSFRc and iSFRc backbones in a circular-shaped network, we assume a network of radius $\Re$, as shown in Fig. 3.18 and Fig. 3.19. Now, again we recall that Z_a, Z_b, Z_c, Z_d, and R are the set of anchor nodes, radial-canal nodes, ring-canal nodes, the number of radial-canals, and the optimal radius of the ring-canal, respectively.

3.9.1 bSFRc backbone in circular-shaped network

Since the anchor nodes initiate radial-canals, it determines the maximum number of radial-canals on bSFRc backbone architecture. For a network of radius $\Re$, as shown in Fig. 3.18, the total number of anchor nodes can be maximum of $2\pi\Re/2r$ around the periphery of the circular-shaped network. On the contrary, total number of ring-canal nodes is estimated as $2\pi R/r$. According to the Lemma 2, we find an

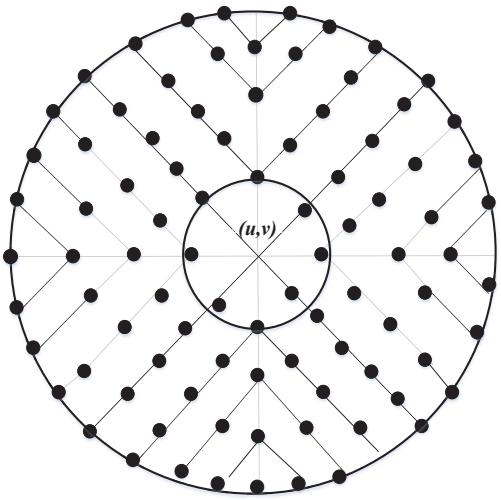

Figure 3.19: iSFRs backbone in circular-shaped network

optimal value of ϕ, and optimal radius (R) of the ring-canal of bSFRc inside the circular network using Eq. (3.39), and Eq. (3.40), respectively.

$$\phi = \frac{\Re}{2r} \tag{3.39}$$

$$R = \frac{\Re}{2} \tag{3.40}$$

The proposed bSFRc backbone in the circular-shaped network is depicted in Fig. 3.18 based on the above optimal values.

3.9.2 iSFRc backbone in circular-shaped network

According to the similar approach, as described in the previous Section 3.9.1, we determine the control variable (ϕ), and the optimal radius (R) of the ring-canal for the iSFRc-backbone in a circular-shaped network.

In the case of iSFRc-backbone in a circular-shaped network, the total number of anchor nodes, excluding the terminal nodes on both sides of the principal axes, can be re-estimated as $4 \times (\Re - r)/r$. On the contrary, the total number of ring-canal nodes on the optimal ring-canal is estimated as $2\pi R/r$.

Therefore, in the light of *Lemma 2*, we find out the optimal radius of the ring-canal for the iSFRc-backbone architecture, as illustrated in Fig. 3.19. The optimal value of the control variable (ϕ), and the optimal radius of the ring-canal are presented in Eq. (3.41), and Eq. (3.42), respectively.

$$\phi = \frac{2(\Re - r)}{\pi r} \tag{3.41}$$

$$R = \frac{2(\Re - r)}{\pi} \tag{3.42}$$

Finally, the proposed iSFRc-backbone in a circular-shaped network is depicted in Fig. 3.19 based on the above optimal values.

3.10 Comparative Discussions on SFR Backbone Architectures

In this section, we summarize various SFR backbone architectures. The key philosophy of designing various SFR-backbones is to spread the backbone nodes over the different regions of the network in such a way that a source node can access at least one of the backbone nodes directly. The SFR backbone consists of two type of canals, i.e., a central *ring-canal*, and a few *radial-canals*. Various SFR backbone architectures, as presented in Fig. 3.20, can largely be classified based on the construction principle of different canals in the network that are discussed as follows.

3.10.1 Radial-canal based SFR-backbone architectures

According to the radial-canal construction, Starfish routing (SFR) backbones can be distinguished in basic SFR (bSFR) and improved SFR (iSFR).

- In bSFR-backbone architectures, the radial-canals are initiated from the anchor nodes located on the periphery of the network and are spread inside toward the central ring-canal, as depicted in Fig. 3.20(a), (c), (e), (g), (i). In these architectures, the radial canals converge to the single central canal (irrespective of its size). Therefore, they suffer from congestion and collision among the nodes during data transmission. These are the key factors of energy wastages of sensor nodes in bSFR-backbone architectures. To mitigate these issues, we develop iSFR-backbone architectures in the network.

- The key philosophy of the improved Starfish (iSFR) backbone architectures is to avoid the convergence of all radial-canals to the network center. Therefore, the radial-canals are diverged from the anchor nodes located on the principal axes to the periphery of the network, as illustrated in Fig. 3.20(b), (d), (f), (h), (j). This strategy significantly prevents congestion and collision around the ring-canal or network center.

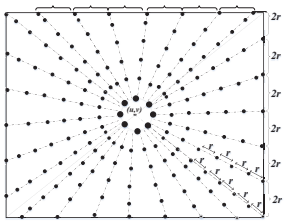

(a) bSFR backbone

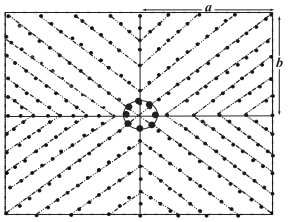

(b) iSFR backbone

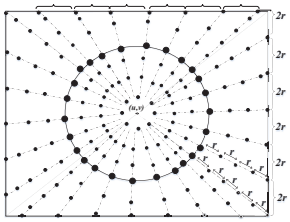

(c) bSFR-circular backbone

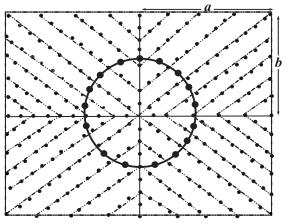

(d) iSFR-circular backbone

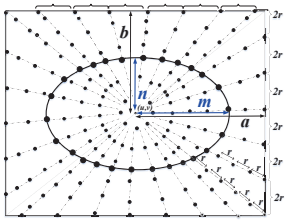

(e) bSFR-elliptical backbone

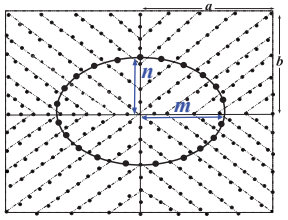

(f) iSFR-elliptical backbone

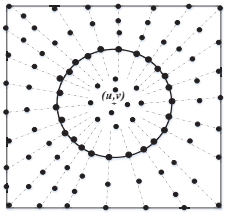

(g) bSFRs in square network

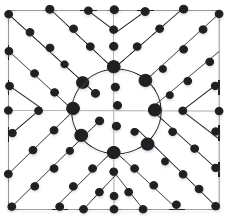

(h) iSFR in square network

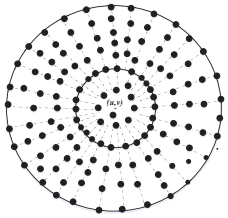

(i) bSFR in circular network

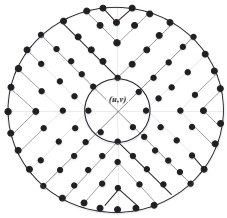

(j) iSFR in circular network

Figure 3.20: Various Starfish routing (SFR) backbone architectures

Table 3.2: Optimal values of ϕ, R, m, and n for various SFR backbones

SN	SFR Type	Area	Optimal value of ϕ	Optimal values of R, m, n
1.	bSFR	$2a \times 2b$	1	-
2.	iSFR	$2a \times 2b$	1	-
3.	bSFR-circular	$2a \times 2b$	$\frac{a+b}{\pi r}$	$R = \frac{a+b}{\pi}$
4.	iSFR-circular	$2a \times 2b$	$\frac{a+b}{\pi r}$	$R = \frac{a+b}{\pi}$
5.	iSFR-circular$_{opt}$	$2a \times 2b$	$\frac{a+b-2r}{\pi r}$	$R = \frac{a+b-2r}{\pi}$
6.	bSFR-elliptical	$2a \times 2b$	$\frac{\sqrt{2}}{\pi}\ (a+b)\ \sqrt{1/(a^2+b^2)}$	$m = \frac{\sqrt{2}\ a}{\pi}\ (a+b)\ \sqrt{1/(a^2+b^2)}$, $n = \frac{\sqrt{2}\ b}{\pi}\ (a+b)\ \sqrt{1/(a^2+b^2)}$
7.	iSFR-elliptical	$2a \times 2b$	$\frac{\sqrt{2}}{\pi}\ (a+b-2r)\ \sqrt{1/(a^2+b^2)}$	$m = \frac{\sqrt{2}\ a}{\pi}\ (a+b-2r)\ \sqrt{1/(a^2+b^2)}$, $n = \frac{\sqrt{2}\ b}{\pi}\ (a+b-2r)\ \sqrt{1/(a^2+b^2)}$
8.	bSFRs	$(2a)^2$	$\frac{2a}{\pi r}$	$R = \frac{2a}{\pi}$
9.	iSFRs	$(2a)^2$	$\frac{2(a-r)}{\pi r}$	$R = \frac{2(a-r)}{\pi}$
10.	bSFRc	$\pi\Re^2$	$\frac{\Re}{2r}$	$R = \frac{\Re}{2}$
11.	iSFRc	$\pi\Re^2$	$\frac{2(\Re-r)}{\pi r}$	$R = \frac{2(\Re-r)}{\pi}$

Labels:

a: Length of a network, b: width of a network,

r: Transmission range of a sensor node, R: Radius of the ring-canal, $\Re$: Radius of a circular network model

m: Major radius of an optimal elliptical ring-canal, n: Minor radius of an optimal elliptical ring-canal

ϕ: Control variable to determine optimal radius of the ring-canal, **bSFR**: Basic Starfish Routing

iSFR: Improved Starfish Routing, **SFRs**: SFR backbone in square-shaped network

SFRc: SFR backbone in circular-shaped network

Moreover, in a separate study, we find the required number of backbone nodes on the SFR backbones for varying number of network sizes. Based on a, b and r, the backbone nodes on bSFR-circular are estimated as $\frac{2\times(2a+2b)}{2r}+\frac{2\times(a+b)}{r}+(\sum_{q=0}^{\lceil\frac{2a}{2r}\rceil-1}\sqrt{(a-qr_1)^2+b^2}\,)/r_1+(\sum_{q=0}^{\lceil\frac{2b}{2r}\rceil-1}\sqrt{(b-qr_2)^2+a^2}\,)/r_2$, where $r_1 = 2a/(\lceil 2a/2r\rceil), r_2 = 2b/(\lceil 2b/2r\rceil)$. On the other hand, in the case of iSFR-circular, the backbone nodes are estimated as $\frac{2\sqrt{(2a)^2+(2b)^2}}{r} + \frac{2\times(a+b)}{r} + (\sum_{q=1}^{\lceil\frac{a}{2r}\rceil-1}\sqrt{(a-qr_1^{'})^2+(a-qr_1^{'}tan\theta_1)^2}\;)/r_1^{'} + (\sum_{q=1}^{\lceil\frac{b}{2r}\rceil-1}\sqrt{(b-qr_2^{'})^2+(b-qr_2^{'}tan\theta_2)^2}\;)/r_2^{'}$, where $r_1^{'} = a/\lceil\frac{a}{2r}\rceil, r_2^{'} = b/\lceil\frac{b}{2r}\rceil$, $tan\theta_1 = b/a$, and $tan\theta_2 = a/b$. Because of the unique SFR backbone architectures, the number of backbone nodes required for iSFR-backbone is lower than that of bSFR-backbone. This can be proved numerically based on these estimation. For instance, in the case of a network of $700 \times 525\ m^2$, iSFR-circular requires less than 100 nodes while bSFR-circular requires more than 300 backbone nodes.

Furthermore, iSFR protocol outperforms bSFR in terms of network QoS and lifetime performances, as per the experimental results discussed in Section 3.12.

3.10.2 Ring-canal based SFR-backbone architectures

According to the ring-canal construction, Starfish routing (SFR) backbones can be classified into three variants that are discussed as follows.

- As a preliminary architecture of SFR, the ring-canal is constructed at the network center whose radius is as maximum as the sensor's transmission range, r. Therefore, it is known as transmission range based SFR-backbones, i.e., bSFR and iSFR, as illustrated in Fig. 3.20(a), and Fig. 3.20(b), respectively. Since the ring-canal's radius is fixed, i.e., equivalent to the sensor's transmission range irrespective of network size, it suffers from more congestion,

interference, forming hotspot zone near the network center. It also affects the QoS and network lifetime of sensor networks. To mitigate these issues for SFR-backbones, it necessitates determining an optimal radius of the circular ring-canal for SFR-backbones.

- In the second category, an optimal ring-canal is constructed for both bSFR and iSFR, as depicted in Fig. 3.20(c), and Fig. 3.20(d), respectively. The optimal radius of the ring-canal is determined based on network size (i.e., a, b), and transmission range of a sensor (r). For both variants of bSFR-circular, and iSFR-circular backbones, the optimal radii of the ring-canals are determined by Eq. (3.15), and Eq. (3.19), respectively. Moreover, the optimal values of ϕ and R for various SFR-backbones are tabulated in Table 3.2.

- The above category determines an optimal radius of the circular ring-canal, irrespective of network size either it is square- or rectangle-shaped. In the case of square area, circular ring-canal would be a good choice. However, it would not be equally appropriate for a rectangular-shaped network. Therefore, optimal ring-canals of bSFR-elliptical, and iSFR-elliptical architectures are constructed, as presented in Fig. 3.20(e), and Fig. 3.20(f), respectively. The optimal radii of the elliptical ring-canals are also determined based on network size (i.e., a, b), and transmission range of a sensor (r). For both variants of bSFR-elliptical, and iSFR-elliptical backbones, the optimal values of ϕ, major-radius (m), and minor-radius (n) are tabulated in Table 3.2. The optimal elliptical ring-canal in a rectangular-shaped network is expected for a significant reduction in end-to-end latency and extending network lifetime that are evaluated in Section 3.12.

We have elaborately discussed the construction of Starfish routing backbones in the above sections. Now, we provide a Markov Chain based theoretical model for end-to-end delay of a packet in Section 3.11. Next, we evaluate the performance results of various SFR-backbones and compare them with the state-of-the-art works through exhaustive simulation studies in Section 3.12.

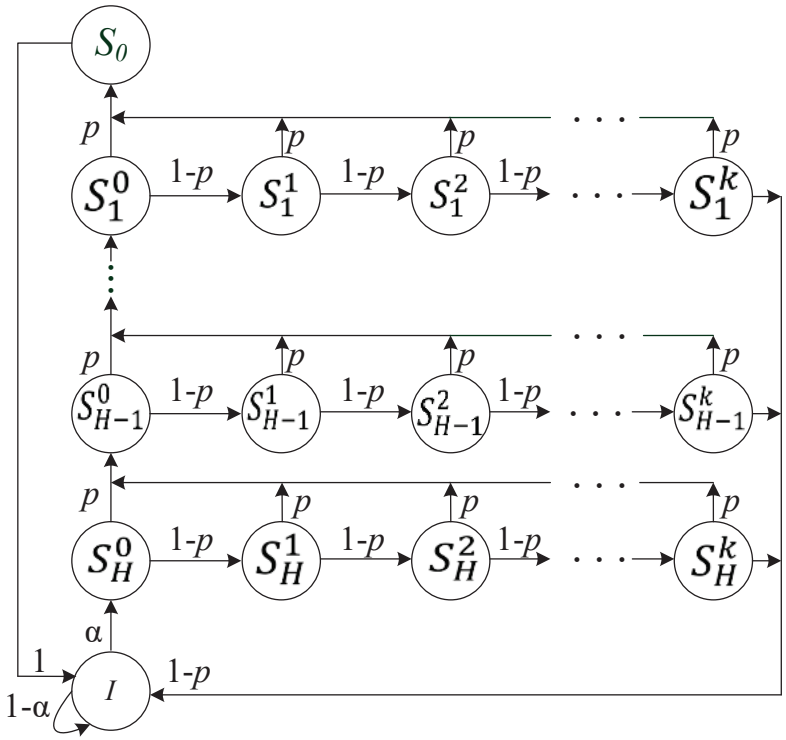

Figure 3.21: Markov chain model for multihop data delivery with retransmissions

3.11 End-to-End Delay Analysis

Here, we perform a probabilistic study to determine the end-to-end packet delivery delay from source nodes to mobile sinks via *ring-* and *radial-canal* nodes on the

Starfish routing backbone. The state-of-the-art works develop theoretical models to analyze average end-to-end latency by considering only the hop-distance between the source and the mobile sink. However, due to the inherent characteristics of sensor nodes, the end-to-end delay of a packet varies substantially depending not only on hop-distance but also on the number of retransmission(s) attempted at each hop. In this section, a Markov Chain-based theoretical model for the packet's end-to-end delay is constructed, taking into account both of the above issues, e.g., hop-distance and the number of retransmission(s).

In the Markov model, shown in Fig. 3.21, the state I is defined as an idle state, where the node has no data to transmit. Let S_h^z represents a state of packet located at h^{th}-hop distance from the sink and z^{th}-transmission or retransmission attempt, where $h \in \{1, 2, \ldots, H\}$ and $z \in \{0, 1, 2, \ldots, k\}$. A packet is dropped at a given hop if all k-number of retransmission attempts are failed. When the sink successfully receives the packet, it is destined at state S_0 in the model.

Given that the packet generation rate, σ, at each source node follows Poisson distribution, the probability that one packet will arrive during a time duration t is expressed as,

$$\alpha = (\sigma t)\ e^{-\sigma t}. \tag{3.43}$$

The success probability (p) of a transmission attempt is binomially distributed, and it is calculated as,

$$p = \mu\alpha\ (1-\alpha)^{m-1}\ (1-e), \tag{3.44}$$

where, μ is the number of nodes willing to transmit in the neighborhood, and e is the probability that a packet contains one or more bit errors [115], [116].

Each state in Markov Chain model, as depicted in Fig. 3.21, belongs to transition probabilities ρ and altogether it produces state distribution vector **(s)** as stated in Eq. (3.45) - Eq. (3.47).

$$\mathbf{s} = [\ \rho_I \quad \overbrace{\rho_H^0 \ \ \rho_H^1 \ \ \rho_H^2 \ldots \ \ \rho_H^k} \quad \ldots \quad \overbrace{\rho_1^0 \ \ \rho_1^1 \ \ \rho_1^2 \ \ \ldots \ \ \rho_1^k} \quad \rho_0]^{'}, \tag{3.45}$$

$$P\ \mathbf{s} = s, \tag{3.46}$$

$$\sum \mathbf{s} = 1. \tag{3.47}$$

For the case, when $H = 3$ and $k = 2$ the distribution vector $\mathbf{s}$ can be written as follows,

$$s = [\ \rho_i \quad \overbrace{\rho_3^0 \ \ \rho_3^1 \ \ \rho_3^2} \quad \overbrace{\rho_2^0 \ \ \rho_2^1 \ \ \rho_2^2} \quad \overbrace{\rho_1^0 \ \ \rho_1^1 \ \ \rho_1^2} \quad \rho_0\ ]^t \tag{3.48}$$

Therefore, for the above instance, the corresponding transition matrix (P) is presented as,

$$P = \begin{bmatrix}
1-\alpha & 0 & 0 & 1-p & 0 & 0 & 1-p & 0 & 0 & 1-p & 1 \\
\alpha & 0 & 0 & 0 & 0 & 0 & 0 & 0 & 0 & 0 & 0 \\
0 & 1-p & 0 & 0 & 0 & 0 & 0 & 0 & 0 & 0 & 0 \\
0 & 0 & 1-p & 0 & 0 & 0 & 0 & 0 & 0 & 0 & 0 \\
0 & p & p & p & 0 & 0 & 0 & 0 & 0 & 0 & 0 \\
0 & 0 & 0 & 0 & 1-p & 0 & 0 & 0 & 0 & 0 & 0 \\
0 & 0 & 0 & 0 & 0 & 1-p & 0 & 0 & 0 & 0 & 0 \\
0 & 0 & 0 & 0 & p & p & p & 0 & 0 & 0 & 0 \\
0 & 0 & 0 & 0 & 0 & 0 & 0 & 1-p & 0 & 0 & 0 \\
0 & 0 & 0 & 0 & 0 & 0 & 0 & 0 & 1-p & 0 & 0 \\
0 & 0 & 0 & 0 & 0 & 0 & 0 & p & p & p & 0
\end{bmatrix} \tag{3.49}$$

Now, we can find the distribution vector at equilibrium using Eq. (3.45) - Eq. (3.47). The solution of the above equations is explained as follows,

$$\rho_i = (1-\alpha)\ \rho_i + (1-p)\ \rho_3^2 + (1-p)\ \rho_2^2 + (1-p)\ \rho_1^2 + \rho_0 \tag{3.50}$$

$$\rho_3^0 = \alpha\ \rho_i \tag{3.51}$$

$$\begin{aligned} \rho_3^1 &= (1-p)\ \rho_3^0 \\ &= \alpha\ (1-p)\ \rho_i \end{aligned} \tag{3.52}$$

$$\begin{aligned} \rho_3^2 &= (1-p)\ \rho_3^1 \\ &= \alpha\ (1-p)^2\ \rho_i \end{aligned} \tag{3.53}$$

$$\begin{aligned} \rho_2^0 &= p\ (\rho_3^0 + \rho_3^1 + \rho_3^2) \\ &= p\ [\alpha\ \rho_i + \alpha\ (1-p)\ \rho_i + \alpha\ (1-p)^2\ \rho_i] \\ &= \alpha\ p\ [1 + (1-p) + (1-p)^2]\ \rho_i \qquad (3.54) \\ &= \alpha\ p\ \gamma\ \rho_i \qquad (3.55) \end{aligned}$$

Assuming,

$$\gamma = [1 + (1-p) + (1-p)^2] \tag{3.56}$$

Similarly, we get,

$$\rho_2^1 = (1-p)\ \rho_2^0 \ = \ \alpha\ p\ \gamma\ (1-p)\ \rho_i \tag{3.57}$$

$$\rho_2^2 = (1-p)\ \rho_2^1 \ = \ \alpha\ p\ \gamma\ (1-p)^2\ \rho_i \tag{3.58}$$

$$\rho_1^0 = p\ (\rho_2^0 + \rho_2^1 + \rho_2^2) \quad = \quad \alpha\ (p)^2\ \gamma\ [1 + (1-p) + (1-p)^2]\ \rho_i \tag{3.59}$$

$$= \quad \alpha\ (p\gamma)^2\ \rho_i \tag{3.60}$$

$$\rho_1^1 = (1-p)\ \rho_1^0 \quad = \quad \alpha\ (p\gamma)^2\ (1-p)\ \rho_i \tag{3.61}$$

$$\rho_1^2 = (1-p)\ \rho_1^1 \quad = \quad \alpha\ (p\gamma)^2\ (1-p)^2\ \rho_i \tag{3.62}$$

$$\begin{aligned} \rho_0 = p\ (\rho_1^0 + \rho_1^1 + \rho_1^2) \quad &= \quad p\alpha\ (p\gamma)^2\ \rho_i\ [1 + (1-p) + (1-p)^2] \\ &= \quad \alpha\ (p\gamma)^3\ \rho_i \\ &= \quad \alpha\ (p\gamma)^H\ \rho_i \end{aligned} \tag{3.63}$$

and,

$$\rho_i = \frac{1}{1 + \alpha\gamma + \alpha p\gamma^2 + \alpha p^2\gamma^3 + \alpha(p\gamma)^3} \tag{3.64}$$

Therefore, from this theoretical analysis, as computing for the instance, $H = 3$ and $k = 2$, the general equations of the solution can be represented as follows,

$$\rho_{h \in H \ldots 0}^{k \in 0 \ldots \tau} = \alpha\ (p\gamma)^{H-h}\ (1-p)^k\ \rho_i \tag{3.65}$$

$$\rho_0 = \alpha\ (p\gamma)^H\ \rho_i \tag{3.66}$$

$$\rho_i = \frac{1}{1 + \alpha \sum_{h=0}^{H-1} p^h \gamma^{h+1} + \alpha(p\gamma)^H} \tag{3.67}$$

$$s = \frac{1}{1 + \alpha\gamma + \alpha p\gamma^2 + \alpha p^2\gamma^3 + \alpha(p\gamma)^3} \begin{bmatrix} 1 \\ \alpha \\ \alpha(1-p) \\ \alpha(1-p)^2 \\ \alpha p\gamma \\ \alpha p\gamma(1-p) \\ \alpha p\gamma(1-p)^2 \\ \alpha(p\gamma)^2 \\ \alpha(p\gamma)^2(1-p) \\ \alpha(p\gamma)^2(1-p)^2 \\ \alpha(p\gamma)^3 \end{bmatrix} \tag{3.68}$$

Therefore, we can now calculate the expected number of transmission- and retransmission-attempts for a packet at each hop as follows,

$$\overline{z} = \sum_{z=0}^{k} z\rho_H^z. \tag{3.69}$$

Assuming that τ represents average delay per packet including processing, transmission, propagation, and queuing delay [117] that can be measured following $\tau = \tau_{proc} + \tau_{trans} + \tau_{prop} + \tau_{queue}$ [118]. Now, we can calculate the expected amount of delay for a packet in one hop as follows,

$$\overline{T} = \tau\ \overline{z}. \tag{3.70}$$

Similarly, we find the expected end-to-end delay for a packet traveling H hops as,

$$T = H \times \overline{T}. \tag{3.71}$$

In the following sections, we evaluate the performances of the studied protocols and discuss the simulation results.

3.12 Performance Evaluation

After the development of Starfish routing (SFR) backbones, we have implemented the *bSFR-circular*, *bSFR-elliptical*, *iSFR-circular*, *iSFR-elliptical*, HexDD [39], and Ring [40] routing-backbones over a sensor network in NS-2 [48], a discrete event network simulator, and after that compared their performances.

3.12.1 Simulation environment

We have considered a WSN of $400 \times 300m^2$ area, where 500 nodes are deployed randomly with uniform distribution. The transmission range (r) of each sensor is set at $90m$; the constant bit rate traffic model is used under UDP for data transmission with a packet size of 512 *bytes* considering 512 $Kbps$ of channel bandwidth and shadowing propagation loss model. For the mobile sink in the network, we have used the random waypoint mobility model, and all other sensor nodes are kept at stationary mode.

Table 3.3: Typical values of path loss exponent (β)

Environment		β
Outdoor	Free space	2
	Shadowed urban area	2.7 to 5
In building	Line-of-sight	1.6 to 1.8
	Obstructed	4 to 6

Table 3.4: Typical values of shadowing deviation (σ)

Environment	σ
Outdoor	4 to 12
Office, hard partition	7
Office, soft partition	9.6
Factory, line-of-sight	3 to 6
Factory, obstructed	6.8

While the mobile sink travels, it must be within sensor's transmission range for successful data transmission. We consider the height of the mobile sink so that it can travel for both obstacle-free and obstructed networks. Therefore, we set the height of the mobile sink during traveling randomly (for different experiments) between $15m$ to $45m$.

In conventional wireless signal propagation model [119], [120], [121], the received power is predicted as a deterministic function of distance where communication range is assumed as an ideal circle. But in practical world the received power at a certain distance of a wireless signal is not deterministic; it is a random variable due to multipath propagation effects. This effect is known as fading effects. Therefore, to achieve a realistic performance from the simulation, shadowing propagation model with $\beta = 2.8$ and $\sigma = 6.0_{dB}$ [122] has been considered in this paper from typical values of these parameters presented in Table 3.3 and Table 3.4. Moreover, the simulation parameters, along with their corresponding values and the burst description of four events considered in the simulation, are tabulated in are summarized in Table 3.5, and Table 3.6, respectively.

Table 3.5: Simulation parameters for backbone performance studies

Parameters	**Value**
Area of the network	$400 \times 300\ m^2$
Type of node deployment	Uniformly random
Number of nodes	500
Transmission range	90 m
Wireless Channel	WirelessPhy/802.15.4
Data packet size	512 $Bytes$ [106] [123]
Bandwidth	512 $Kbps$ [106]
Propagation model	Shadowing loss model [122]
Application type	Event-driven
Sink mobility model	Random way point
Initial energy of a sensor node	$6.0J$
Tx power	$0.023W$
Rx power	$0.018W$
Idle power	$0.037mW$
Sleeping power	$0.003mW$
Simulation time	1 hour

3.12.2 Performance metrics

The efficiency of the proposed protocol has been demonstrated by using the standard performance metrics that are described as follows.

- *Average throughput* is measured as the number of data bytes successfully received by the sink per unit time. The higher value represents better per-

Table 3.6: Event and burst descriptions for backbone performance studies

	Event A	**Event B**	**Event C**	**Event D**
Burst 1	30s - 40s	90s - 100s	130s - 140s	375s - 385s
Burst 2	125s - 135s	200s - 210s	380s - 390s	565s - 575s
Burst 3	425s - 435s	660s - 670s	740s - 750s	760s - 770s

formance.

- *Average end-to-end packet delivery delay* is the average time difference between the packet reception time at the sink and packet generation time at the source. A lower value indicates an improved performance.

- *Packet delivery ratio* is the ratio of the number of received packets at the sink to the generated packets by the source nodes. The higher value represents better performance.

- *Standard deviation (η) of residual energy* is the average dispersion among the residual energy levels on backbone nodes (Z) and can be calculated as follows,

$$\eta = \sqrt{\frac{1}{|Z|} \sum_{z=1}^{|Z|} (E_{res}(z) - \mu)^2}, \tag{3.72}$$

where, $E_{res}(z)$ is the node z's residual energy, and the mean residual energy of all backbone nodes is indicated by μ. It specifies the distribution of the energy consumption among the backbone sensors. The η value is expected to be small cause it indicates the better ability of the *Starfish routing backbone* to balance energy consumption.

- *Network lifetime* is calculated from the deployment time of the network to the time at which a backbone node dies and becomes unreachable from neighboring source or backbone nodes in the network. We consider it assuming that when it takes considerably long time to die a backbone node, the same phenomena will be repeated for the rest of the backbone. The lifetime of a sensor network is expected to be high, indicating the ability of an event to report over the SFR-backbones during the simulation period.

- *Operational overhead* is measured as the ratio of total control bytes exchanged during the whole simulation period to the total amount of data bytes delivered to the sink. A smaller value indicates better performance.

3.12.3 Simulation results

The simulation experiments are run 30 times with different random seed values for an On-Off application and taken the average for each data point in the graph. The events in the network happen randomly at different places, and random sources initiate flows that remain unchanged over the simulation period.

3.12.3.1 Impacts of varying speeds of the mobile sink

We evaluated the performances of the studied protocols for varying sink speeds from $1ms^{-1} \sim 6ms^{-1}$ which are corresponding to pedestrian speed through low-speed vehicles. In this experiment, the network size was fixed at 400×300 m^2, transmission range of sensor nodes was set at $90m$.

1. *Throughput performances*

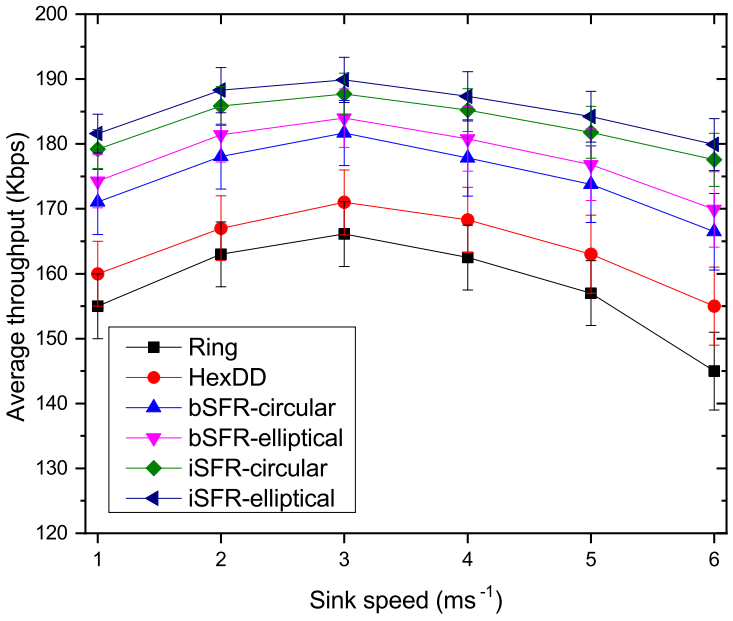

Figure 3.22: Average throughput for varying speeds of the mobile sink

The results, as shown in Fig. 3.23, depict that *average throughput* steadily increases with the sink speed up to $3ms^{-1}$ in all the studied protocols. But for higher speeds of the sink, *average throughput* decreases sharply due to faster changes of routing path caused by sink mobility. The average throughput for all variants of *Starfish routing (SFR) backbones* is better than those of HexDD [39] and Ring [40] strategies because of faster data communication over high-speed backbone in the network. This is achieved through spreading backbone nodes on the *ring-canal* and *radial-canals* that ensure balanced data traffic load throughout the network.

Moreover, the improved Starfish routing backbones, e.g., *iSFR-circular* and *iSFR-elliptical*, deliver higher throughput than its basic one, e.g., *bSFR-circular* and *bSFR-elliptical*, due to significant reduction of collisions and

interferences near *ring-canal* of the network.

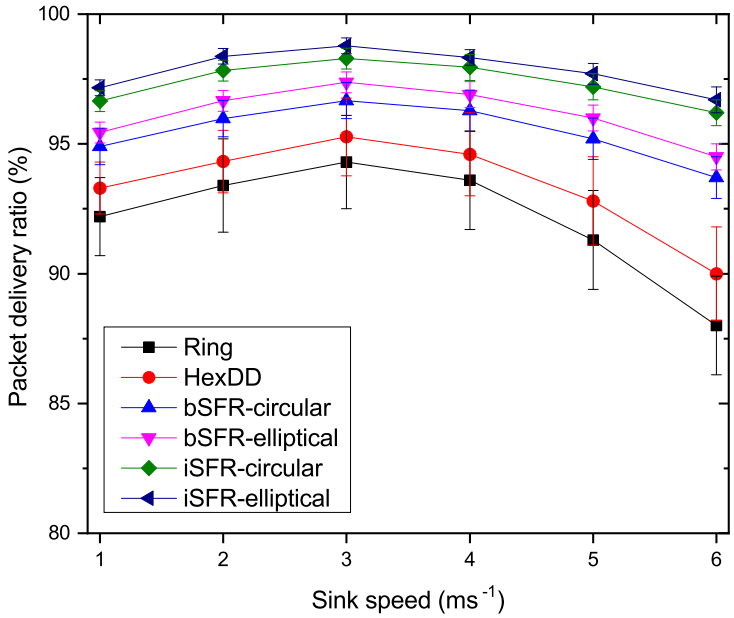

Figure 3.23: Packet delivery ratio for varying speeds of the mobile sink

Furthermore, from the experimental results in Fig. 3.23, it is clearly observed that elliptical ring-canal based SFR-backbone architectures, e.g., *iSFR-elliptical* and *bSFR-elliptical*, respectively outperform *iSFR-circular* and *bSFR-circular*, due to suitably fitted on the optimal size of elliptical ring-canal in a rectangular-shaped network. These experimental results prove the strength of *iSFR-elliptical* to achieve higher data throughput among all variants of SFR backbones.

2. *Packet delivery rate (PDR) performances*

For the same reasons as discussed for data throughput, the studied protocols show the higher *packet delivery ratio (PDR)* with increasing sink speed, as

illustrated in Fig. 3.24, and later, the *PDR* decreases sharply with faster speeds of the sink.

In the results, the PDR performances for all variants of *Starfish routing (SFR) backbones* is better than those of HexDD [39] and Ring [40] strategies due to quick data transmission over the high-speed Starfish backbones in the network. It happens because of ensuring balanced data traffic load throughout the backbone nodes in sensor networks.

Moreover, the improved Starfish routing backbones, e.g., *iSFR-circular* and *iSFR-elliptical*, deliver higher PDR than basic Starfish routing backbones, e.g., *bSFR-circular* and *bSFR-elliptical*. This performance proves the significant benefits of iSFR over bSFR due to mitigating collisions and interferences near *ring-canal* of the network.

Furthermore, from the PDR performances, it is clearly observed that elliptical ring-canal based SFR architectures outperform SFR-circular ones due to optimally fitted elliptical ring-canal in the network. These experimental results also show the strength of *iSFR-elliptical* to achieve higher PDR as well as prove the advantages of using the mobile sink in sensor networks.

3. *End-to-end packet delivery delay performances*

The *average end-to-end packet delivery delay* is decreased for all the studied backbone strategies while the sink speed is around $3ms^{-1}$, as shown in Fig. 3.25. It happens because the sink mobility significantly reduces the average hop distance of the transmitted data packets. However, the *end-to-end delay* again increases with the increasing sink speed as the data packets had to route more hops to reach the sink. Besides, higher sink mobility causes

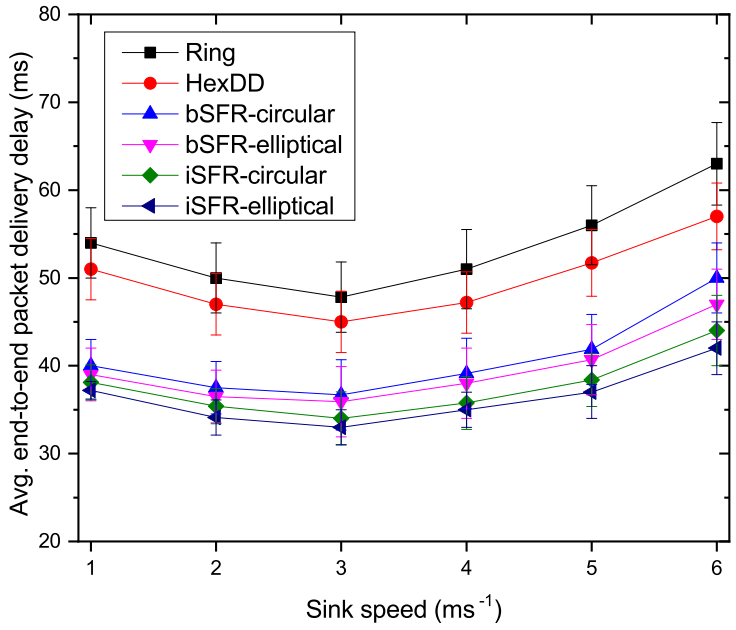

Figure 3.24: End-to-end packet delivery delay for varying speeds of the mobile sink

stale sink location information, increasing the retracing time for localization.

In the results, we notice that the *end-to-end packet delivery delay* performances for all variants of *Starfish routing (SFR) backbones* is better than those of HexDD [39] and Ring [40] strategies because it doesn't require any query for sink's fresh location. Moreover, rather than three principal-diagonals in HexDD, more *radial-canals* can directly transmit data to the sink, that helps our proposed *Starfish routing backbone* including all variants to minimize the *end-to-end packet delivery delay*.

Moreover, for the improved Starfish routing backbones, e.g., *iSFR-circular* and *iSFR-elliptical*, *end-to-end packet delivery delay* is lower than basic Starfish routing backbones, e.g., *bSFR-circular* and *bSFR-elliptical*. This performance proves the significant benefits of iSFR over bSFR due to form-

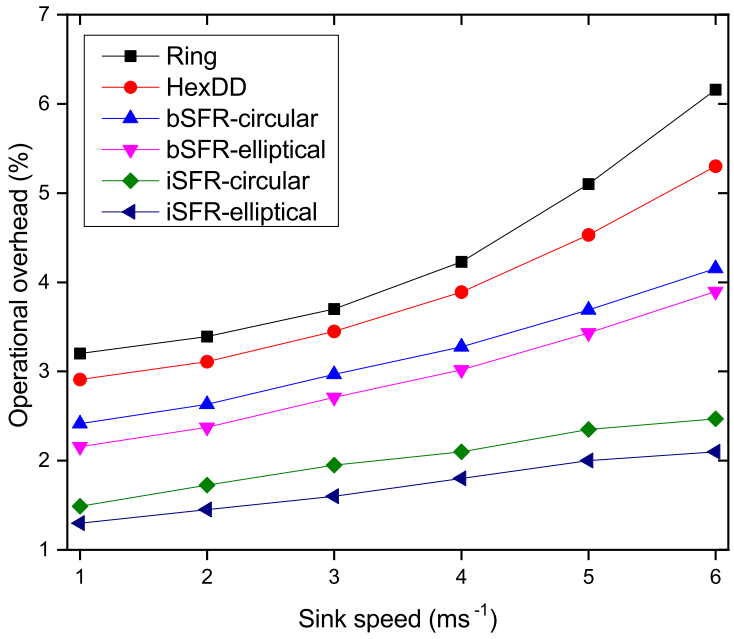

Figure 3.25: Operational overhead for varying speeds of the mobile sink

ing HSB with optimal number of backbone nodes on SFR architectures.

Furthermore, it is noteworthy that the elliptical ring-canal based SFR architectures outperform SFR-circular ones in terms of the *end-to-end packet delivery delay* performance because of developing an optimal elliptical ring-canal in the network. These experimental results also show the strength of *iSFR-elliptical* for real-time applications in sensor networks.

4. *Operational overheads*

The *operational overhead* is the metric to measure the effectiveness of the SFR backbones in the network. For varying sink speeds, the *operational overhead* of all studied protocols increase linearly, as shown in Fig. 3.26. However, the proposed SFR backbones remain in lower operational overhead compared to

other studied protocols, e.g., HexDD and Ring. This is caused due to preformed routing-backbone with *ring-* and *radial-canals* and *guaranteed single-hop* access to the backbone. For the operational procedure of Ring routing, at first, source node gets mobile sink's present location and then it forward data to the mobile sink. Due to faster sink's mobility, the source node has to follow footprint of the mobile sink to deliver data. It significantly increases overhead during data transmission in the network. Moreover, in the case of HexDD protocol, there are only six rendezvous regions meeting at network center through which data are delivered to the mobile sink. It also needs query for data and reverse feedback for data delivery. Therefore, operational overheads of the studied protocols, e.g., HexDD and Ring, are higher than iSFR variants. Furthermore, iSFR-elliptical architecture has advantages over SFR's circular and basic SFR variants.

From the above discussion, it is observed that neither very slow nor very high-speed mobility of the sink is beneficial; rather a moderate speed improves network performances for all studied backbone strategies. However, *Starfish routing backbone* outperforms HexDD and Ring backbones due to fair distribution of data traffic over backbone nodes within the network, and iSFR-elliptical architecture gets advantages of optimal elliptical ring-canal over its circular and basic SFR variants.

3.12.3.2 Impacts of varying sizes of networks

The sink speed is not the only parameter affecting the performances in sensor networks. The network size, in terms of its length and width, also affects the scalability and efficiency of routing backbones significantly. It happens due to the fact that the density of the network or traffic load depends on the network size.

We have evaluated the performances of the studied protocols for varying sizes of networks from $200 \times 150m^2 \sim 700 \times 525m^2$, while a fixed number of 500 sensor nodes are deployed randomly. In this experiment, the sink speed is fixed at $3ms^{-1}$, transmission range of sensor nodes is set at $90m$.

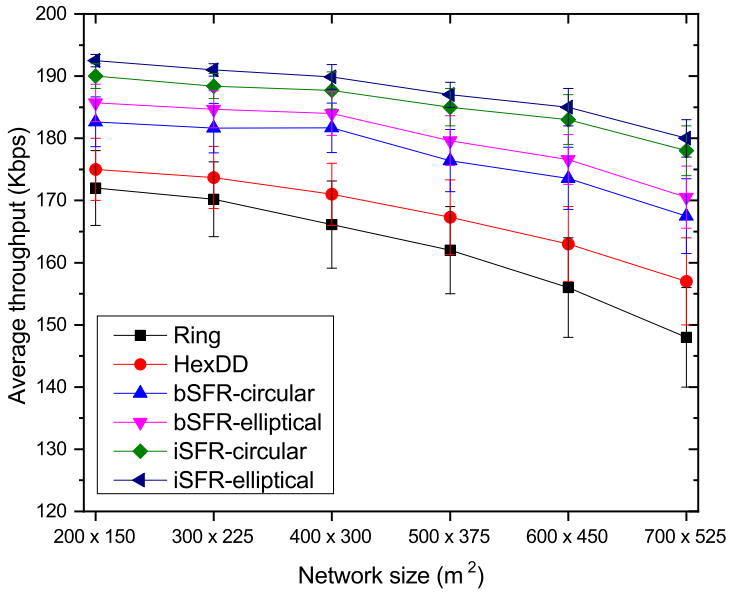

Figure 3.26: Average throughput for varying sizes of networks

1. *Throughput performances*

   The graphs of Fig. 3.27 illustrate that the *average throughput* steadily decreases in all the studied protocols. This happens because a fixed number of sensor nodes are deployed in increasing size of networks, which trivially reduces the probability of event notification by source nodes in the network. The average throughput for all variants of *Starfish routing (SFR) backbones* is better than those of HexDD [39], and Ring [40] strategies because of faster data communication over HSB and guaranteed single-hop access to at least

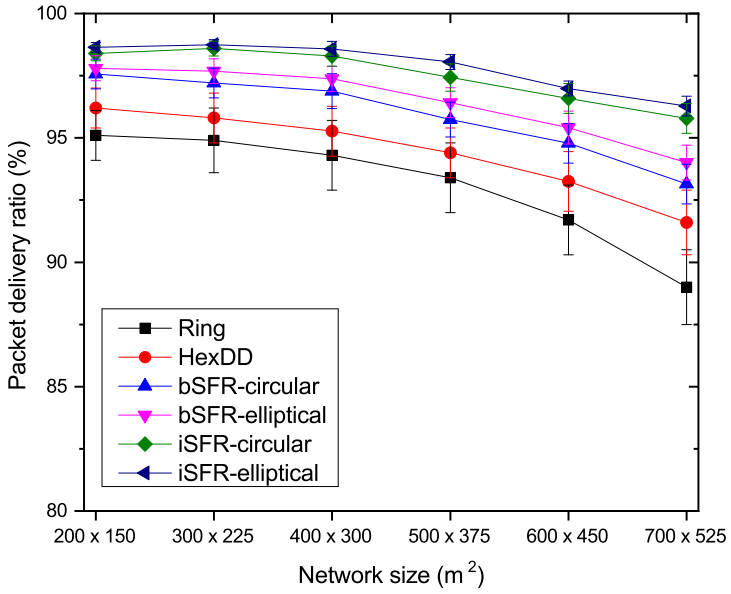

Figure 3.27: Packet delivery ratio for varying sizes of networks

one of the backbone nodes in the network. This is achieved through spreading backbone nodes on the SFR architectures that also ensure balanced data traffic load throughout the network.

Moreover, for the iSFR backbones, e.g., *iSFR-circular* and *iSFR-elliptical*, the *average throughput* is higher compared to its basic ones, e.g., *bSFR-circular* and *bSFR-elliptical*, due to significant reduction of collisions and interferences near *ring-canal* of the network. Furthermore, the elliptical ring-canal based SFR outperforms all the studied protocols because of its optimal structure in the network.

2. *Packet delivery rate (PDR) performances*

The studied protocols show the decreasing *packet delivery ratio (PDR)* with increasing network size, as shown in Fig. 3.28. In the results, the PDR per-

formances for all variants of *Starfish routing (SFR) backbones* are better than those of HexDD [39] and Ring [40] strategies due to quick data transmission over the HSBs in the network. Moreover, the improved Starfish routing backbones, e.g., *iSFR-circular* and *iSFR-elliptical*, deliver higher PDR than their corresponding basic SFR variants, e.g., *bSFR-circular* and *bSFR-elliptical*. This performance proves the significant benefits of iSFR over bSFR.

It is beyond stating to explain that *iSFR-elliptical* outperforms overall studied protocols due to its improved structure and existence of optimal elliptical ring-canal in the network. Besides, the higher *PDR* performance proves the suitability of *iSFR-elliptical* for large networks.

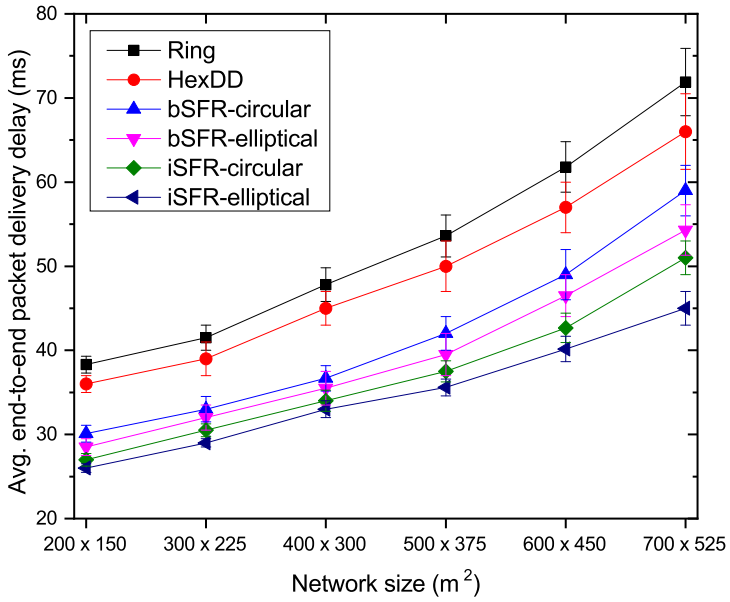

Figure 3.28: End-to-end packet delivery delay for varying sizes of networks

3. *End-to-end packet delivery delay performances*

The *average end-to-end packet delivery delay* is increased linearly for all the

studied backbone strategies with increasing sizes of networks, as shown in Fig. 3.29. This happens due to increasing average hop distance between the source to the sink. Besides, it is noticed that all variants of the *Starfish routing backbone* requires the lowest *end-to-end packet delivery delay* compared to the state-of-the-art works because of guaranteed single-hop access to the backbone nodes. This proves the suitability of *Starfish routing backbone* for delay-deadline-based real-time applications.

In the case of the improved Starfish routing backbones, e.g., *iSFR-circular* and *iSFR-elliptical*, *end-to-end packet delivery delay* is lower than basic Starfish routing backbones, e.g., *bSFR-circular* and *bSFR-elliptical*. This performance proves the significant benefits of iSFR over bSFR due to forming HSB with an optimal number of backbone nodes on SFR architectures.

Furthermore, it has already been discussed that the elliptical ring-canal-based SFR architectures outperform all studied protocols because of forming an optimal elliptical ring-canal in the network. The lowest end-to-end delay performance of the *iSFR-elliptical* shows its strength and emphasizes deploying in sensor networks for real-time applications.

4. *Operational overheads*

The *operational overhead* performance indicates the operational and functional effectiveness of a protocol to a great extend. In Fig. 3.30, the operational overhead steadily increases in all the studied protocols with the increasing size of networks. This happens because more control packets are transmitted for data delivery for increasing size of networks. Similar to the above performance results, the proposed SFR backbones remain in lower oper-

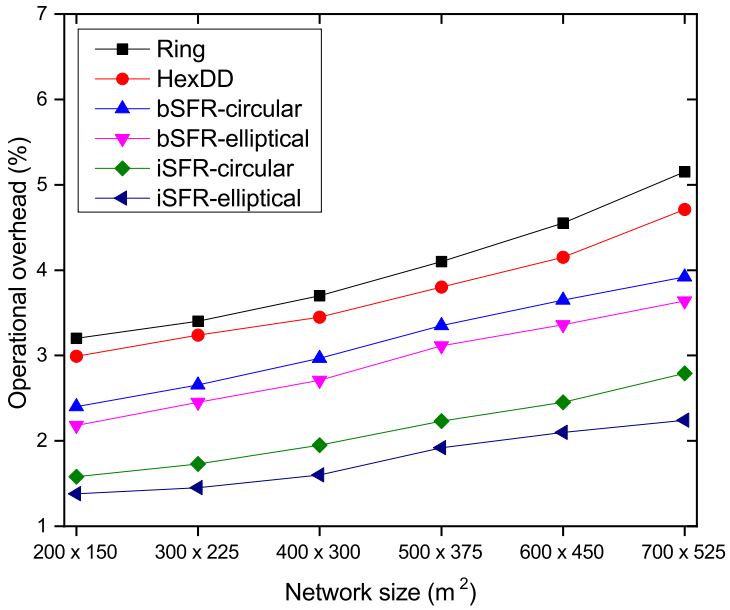

Figure 3.29: Operational overhead for varying sizes of networks

ational overhead compared to other studied protocols, e.g., HexDD and Ring. This is caused due to minimum control packet transmitted over preformed SFR backbones. Moreover, iSFR-elliptical architecture gets advantages over its iSFR-circular and bSFR variants.

We can conclude the above results and discussions that spreading data routing loads over nodes from different areas of the network helps the *Starfish routing backbones* to achieve a higher level of scalability compared to the studied protocols. In the following section, we discuss the performances of network lifetime for the proposed SFR backbones.

3.12.3.3 Effects on network lifetime

In this work, we have developed a high-speed backbone in sensor networks, namely SFR, through ring-canal and radial-canals. To ensure continuous data routing over the SFR backbone, all nodes are always connected. The efficiency of SFR backbones in sensor networks is measured on how long the backbone nodes remain connected for data delivery. Therefore, we consider network lifetime as the duration from the network deployment to the time at which the first backbone node dies in the network. The lifetime of a sensor network is expected to be high, indicating the ability of an event to report over the SFR-backbones. In these experiments, we have set the simulation parameters for varying sink speeds and different sizes of networks, respectively, as similar as described in the corresponding Sections 3.12.3.1 and 3.12.3.2, to investigate the effects on *network lifetime* of the studied state-of-the-art-works.

1. *Network lifetime for varying sink speeds*

   The results, as illustrated in Fig. 3.31, show that the *network lifetime* increases steadily with the sink speed up to $3ms^{-1}$ in all the studied protocols. But for higher speeds of the sink, *network lifetime* decreases sharply due to notifying the mobile-sink location more frequently to all other backbone nodes, and thus it increases energy consumption than that of moderate sink speeds. The *network lifetime* for all variants of SFR backbones is better than those of Ring and HexDD routing strategies because of avoiding unnecessary broadcasting for sink location updating through sensor nodes (in ring), or to transmit data over only three principal diagonals (in HexDD) protocols.

   Moreover, the improved Starfish routing backbones, e.g., *iSFR-circular* and *iSFR-elliptical*, have higher network lifetime than its basic one, e.g.,

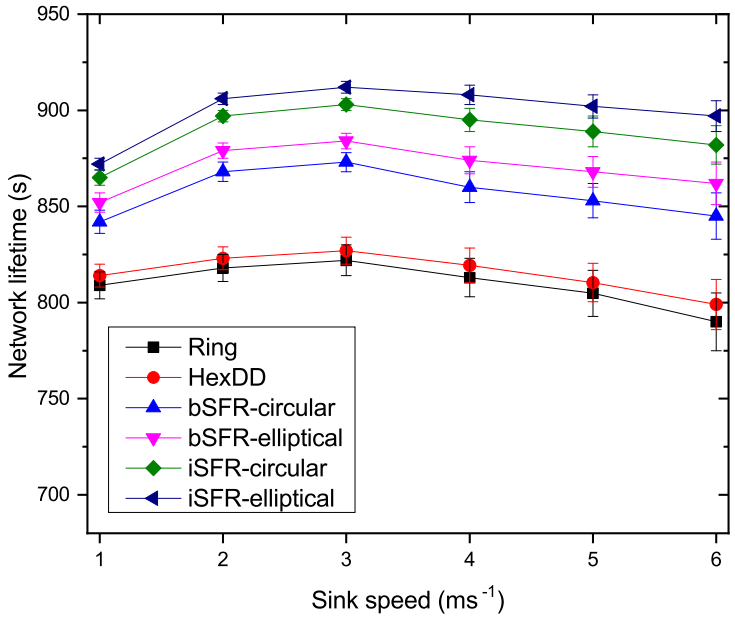

Figure 3.30: Network lifetime for varying speeds of the mobile sink

bSFR-circular and *bSFR-elliptical*, due to significant reduction of energy wastage from collisions and interferences near *ring-canal* of the network.

Furthermore, from the experimental results in Fig. 3.31, it is clearly observed that elliptical ring-canal based SFR-backbone architectures, e.g., *iSFR-elliptical* and *bSFR-elliptical*, respectively outperform *iSFR-circular* and *bSFR-circular*, due to optimally fitted ring-canal on the iSFR-elliptical in the network.

2. *Network lifetime for varying sizes of networks*

The graphs of Fig. 3.32 depict that the *network lifetime* steadily decreases in all the studied protocols, e.g., HexDD and Ring, with increasing size of networks. This happens because more hops are required to deliver data packets for a larger network, and thus backbone nodes on the *ring-* and *radial-canals*

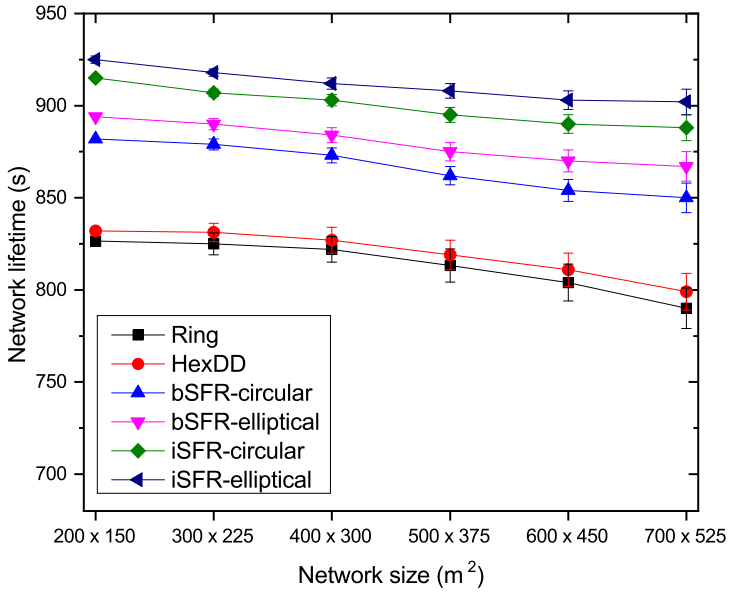

Figure 3.31: Network lifetime for varying sizes of networks

consume more energy than that of smaller networks.

Moreover, the improved Starfish routing backbones, e.g., *iSFR-circular* and *iSFR-elliptical*, have higher network lifetime than its basic one, e.g., *bSFR-circular* and *bSFR-elliptical*, for the similar reasons as discussed above. Furthermore, from the experimental results in Fig. 3.32, it is clearly observed that the iSFR-elliptical backbone outperforms *iSFR-circular*, *bSFR-circular*, and bSFR-elliptical because of optimal size of the ring-canal in the network.

3.12.3.4 Effects on standard deviation of residual energy

In the previous section, we studied network lifetime performances. What the key influences of the Starfish routing backbones are to improve the lifetime of sensor networks are further investigated in this section. It is noteworthy to state that the

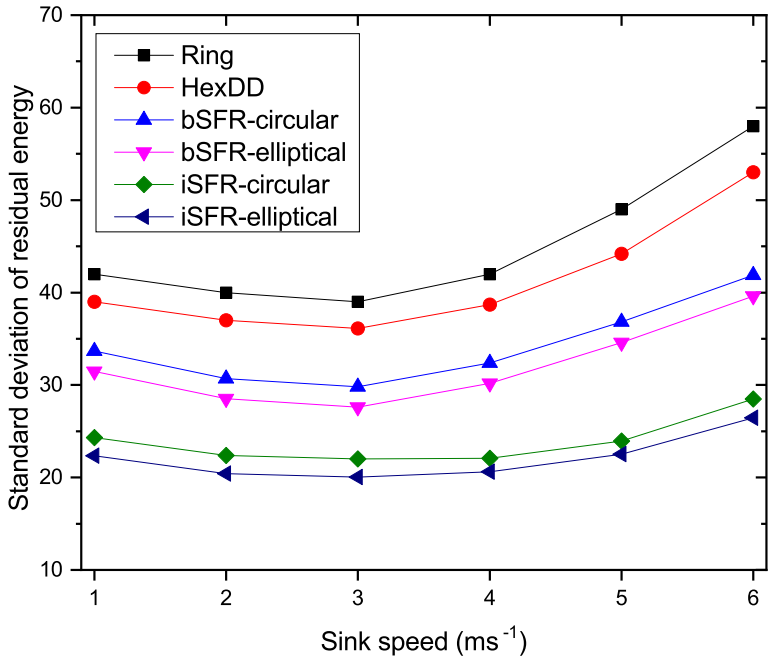

Figure 3.32: Standard deviation of residual energy for varying speeds of the sink

SFR architectures distribute backbone nodes over the *ring-canal* and *radial-canals* to ensure uniform energy consumption throughout the network. This is why we investigated the standard deviation of residual energy of backbone nodes while it is encountered the first backbone node is dead.

In these experiments, we have set the simulation parameters for varying sink speeds and different sizes of networks, respectively, as similar as described in the corresponding Section 3.12.3.1, and Section 3.12.3.2, to investigate the effects on *standard deviation of sensor's residual energy* of the studied state-of-the-art-works.

1. *Sensor's energy-deviation for varying sink speeds*

   The *standard deviation of residual energy*, as shown in Fig. 3.33, is decreased

for all the studied backbone strategies while the sink speed is around $3ms^{-1}$. It happens due to the fact that the sink mobility significantly reduces long-distance packet transmission or minimizes the average hop distance of the packets. However, the deviations start to increase when the sink speed exceeds $3ms^{-1}$ due to notifying the mobile-sink location more frequently to all other backbone node or excessive energy consumption for propagating extra messages to retrace the mobile sink.

In the results, we find that the *standard deviations of residual energy* for all variants of *Starfish routing (SFR) backbones* are the lowest comparing to HexDD [39] and Ring [40] strategies. This is caused due to distributing routing loads to many backbone nodes, e.g., *ring-canal* and *radial-canals*, in all variants of SFR architectures. It implies that energy consumption is rationally distributed among the nodes throughout the network. This operational philosophy influences achieving the lowest energy deviations of sensors (specially backbone nodes) for all variants of SFR architectures. Besides, sink mobility provides globally less energy consumption, and thus it has a great impact to increase network lifetime for Starfish routing backbones, as described in Section. 3.12.3.3.

Moreover, for the improved Starfish routing backbones, e.g., *iSFR-circular* and *iSFR-elliptical*, *standard deviations of residual energy* is lower than basic Starfish routing backbones, e.g., *bSFR-circular* and *bSFR-elliptical*. This performance proves the significant benefits of iSFR backbone architecture over bSFR ones due to preventing convergence of all radial-canals to the centra ring-canal.

Furthermore, it is noteworthy that the energy-deviation of iSFR-elliptical

architecture outperforms that of iSFR-circular and bSFRs because of developing an optimal elliptical ring-canal in the network. These experimental results strengthen the formation of the iSFR-elliptical backbone in sensor networks to extend network lifetime through balanced energy consumption.

2. *Sensor's energy-deviation for varying sizes of networks*

   The *standard deviations of residual energy* is increased linearly for all the studied backbone strategies, e.g., Ring and HexDD, with increasing size of networks, as shown in Fig. 3.34. This happens due to increasing energy expenditure for longer hop distances between the source to the sink. Besides, it is noticed that all variants of the *Starfish routing backbone* exhibit lower *standard deviations of residual energy* compared to the state-of-the-art works because of balanced energy consumption throughout the network. This proves the scalability of *Starfish routing backbones* to enhance network lifetime for very large sensor networks.

   In the case of the improved Starfish routing backbones, e.g., *iSFR-circular* and *iSFR-elliptical*, *standard deviations of residual energy* is lower than basic Starfish routing backbones, e.g., *bSFR-circular* and *bSFR-elliptical*. This performance proves the significant benefits of iSFR over bSFR due to avoiding the convergence of radial-canals to the ring-canal on SFR architectures. Furthermore, it has already been discussed that the elliptical ring-canal-based SFR architectures outperform all studied protocols because of forming an optimal elliptical ring-canal in the network. The lowest standard deviations of residual energy of the *iSFR-elliptical* show its strength to significant improvement of network lifetime.

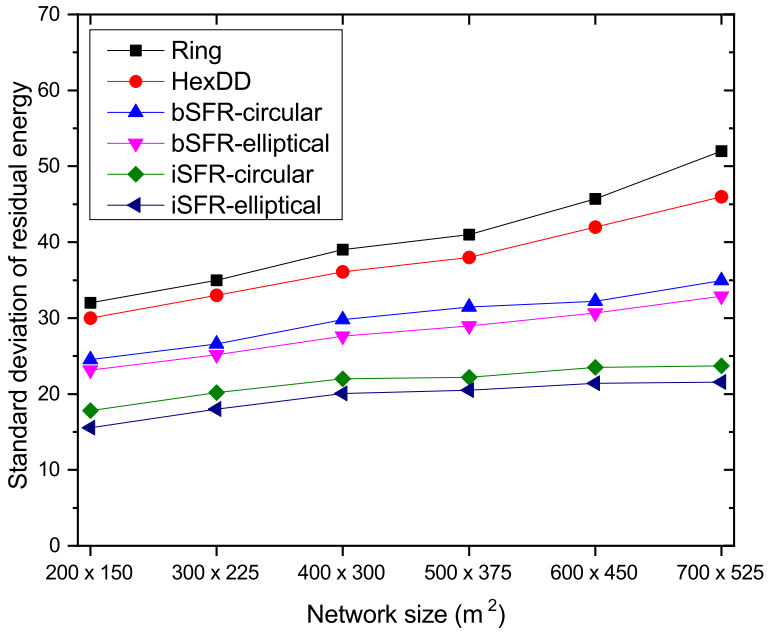

Figure 3.33: Standard deviation of residual energy for varying sizes of networks

These experimental results substantiate the efficiency of *Starfish routing backbone* over HexDD and Ring backbones to achieve extended network lifetime through minimizing energy-deviations in the network.

3.12.3.5 Impacts of varying sizes of ring-canal

We evaluated the performances of the proposed bSFR-circular routing backbone for varying sizes of control variable, ϕ, to investigate the impact of increasing sizes of ring-canal on network performances and lifetime performances. In this experiment, we varied the value of ϕ from 0.1 - 3.0, and the network area was fixed at 700×525 m^2 [110], [114].

The results, as shown in Fig. 3.34, depict that *average throughput* increases with the growing values of ϕ. But for higher values of ϕ, while it is around the

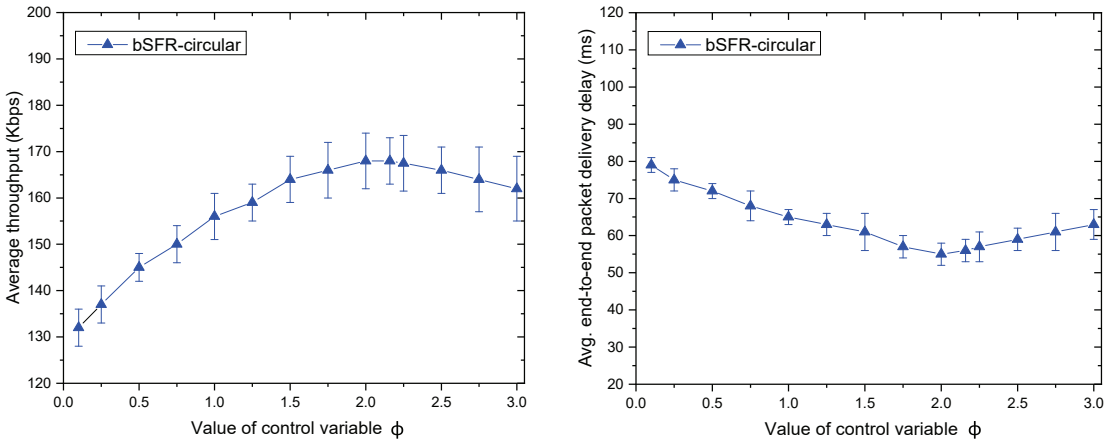

(a) Data throughput (b) End-to-end delay

Figure 3.34: Impacts of varying values of ring-canal control variable, ϕ

optimal value of ϕ, *average throughput* decreases monotonically.

From the simulation results, we also investigated average end-to-end data delivery delay. In Fig. 3.34, initially, end-to-end delay decreases around the optimal value of ϕ, and, later, it starts increasing steadily for larger value of ϕ greater than the optimal value of ϕ.

On the other hand, the *network lifetime* also increases with the rising values of ϕ. But for higher values of ϕ, while it is near to the optimal value of ϕ, *network lifetime* decreases monotonically.

Finally, from these experimental results for varying sizes of ring-canal, it is clearly observed that the optimal size of the ring-canal in a network has significant impact on network performances as well as network performances. The results prove the strength of the optimization model to determine the optimal values of the control value ϕ for a given network.

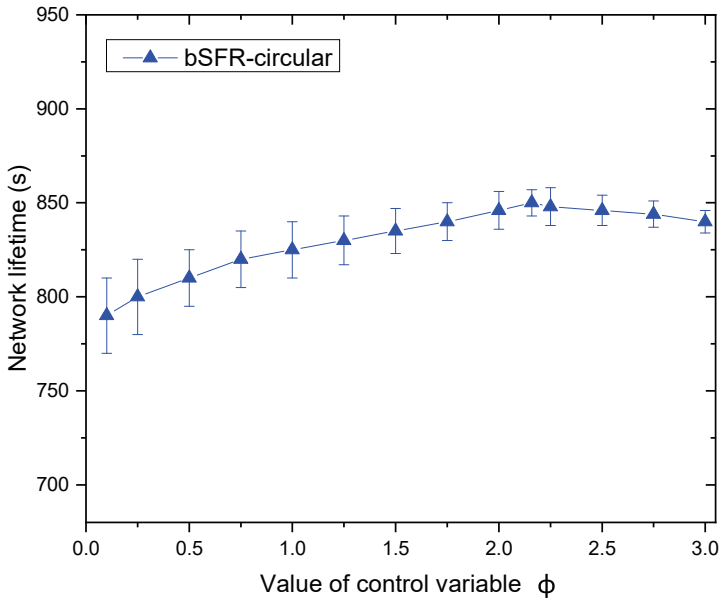

Figure 3.35: Network lifetime for varying values of ϕ

3.13 Summary

In this chapter, we have developed the *Starfish (SFR) routing* backbone for sensor network that can minimize the *end-to-end data delivery delay* and extend *network throughput* and *lifetime*. The distributed backbone-nodes over *ring-* and *radial-canals* on the *Starfish routing backbone* significantly contribute to increase the *network performances* as well as *network lifetime*. Moreover, the dynamic scalability of the *ring-canal* size and the number of *radial-canals* is maintained based on the *transmission range* of sensor nodes and the size of *network area*. The above key characteristics of the *Starfish routing backbone* significantly outperform the state-of-the-art works.

The experimental results, as summarized in the Table 3.7, presented the performance improvements of the proposed SFR backbone over the state-of-the-art works

Table 3.7: Performance improvements of the proposed SFR backbone over the state-of-the-art works

	Ring [40]		**HexDD [39]**	
Control variable	Area	Speed	Area	Speed
Data throughput	+15.68 %	+17.28 %	+11.82 %	+12.94 %
Packet delivery ratio	+5.21 %	+6.23 %	+3.68 %	+4.79 %
End-to-end delay	-33.20 %	-32.08 %	-28.37 %	-26.96 %
Operational overhead	-55.75 %	-59.58 %	-52.34 %	-55.38 %
Network lifetime	+12.05 %	+11.13 %	+11.17 %	+10.31 %
Stdev. of residual energy	-51.71 %	-50.62 %	-47.71 %	-46.31 %

(e.g., Ring and HexDD routing strategies) based on the evaluation metrics for varying size of networks and sink speeds. These results substantiate the efficiency of *Starfish routing backbone* over state-of-the-art works.

Chapter 4

Maximizing Lifetime of Starfish Routing Backbone

In this chapter, we formulate an optimization framework for maximizing lifetime of an obstructed sensor network containing Starfish routing (SFR) backbone along with necessary theoretical proofs and experimental results.

4.1 Introduction

In this era of Industry 4.0 [10], [11], sensor networks play important roles in collecting data from wide-range of real-time applications, including industrial process monitoring, nuclear power plant monitoring [2], precision agriculture, smart grid [3], big-data gathering, e-health [15], etc. In the upcoming years, the sensed data will lead to developing embedded intelligent systems for most industrial and domestic applications [113], [124], [125]. The efficiency of these real-time applications highly depends on delivering data within the bounded delay deadline and minimizing end-to-end data delivery delay. Consequently, sensor networks inherently focus on efficient data routing so that energy consumption is minimized and network lifetime is maximized. In mobile-sink based sensor networks, the sink typically col-

lects data traveling across the network, and this technique has already been proven not only to enhance the network lifetime but also to minimize average end-to-end data collection latency to a great extent compared to its static counterpart [26], [27]. However, still, there is room to optimize the network lifetime further while maintaining delay deadlines for real-time applications.

The problem of maximizing the lifetime of sensor networks has been well studied in the literature [92], [103]. The primitive strategies follow optimal coverage and connectivity [104], opportunistic transmission schemes, dynamic beam-forming [105] [106], etc. Further improvement of network lifetime is achieved through greedy energy-efficient routing, clustering techniques, and machine learning approaches [107], etc. Though the strategies can achieve an extended network lifetime, they lack delay deadlines for real-time applications. In the literature works, data collection strategies using a mobile sink are broadly grouped into two categories: *direct-contact based* and *rendezvous-node based*. In the former strategy [18], [19], [28], the mobile sink periodically travels to all source sensor nodes and collects sensed data directly from them. Even though this strategy can completely avoid message-relay overheads and increase network lifetime, the strategy sacrifices application delay-deadline. Therefore, it's not suitable for real-time data collection applications. Moreover, it increases the traveling path length for the mobile sink, causing higher data delivery latency.

On the other hand, in *rendezvous-node based* data collection strategy [29], [30], [31], a mobile sink only visits and collects data from a few rendezvous nodes over a designated tree-like backbone [90], cluster-heads [91], [93] or routing-backbones (e.g., Fish-bone [41], Honeycomb [83], etc.), instead of visiting all sensor nodes in the network. However, both strategies have considered the random sink mobility

model rather than finding an efficient data collection scheduling based on data arrival rate, sojourn duration at rendezvous nodes, etc.

Moreover, exhaustive visits through all rendezvous nodes on cluster-heads or backbone nodes also become infeasible for real-time applications due to violation of application delay-deadline. Thus, the problem of determining an optimal set of rendezvous nodes together with sojourn duration at each of them aiming to maximize network lifetime for a time-constraint application is still challenging. Moreover, the presence of obstacles in the network and heterogeneous data generation rates of sensor nodes, a data collection strategy that might further enhance network performances and lifetime of the network, has not yet been well-explored in the literature. Therefore, it necessitates developing a data collection scheduling for a real-time application in an obstructed network aiming to maximize network lifetime. It is noteworthy that an obstructed network may contain a building, tree, pond, lake, forest, mountain, etc. For this reason, we concentrate on exploring efficient data collection scheduling to maximize network lifetime, ensuring uniform energy consumption throughout the network for a real-time application.

In this Chapter, we develop a novel data collection scheduling, namely *Starfish*, for a mobile sink in an obstructed sensor network adopting a Starfish routing (SFR) backbone that spreads backbone nodes throughout the network to achieve single-hop accessibility from any source node. The proposed a Starfish data collection schedule addresses the problem of determining an optimal set of backbone nodes over the SFR backbone, together with corresponding sojourn durations to maximize network lifetime. This mechanism is also driven by time-constraints of underlying applications and data generation rates around the backbone nodes. The key contributions of this work are summarized as follows:

- We formulate the problem of maximizing the lifetime of an obstructed network as a mixed-integer linear programming (MILP) that finds an optimal set of rendezvous nodes along with corresponding sojourn durations.
- The proposed Starfish data collection schedule of a mobile sink maintains applications requirements on end-to-end data delivery delay.
- It also guarantees loop-free travel-scheduling among the rendezvous nodes, ensuring balanced energy consumption as well as reduced data delivery delay.
- An experimental analysis, performed in network simulator (e.g., NS-2) [48], shows significant performance improvements on network lifetime, end-to-end delay, data throughput over the state-of-the-art works.

Fig. 4.1 presents the major phases Starfish data collection scheduling to maximize network lifetime throughout the Chapter. The chapter is organized as follows. In Section 4.2, we focus on the issues that are to be addressed to maximize the network lifetime. Then, we discuss the network model in an obstructed environment, assumptions, energy model, etc., in Section 4.3. After that, we develop lifetime maximization franework through the proposed Starfish data collection scheduling of a mobile sink in the obstructed network in Section 4.4. The Section 4.5 discusses on the performance evaluation results, and finally, we conclude the Chapter in Section 4.6.

4.2 Problem Statement

The problem of maximizing the lifetime of sensor networks for a time-constraint application is still challenging. Moreover, the presence of obstacles in the network

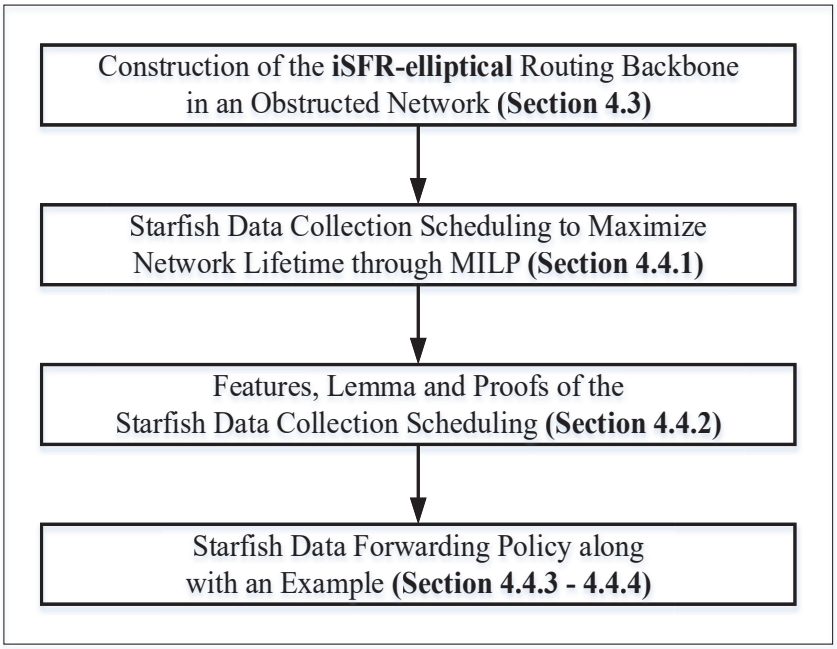

Figure 4.1: Block diagram of the Starfish Scheduling to maximize network lifetime

and heterogeneous data generation rates of sensor nodes become more complicated to maximize network lifetime. In such a network environment, this is crying necessity to develop an efficient data collection scheduling for a real-time application to extend network lifetime. The key factors to maximize network lifetime are to ensure uniform energy consumption and sink's data collection schedule jointly based on data generation rates throughout the network. Therefore, we maintain uniform energy consumption throughout the network by adopting Starfish routing backbone with an elliptical ring-canal (iSFR-elliptical), as developed in Chapter 3, in an obstructed network.

Therefore, we determine an optimal set of rendezvous nodes and corresponding sojourn durations to maximize network lifetime. This mechanism is also driven by

the time constraints of underlying applications and data generation rates around the backbone nodes. In other words, the network lifetime maximization problem is translated as maximizing sojourn durations over an optimal set of sojourn locations in the network, maintaining the application's delay-deadline, data generation rates, and sensor's residual energy. In the subsequent sections, we discuss network model followed by Starfsih data collection scheduling with a mobile sink.

4.3 Network Model and Assumptions

This section introduces the network model of an obstructed sensor network of $2a \times 2b\ m^2$ $(a \geq b)$ area with network-center at (u, v), as shown in Fig. 4.2. Here, obstacle means a bounded area in a sensor network across which a mobile sink cannot travel (e.g., forest, ponds, hills, mountains, etc.). The network contains a mobile sink (acts as a central controller) that travels throughout the network to collect sensed data from nodes. We assume, $\mathbb{N}$ is the set of stationary sensor nodes in the network, each having initial residual energy ε^0, and transmission range r $(0 < r < b)$. Since connectivity among sensor nodes and mobile sink needs to be guaranteed to receive all sensed data for future processing, we have adopted one of the SFR vatiants, namely iSFR-elliptical backbone in the obstructed network that is discussed in brief as follows.

4.3.1 iSFR-elliptical backbone in an obstructed network

The detailed construction procedures of the improved Starfish routing backbone with an elliptical ring-canal (iSFR-elliptical) is discussed in the previous Chapter 3. We recall that the iSFR-elliptical backbone consists of *ring-canal* nodes ($\mathbb{Z}$) and

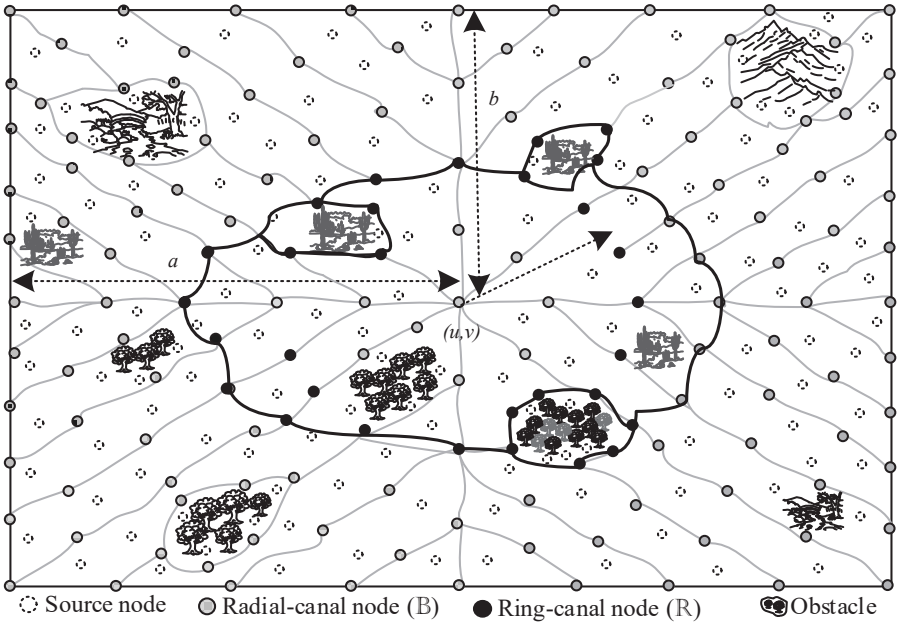

Figure 4.2: Network model and SFR backbone in an obstructed-network

radial-canal nodes ($\mathbb{B}$). The *ring-canal* nodes (e.g., $\mathbb{Z} \subset \mathbb{N}$) are selected every r distance interval over optimal elliptical ring-canal. In the case of *radial-canals*, at first, a few designated nodes are chosen every $2r$ distance away along principal-axes. Then the *radial-canals* are prolonged toward the edge of the network parallel to both principal-diagonals. Finally, the radial-canal nodes (e.g., $\mathbb{B} \subset \mathbb{N}$) are selected over principal axes, principal diagonals, and all radial-canals approximately every r distance away; and thereafter these nodes are connected to construct the iSFR-elliptical backbone. Since the network model contains obstacles in the network, the central controller selects backbone nodes for both ring-canal and radial-canal surrounding the obstacle following the obstacle-detection strategy, as described in [23].

Table 4.1: Notations for the Starfish data collection scheduling

Symbols	**Descriptions**
$2a \times 2b$	Network area
$\mathbb{N}$	Set of all sensor nodes
r	Transmission range of a sensor node
R	Optimal radius of the ring-canal
T	Minimum value of application delay-deadline
C	Set of cycles be completed by mobile sink
D^c	The worst-case end-to-end delay of a packet in a cycle c
σ_m^c	Data arrival rate at sojourn location m in cycle c
S_m^c	Sojourn duration at m in a cycle c
$\mathbb{B}$	Set of nodes on radial-canal
$\mathbb{Z}$	Set of nodes on the ring-canal
$\mathbb{R}^c$	Power set on ring-canal nodes $\mathbb{Z}$ during cycle c
$\mathbb{M}_n^c$	Set of optimally selected sojourn locations during cycle c
ε_m^0	Initial residual energy of a node
e_m^c	Total energy required at m in cycle c
E	Energy expenditure to transmit one bit of data
$\tilde{E}$	Energy expenditure to receive one bit of data
q_m^c	Bit-length of a packet at m in cycle c
A^c	Set of sink's traveling-arcs in cycle c
f_{lm}^c	A variable determining sink from l to m at cycle c
h_m^c	A variable determining sink's sojourn at m in a cycle c
$\overline{\delta}$	The expected end-to-end delay per hop for a packet
H^c	Hop-distance for a packet in a cycle c
$\rho_{H^c}^{z^c}$	Inter-hop transition probability of a packet

4.3.2 Energy model

In this work, we consider the classic energy consumption model for a sensor node, as described in [59] [101]. Since most of the energy is dissipated during transmitting and receiving states of a node, the energy consumption for transmission (E) and reception ($\tilde{E}$) for l-bit message over a distance d is measured as follows.

$$E(l,d) = E_{transmit}(l,d) = \begin{cases} l\xi_{elec} + l\xi_{fs}d^2 & \text{if } d < d_0 \\ l\xi_{elec} + l\xi_{amp}d^4 & \text{if } d \geq d_0 \end{cases} \tag{4.1}$$

$$\tilde{E}(l) = E_{receive}(l) = l\xi_{elec} \tag{4.2}$$

In the equations, ξ_{elec}, ξ_{fs}, and ξ_{amp} represent energy dissipated by the electronic circuit, required power for amplification in free space, and for multipath attenuation model, respectively. The electronics energy depends on the factors such as digital coding, modulation, etc. If the transmission distance d is less than the threshold value d_0, as considered a boundary value between free space and multipath, the power amplification loss adopts as a free space model. On the other hand, if the transmission distance is greater than or equal to the threshold value d_0, the multipath attenuation model is adopted.

The details of the proposed optimal data collection scheduling, namely *Starfish data collection scheduling*, are explained to maximize network lifetime and improve data collection efficiency in Section 4.4. The symbols and notations are summarized in Table 4.1.

4.4 Starfish Data Collection Scheduling

In this section, we develop an optimal data collection scheduling of a mobile sink so that lifetime of a sensor network can be maximized while maintaining application delay-deadline. In the network, a mobile sink visits any set element of $\mathbb{R}^c$ in each cycle $c \in C$, where $\mathbb{R}^c$ denotes the power set on $\mathbb{Z}$ ($i.e., \mathbb{R}^c = P(\mathbb{Z})$), and $C = \{0, 1, 2, \dots\}$. This choice is motivated by the fact that data collection over the optimal size of elliptical-canal of iSFR-elliptical backbone offers minimum energy expenditure in the network, as explained Chapter 3. Moreover, the computational complexity of finding optimal sojourn locations over the elliptical ring-canal nodes would be less compared to that when all nodes are explored. The following subsections describe the *Starfish data collection scheduling* in detail.

4.4.1 Optimal data collection scheduling to maximize lifetime

In the proposed scheduling, we assume, a mobile sink sojourns (or halts) at sojourn location $m \in \mathbb{M}_n^c$ and $\mathbb{M}_n^c \in \mathbb{R}^c$ for a duration of S_m^c in a cycle c, where $n = \{1, 2, \dots, |\mathbb{R}^c| - 1\}$. Since the network contains obstacles among nodes, arc set is defined as follows, $A^c = \{(l, m) : f_{lm}^c = 1\}$, where $f_{lm}^c = 1$ indicates that there exists a traveling path avoiding obstacles between sojourn locations $l \in \mathbb{M}_n^c$ and $m \in \mathbb{M}_n^c$ in a cycle $c \in C$; 0 otherwise. The sojourn duration of the mobile sink at a rendezvous node in a particular cycle depends on the data arrival rate. Here, sojourn locations are those that are optimally selected among rendezvous nodes in a cycle. We assume σ_m^c and S_m^c are, respectively, the data arrival rate, and the sojourn duration at corresponding location $m \in \mathbb{M}_n^c$ in a cycle $c \in C$. The sojourn

duration S_m^c is measured as follows,

$$S_m^c = \frac{\sigma_m^c}{\sum_{j \in \mathbb{Z}} \sigma_j^c} \times \ D^c, \ \forall c \in C, \forall m \in \mathbb{M}_n^c \tag{4.3}$$

where D^c is the worst-case end-to-end data collection latency from the farthest source node of the network to the mobile sink for any cycle c. Since the central controller is aware of both data arrival rate at each rendezvous node on the ring-canal and sink travels around the preformed ring-canal, it can determine the worst-case end-to-end delay D^c for a network instance [110]. To support real-time applications, the worst-case end-to-end delay D^c for a cycle cannot exceed the minimum value of application delay-deadline T (i.e., $D^c \leq T$).

Now, we assume ε_m^c be the residual energy of a rendezvous node $m \in \mathbb{M}_n^c$ at a particular cycle $c \in C$. While routing data, a node requires energy E and $\tilde{E}$ for transmitting and receiving each bit, respectively. Therefore, the total energy required by a rendezvous node $m \in \mathbb{M}_n^c$ during sojourn period S_m^c can be computed as,

$$e_m^c = S_m^c \cdot \sigma_m^c \cdot q_m^c \cdot (E + \tilde{E}), \ \forall m, \ \forall c, \tag{4.4}$$

where q_m^c is the bit-length of a packet. While selecting a sojourn location $m \in \mathbb{M}_n^c$ in a cycle c, its residual energy ε_m^c must be greater than the required energy e_m^c. At the end of a cycle, the residual energy of a rendezvous node is updated as, $\varepsilon_m^{c+1} = \varepsilon_m^c - e_m^c$. At the initial cycle, i.e., $c = 0$, ε_m^0 is considered as the initial residual energy and energy expenditure, $e_m^0 = 0$.

The key objective of the proposed *Starfish data collection scheduling* is to maximize network lifetime that is translated as maximizing sojourn duration over the optimal set of rendezvous nodes of the Starfish routing backbone. A rendezvous node is interpreted as a sojourn location when the mobile sink halts

for a certain duration to collect data. We maximize total duration to maximize the network lifetime since the sink's data collection lasts until the network is dead. The objective function and the constraints of the mixed-integer linear program (MILP) are formulated as follows.

Maximize :

$$L = \underset{\mathbb{M}_n^c \in \mathbb{R}^c}{\operatorname{argmax}} \sum_{\forall c \in C} \sum_{\forall m \in \mathbb{M}_n^c} S_m^c, \tag{4.5}$$

subject to,

$$e_m^c < \varepsilon_m^c, \quad \forall c \in C, \ \forall m \in \mathbb{M}_n^c \tag{4.6}$$

$$\sum_{m \in \mathbb{M}_n^c} e_m^c h_m^c / S_m^c < \sum_{m \in \tilde{\mathbb{M}}_n^c} e_m^c h_m^c / S_m^c, \forall c, \forall \tilde{\mathbb{M}}_n^c \tag{4.7}$$

$$h_m^c \in \{0, 1\}, \ \forall c \in C \tag{4.8}$$

$$D^c \leq T, \ \forall c \in C \tag{4.9}$$

$$\begin{gathered} \mathbb{P}^c(j \overset{k}{\rightsquigarrow} m) = True, \forall j \in \mathbb{Z} \cup \mathbb{B}, \exists k \in \mathbb{Z} \cup \mathbb{B} \cup \emptyset, \\ \exists m \in \mathbb{M}_n^c, \forall c \in C \end{gathered} \tag{4.10}$$

$$\begin{gathered} w_l^c - w_m^c + |\mathbb{M}_n^c| \cdot f_{lm}^c \leq |\mathbb{M}_n^c| - 1, \ \forall (l, m) \in A^c, \\ \forall c \in C \end{gathered} \tag{4.11}$$

$$0 \leq w_l^c < w_m^c, \ \forall c \in C \tag{4.12}$$

$$f_{lm}^{c} \in \{0,1\},\ \forall c \in C \tag{4.13}$$

Here, Eq. (4.5) is the objective function, and Eq. (4.6) - Eq. (4.13) are the constraints. The **objective function** schedules the mobile sink so that it can maximize network lifetime L, which is translated as finding out optimal sets of rendezvous nodes $\mathbb{M}_n^c$ to maximize sojourn durations for allowable cycle $c \in C$. In the objective function, sojourn duration S_m^c is related to the data arrival rate at that location in a cycle c that is measured following Eq. (4.3).

We formulate the network lifetime maximization problem in the MILP framework in such a way that the mobile sink persistently travels over sojurn locations until the residual energy of the corresponding backbone node is exhausted. The **energy constraint** in Eq. (4.6) finds candidate RNs on the ring-canal to be selected as a sojourn location, if and only if energy expenditure e_m^c in a cycle c is less than the remaining residual energy ε_m^c of the node. At the end of a cycle, residual energy of RNs is updated as $\varepsilon_m^{c+1} = \varepsilon_m^c - e_m^c$ in order to discover its feasibility to be a sojourn location in the next cycle.

The **energy efficiency constraint** in Eq. (4.7) helps us to single out all the alternative paths that are not as energy-efficient as the selected one $\mathbb{M}_n^c$ in a cycle. In Eq. (4.7), the set of all alternative paths $\tilde{\mathbb{M}}_n^c \in \tilde{\mathbb{R}}^c$ and $\tilde{\mathbb{R}}^c = \{\mathbb{R}^c \setminus \mathbb{M}^c\}$. Both constraints in Eq. (4.6) and Eq. (4.7) force to select a set of energy-efficient rendezvous nodes as sojourn locations for a cycle c so that energy consumption is minimized per unit time. Moreover, as there exists at least one energy-efficient path during data collection for each cycle, the lifetime of the network is maximized for all completed cycles. Eq. (4.8) defines a **binary variable** h_m^c that determines whether the mobile sink sojourns at m in a cycle c or not. Therefore, the constraints in Eq. (4.6) - Eq. (4.8) jointly select $\mathbb{M}_n^c$ among ring-canal nodes in the

network.

The **quality of service (QoS) constraint** in Eq. (4.9) ensures that the worst-case end-to-end delay D^c for a cycle cannot exceed the minimum value of application delay-deadline T. The worst-case end-to-end delay D^c is bounded by hop-distance $H^c_{min} \leq H^c \leq H^c_{max}$ that is estimated using Lemma 3 in the light of detailed analysis stated in Section 3.11. This QoS constraint guarantees the effectiveness of the data collection schedule for a real-time application in the network.

The **connectivity constraint** in Eq. (4.10) ensures that there exists at least one path from any backbone node $j \in \mathbb{Z} \cup \mathbb{B}$ to a sojourn location $m \in \mathbb{M}^c_n$, either directly or via a forwarding backbone node $k \in \mathbb{Z} \cup \mathbb{B}$. Since there exists a Starfish routing backbone in the network and it guarantees single-hop connectivity of at least one backbone node from any source node, the connectivity constraint in Eq. (4.10) holds until the network is dead.

In the network, the mobile sink travels to the selected sojourn locations over the elliptical-canal nodes, where sub-loop nodes may exist due to the presence of obstacles. Therefore, the **sub-tour prevention** constraints in Eq. (4.11) and Eq. (4.12) jointly determine the order of visiting sojourn locations and ensure that no sub-tour would be formed among the sojourn locations.

At last, f^c_{lm} in Eq. (4.13) represents a **binary variable**, used in Eq. (4.11), that determines whether the mobile sink travels from sojourn location l to m among backbone nodes during path selection. Therefore, if $f^c_{lm} = 1$, then $w^c_l < w^c_m$. Since each sojourn location $m \in \mathbb{M}^c_n$ is associated with a weight $w^c_m > 0$ and an increasing weight (i.e., $w^c_l < w^c_m$) is maintained for each visiting sojourn location, it inherently prevents forming any sub-loop of a path for the mobile sink during traveling sojourn locations.

Finally, the formulation maximizes sojourn duration over the optimal set of sojourn locations for a maximum number of cycles until the residual energy of iSFR-elliptical backbone nodes is exhausted. This inherently helps to achieve an extended network lifetime during data collection in the network.

4.4.2 Features of the proposed scheduling

In this subsection, we explain different characteristics of the proposed *Starfish schedule*. We analyze the worst-case end-to-end data delivery delay using Lemma 3, and Lemma 4, in the light of end-to-end delay analysis formulated in the Section 3.11. Since the network may contain sub-cycle nodes on the ring-canal due to the presence of obstacles, the proposed *Starfish scheduling* could be inefficient if the mobile sink travels over sub-cycles. Therefore, we present Lemma 5 to prove that the MILP model avoids sub-loop among the sojourn locations for any cycle c. Finally, Lemma 6 proves that the selected set of sojourn locations $\mathbb{M}_n^c$ for a cycle c over the iSFR-elliptical backbone is optimally selected.

Lemma 3. *For a given network* $2a \times 2b$ $(a \geq b > r)$ *containing a SFR-circular backbone and sensor nodes with transmission range* r*, the extreme hop-distance* H^c *is bounded by* $\lceil (b-R)/r \rceil \leq H^c \leq \lceil (\sqrt{a^2+b^2} + R(\pi - 1))/r \rceil$ *for a data packet.*

Proof. In the network, the minimum hop distance of a packet to the ring-canal typically exists along the minor axes. Thus, the minimum hop distance is bounded by $H^c_{min} = \lceil (b-R)/r \rceil$, since $b \leq a$. Accordingly, the maximum hop distance from the farthest node (e.g., the corner node of the network) to the mobile sink is typically bounded by two reference distances, e.g., corner node to the ring-canal node, and then to the farthest opposite node around the ring-canal. The longest distance from the corner node to the ring-canal lies along the principal diagonal

that is approximated around $\sqrt{a^2+b^2}-R$. Meanwhile, since the sink visits around the ring-canal, the longest traveling path to the farthest opposite node is estimated as half-perimeter of the ring-canal, i.e., πR. Therefore, the maximum hop-distance H^c_{max} is estimated as $\sqrt{a^2+b^2}-R+\pi R$, and thus the extreme hop-distance for a packet is bounded by $\lceil (b-R)/r \rceil \leq H^c \leq \lceil (\sqrt{a^2+b^2}+R(\pi-1))/r \rceil$, and hereby, Lemma 3 is proved. □

Lemma 4. *Given that $\overline{\delta}$ is the expected end-to-end data delivery delay of a packet for one hop (including medium access, processing, queuing delay, propagation, transmission, retransmission) in a network, then the worst-case end-to-end data delivery delay $D^c = \overline{\delta^c} \times H^c_{max}$ for a packet traveling H^c_{max} hop in a cycle $c \in C$.*

Proof. Since the network contains obstacles, the end-to-end delay (i.e., δ) of a packet greatly depends on both hop-distance from the source node to the mobile sink and the number of retransmission(s) at each hop.

To prove the Lemma 4, in the light of Section refsec:ch3theorymodel, we assume $\rho^{z^c}_{H^c}$ be the inter-hop transition probability of a packet in a Markov chain model for a cycle c, where hop $H^c \in \{1, 2, \ldots, H_{max}\}$ and retransmission attempt per hop till success $z^c \in \{0, 1, 2, \ldots, \phi\}$. Therefore, the expected retransmission attempt for a packet is expressed as $\overline{z^c} = \sum_{z^c=0}^{\phi} z^c \rho^{z^c}_{H^c}$, and the expected delay is expressed as $\overline{\delta^c} = \delta\ \overline{z^c}$ for a packet.

Finally, the average end-to-end data delivery delay for a data packet traveling maximum H^c_{max} hops is expressed as $D^c = \overline{\delta}^c \times H^c_{max}$, which is bounded by extreme hop-distance H^c, as computed in Lemma 4, and thus it is proved. □

Lemma 5. *Given that $w^c_l \leq w^c_m$, as stated in Eq. (4.12), the optimal data collection scheduling of a mobile sink in the Starfish routing backbone is sub-cycle free for $l, m \in \mathbb{M}^c_n$ and $c \in C$.*

Proof. Suppose, for the sake of contradiction, the hypothesis is not true. Then there exists the constraint $w_l^c \leq w_m^c$ for which there is a sub-cycle between sojourn locations such that $\mathbb{M}_n^c = \{l, l_2, l_3, \ldots, m, l\}$ in a cycle c.

According to the constraint in Eq. (4.11) of the MILP formulation, the mobile sink travels from l to l_2 that follows $w_l^c \leq w_{l_2}^c$. Similarly, for the sub-cycle through $\{l, l_2, l_3, \ldots, m, l\}$, it also maintains $w_l^c \leq w_{l_2}^c \leq w_{l_3}^c \leq w_m^c \leq w_l^c$.

Now, as on hypothesis, since the mobile sink also travels from m to l maintaining $w_m^c - w_l^c + |\mathbb{M}_n^c| \cdot f_{ml}^c \leq |\mathbb{M}_n^c| - 1$, that gives $w_m^c \leq w_l^c - 1$. However, this contradicts the given fact $w_l^c \leq w_m^c$. Since we have arrived at a contradiction, our original supposition that there exists a sub-cycle between sojourn locations l and m in a cycle c could not be true.

Thus, the optimal data collection scheduling by mobile sink over the Starfish routing backbone is sub-cycle free for a particular cycle c, and hereby the Lemma 5 is proved. □

Lemma 6. *Given that* $\forall c\ \forall \tilde{\mathbb{M}}_n^c\ \sum_{m \in \mathbb{M}_n^c} e_m^c h_m^c / S_m^c < \sum_{m \in \tilde{\mathbb{M}}_n^c} e_m^c h_m^c / S_m^c$*, as stated in Eq. (4.7), the selected set* $\mathbb{M}_n^c \in \mathbb{R}^c$ *of sojourn locations for a cycle* c *over the Starfish routing backbone is optimal.*

Proof. Suppose, for the sake of contradiction, the hypothesis is not true. Then there exists an $\tilde{\mathbb{M}}_n'^c \neq \mathbb{M}_n^c$ that maximizes the sojourn duration S_m^c.

According to the MILP formulation, the key philosophy of energy efficiency constraint in Eq. (4.7) is to single out a set $\mathbb{M}_n^c$ from $\mathbb{R}^c$.

Now, as on hypothesis, for the selected set $\tilde{\mathbb{M}}_n'^c$ of rendezvous nodes for a cycle c, it maintains $\sum_{m \in \tilde{\mathbb{M}}_n'^c \in \tilde{\mathbb{R}}_n^c} e_m^c h_m^c / S_m^c < \sum_{m \in \mathbb{M}_n^c} e_m^c h_m^c / S_m^c$. However, this inequality contradicts according to the constraint in Eq. (4.7) to achieve maximum sojourn duration S_m^c for a particular cycle c simultaneously with $\mathbb{M}_n^c$, since $\tilde{\mathbb{M}}_n'^c \neq \mathbb{M}_n^c$ and

$\tilde{\mathbb{M}}_n'^c \in \tilde{\mathbb{M}}_n^c \in \tilde{\mathbb{R}}^c = \{\mathbb{R}^c \backslash \mathbb{M}_n^c\}$. Hence we have arrived at a contradiction, our original supposition that the selected set $\tilde{\mathbb{M}}_n'^c$ of rendezvous nodes is optimal in a cycle c could not be true simultaneously with any other alternative set of rendezvous nodes.

Therefore, the selected set $\mathbb{M}_n^c \in \mathbb{R}^c$ of rendezvous nodes for a cycle c over the Starfish routing backbone is optimal, and consequently, it is true for all cycle $c \in C$, and hereby the Lemma 6 is proved. □

Now, the data forwarding policy and an illustrative example of the proposed real-time data collection to maximize network lifetime are presented in the following sections, 4.4.3, and 4.4.4, respectively.

4.4.3 Data forwarding policy

After selection of an optimal set of sojourn locations following the above MILP framework, the mobile sink (or a central controller) notifies all nodes both the selected sojourn locations $m \in \mathbb{M}_n^c$ and corresponding sojourn duration S_m^c at the beginning of each cycle $c \in C$. Since the network runs real-time applications, it follows a continuous forwarding policy to send data to the mobile sink over ring-canal and radial-canal nodes of the Starfish routing backbone.

The key philosophy of the continuous forwarding policy employed by backbone nodes is to send data to the mobile sink immediately. If a source node senses data within the transmission range of a ring-canal node, it immediately forwards data to the nearest ring-canal node. Afterward, the ring-canal node takes responsibility to send data to the mobile sink. If any source node is out of transmission range of the ring-canal, it transmits data to the nearest radial-canal node; then, the node immediately forwards data to the closest ring-canal node. As soon as a ring-canal node collects data from the source nodes, or radial-canal nodes, or neighbor nodes,

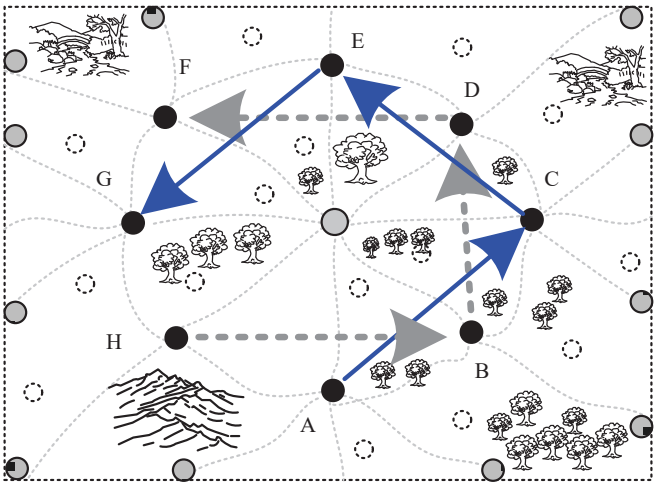

Figure 4.3: Data forwarding in obstructed network environment

it instantly forwards data over backbone nodes to the current sojourn location $m \in \mathbb{M}_n^c$ of the mobile sink for a cycle c. Here, we consider the shortest routing path in the network that is implemented in [110]. When a ring-canal node runs out of energy, it migrates the role to neighboring node(s), maintaining the circular property of the ring-canal. This continuous data forwarding policy minimizes end-to-end delay significantly, even in an obstructed network environment. The simulation results prove the efficiency of the proposed *Starfish scheduling* to maximize network lifetime that are explained in Section 4.5.

4.4.4 An illustrative example

We consider a set of rendezvous nodes $\{A, B, C, \ldots, H\}$ on the ring-canal, as shown in Fig. 4.3. Due to the presence of obstacles in the network, the mobile sink cannot travel to every rendezvous node from any of those. Table 4.2 shows the traveling route matrix of the mobile sink among the rendezvous nodes $\{A, B, C, \ldots, H\}$ in

the presence of obstacles. When the mobile sink halts at a sojourn location A, it can only travel either to C or H due to obstacles in the network. Similarly, in the case of halting at B, it can travel only to $\{D, F, H\}$. Now, the key philosophy of the proposed *Starfish* data collection scheduling is to determine the optimal set of sojourn locations based on data arrival rates, energy expenditures at corresponding rendezvous nodes so that the mobile sink can travel through a sub-loop free path. As an example, we consider the maximum delay-deadline of real-time application is $250ms$ and data arrival rates at corresponding rendezvous nodes $\{\sigma_A^c, \sigma_B^c, \sigma_C^c, \ldots, \sigma_H^c\}$ are tabulated in Table 4.3.

Table 4.2: Traveling route matrix for mobile sink

	A	B	C	D	E	F	G	H
A	-	0	1	0	0	0	0	1
B	0	-	0	1	0	1	0	1
C	1	0	-	0	1	0	1	1
D	0	1	0	-	1	1	0	1
E	0	0	1	1	-	1	1	0
F	0	1	0	1	1	-	1	1
G	0	0	1	0	1	1	-	1
H	1	1	1	1	0	1	1	-

According to the proposed *Starfish scheduling*, at first, the central controller (or the sink) finds a set $\mathbb{R}^c$ as a power set on the ring-canal nodes $\mathbb{Z}$. When the MILP framework runs, the central controller selects the most energy-efficient set of sojourn locations $\mathbb{M}_n^c$ for a cycle c to maximize sojourn duration. Meanwhile, it computes energy expenditures over the sets of $\mathbb{R}^c$ based on available traveling paths

Table 4.3: Data arrival rates (packet/sec) and set of sojourn locations

c	σ_A^c	σ_B^c	σ_C^c	σ_D^c	σ_E^c	σ_F^c	σ_G^c	σ_H^c	$\mathbb{M}_n^c$
1	40	7	20	10	30	13	35	17	{A,C,E,G}
2	10	35	16	40	10	45	8	50	{H,B,D,F}
3	40	10	30	50	20	12	45	13	{G,A,C,D}
4	50	10	20	40	12	45	20	38	{F,D,A,H}

of the mobile sink in the presence of obstacles and data arrival rates, as mentioned in Table 4.2 and Table 4.3, respectively. In this example, *Starfish scheduling* finds a set of sojourn locations $\mathbb{M}_n^1 = \{A, C, E, G\}$, for $c = 1$, and then it determines the sojourn duration at corresponding sojourn locations (using Eq. (4.3)). For an efficient routing of data packets throughout the network, the central controller acknowledges selected sojourn locations ($m \in \mathbb{M}_n^c$) along with corresponding sojourn duration $\{S_A^1, S_C^1, S_E^1, S_G^1\}$ before starting data collection.

Similarly, *Starfish scheduling* gets another set of sojourn locations $\mathbb{M}_n^2 = \{H, B, D, F\}$ for the second cycle $c = 2$ satisfying the required constraints in Eq. (4.6) - Eq. (4.13), and so on until the network is dead. The lifetime of the network can be estimated when the central controller finds the maximum number of cycles. As soon as the central controller determines the optimal set of sojourn locations, it acknowledges the ring-canal nodes along with sojourn duration. Afterward, each designated sojourn location broadcasts locally to the neighbors on the radial-canal backbone nodes so as to forward their sensed data up to the sojourn locations.

In continuous data forwarding policy, a source node immediately forwards sensed data to the nearest ring-canal node directly (or via the radial-canal nodes).

Since each ring-canal node (or rendezvous node) is aware of the data collection schedule along with sojourn duration, it instantly forwards data to the mobile sink via sojourn location $m \in \mathbb{M}_n^c$. This data forwarding policy minimizes end-to-end packet delivery delay significantly for real-time applications, even in an obstructed network environment.

In the following section, we have carried out an exhaustive experimental analysis to compare the proposed Starfish data collection scheduling with the state-of-the-art works. The details of simulation results are discussed in Section 4.5.

4.5 Performance Evaluation

This section presents the performances of the proposed *Starfish* data collection scheduling compared with recent works such as Viable Path-based scheduling (VPS) [43] and Landmark-assisted scheduling (LAS) [44] in network simulator (e.g., NS-2) [48].

4.5.1 Setup environment

In the simulation setup, a WSN of $600 \times 450m^2$ area is considered, where sensor nodes are randomly deployed following uniform random distribution having node density 0.002 per unit area. In the network, each sensor has a transmission range $90m$, and initial energy of $6J$. In the simulation, constant bit rate (CBR) traffic is modeled while data are transmitted under UDP protocol, 512 *bytes* of each data packet is transmitted over 512 $Kbps$ of channel bandwidth. The values of simulation parameters in a network environment are listed in Table 4.4.

Table 4.4: Simulation parameters for Starfish-schedule studies

Parameters	**Values**
Network area	$600 \times 450\ m^2$
Deployment type	Uniform random
Node density	$0.002m^{-2}$
Transmission range	$90\ m$
MAC	WirelessPhy/802.15.4
Size of data packet	$512\ Bytes$
Channel bandwidth	$512\ Kbps$
Application type	Event-driven
Initial node energy	$6J$
Tx power	$0.023W$
Rx power	$0.018W$
Idle power	$0.037mW$
Sleeping power	$0.003mW$
d_0	$70m$
Simulation time	$1000s$

4.5.2 Evaluation metrics

The following six evaluation metrics [110] have been used to gauge the performances of the studied data collection scheduling systems.

- *Network lifetime* is calculated from the deployment time of the network to the time at which a backbone node dies and becomes unreachable from neighboring source or backbone nodes in the network. We consider it assuming

that when it takes considerably long time to die a backbone node, the same phenomena will be repeated for the rest of the backbone. The lifetime of a sensor network is expected to be high, indicating the ability of an event to report over the SFR-backbones during the simulation period.

- *Standard deviation of residual energy* refers to the distribution of backbone nodes' residual energy when the lifetime of a network is exhausted. This measure is expected to be the smallest so that energy consumption among the backbone nodes is balanced to enhance network lifetime.

- *Data throughput* refers to the average data rate of successful data that is received by the mobile sink. The higher value of throughput is expected for better network performance.

- *Packet delivery ratio (PDR)* refers to the ratio between the number of data packets successfully delivered to the mobile sink and the number of packets generated by the source node within a certain application delay deadline. The higher value of PDR represents the reliability of the data routing over the backbone nodes.

- *Average end-to-end (e2e) packet delivery delay* refers to the difference in time delay from generation time of a packet to its reception time. The lower value of e2e packet delivery delay indicates the effectiveness of data collection scheduling for real-time applications.

- *Operational overhead* refers to the ratio of network control bytes exchanged to the data bytes received by the mobile sink during experimental evaluation. Performance is better when the operational overhead is lower.

4.5.3 Experimental results

We performed 50 times of simulation experiments with different randomly generated seed values, and the average result is plotted for each data point in the graph. In the network, if there is no direct, line-of-sight path between the transmitter and the receiver due to obstacles, data propagation is bounced off objects, and it causes multipath fading with path loss exponent value of 2-4. However, the simulation trace file data depicted that the average value of the path loss exponent used by the transmitters during the experiments was 2.8. We considered 250 ms for the maximum delay-deadline of application and events in the simulation experiments randomly at 30 different locations. Table 4.5 provides events with corresponding burst duration for the experiment.

Table 4.5: Events and burst descriptions for Starfish schedule

	Event-A	**Event-B**	**Event-C**	**Event-D**
Burst-1	10s-20s	70s-80s	110s-120s	365s-375s
Burst-2	105s-115s	190s-200s	370s-380s	570s-580s
Burst-3	430s-440s	650s-660s	730s-740s	750s-760s

4.5.3.1 Impacts of varying data generation rates

This section presents the performances of the studied protocols for varying data generation rates $1 - 8$ $packets/second$. In the experiment, the network size was fixed at 600×450 m^2, sink speed was fixed at 6 $meter/second$, and the number of obstacles was fixed at 40, occupying around 15% of the corresponding network area.

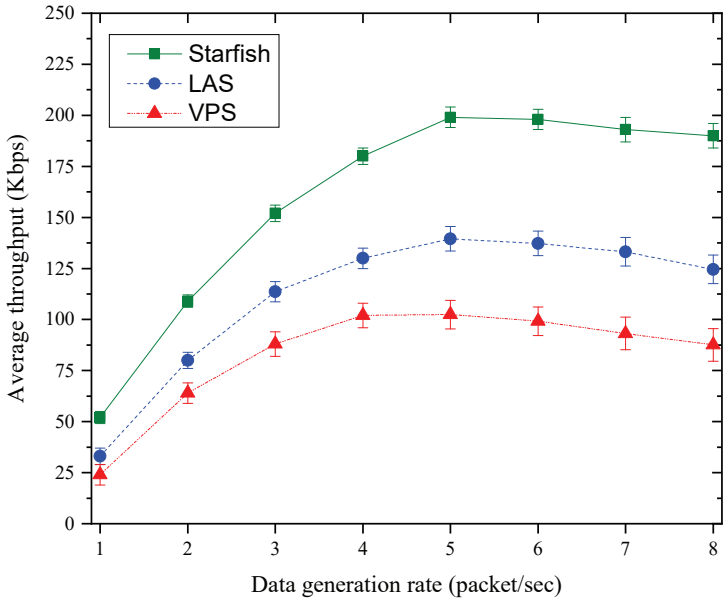

Figure 4.4: Average throughput for varying rates of data generation

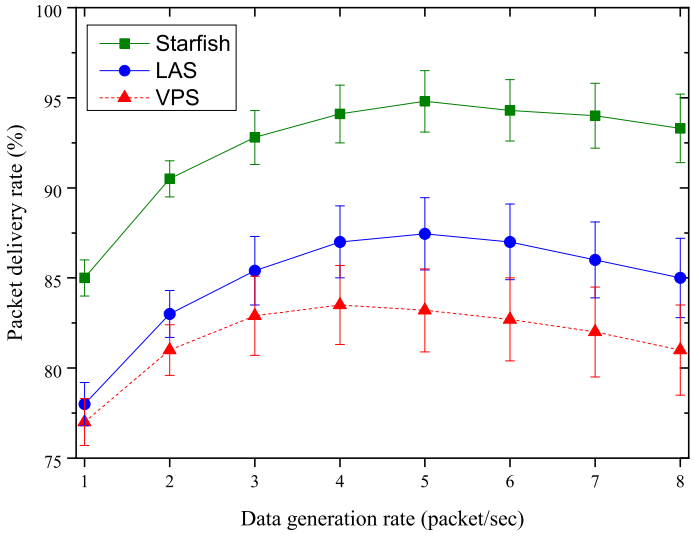

Figure 4.5: Packet delivery ratio for varying rates of data generation

The graphs, as shown in Fig. 4.4, illustrate that *average data throughput* (within delay-deadline) rises sharply with the increasing rate of packet generation in all the studied protocols. This is trivial because of generating more packets and successful reception of these packets by the mobile sink. It is obvious that the proposed *Starfish* data collection scheduling is effective in terms of bandwidth utilization as the rate of packet generation increases. However, for a higher rate of data generation (e.g., more than 5 packets/second), *data throughput* decreases steadily due to the exceeding maximum channel bandwidth, buffer overflow, and packet drop, etc. The average throughput for the proposed data collection scheduling over Starfish backbone is significantly higher than those of VPS [43], and LAS [44] strategies because faster data forwarding is offered over starfish routing backbone and continuous data collection scheduling from the optimal number of sojourn locations on the ring-canal. It is noteworthy that both sojourn location and duration are selected based on corresponding data arrival rates.

For similar reasons, the proposed scheduling over the *Starfish* routing backbone exhibits higher *PDR* with progressive data generation rate in the simulation experiments, as depicted in Fig. 4.5, and afterward, *PDR* declines steadily for a higher rate of data generation. These results prove the reliability of using *Starfish* scheduling for real-time applications in the network.

On the contrary, the *average end-to-end packet delivery delay* within the application delay-deadline is decreased with the progressive rate of data generation, as illustrated in Fig. 4.6. It occurs because the sink's mobility significantly reduces the vicinity length from source nodes to the mobile sink. Moreover, the proposed *Starfish* scheduling performs better than VPS [43], and LAS [44] strategies, because sink's mobility is governed by data arrival rates at rendezvous nodes, and there is

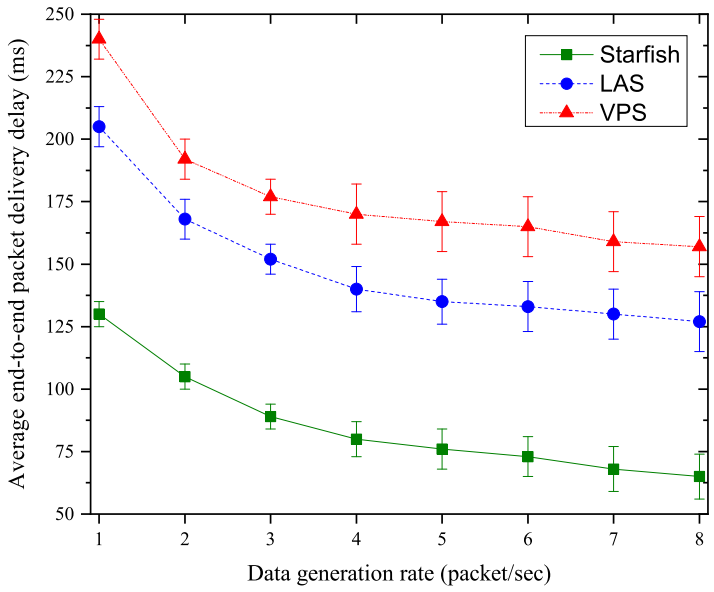

Figure 4.6: End-to-end delay for varying rates of data generation

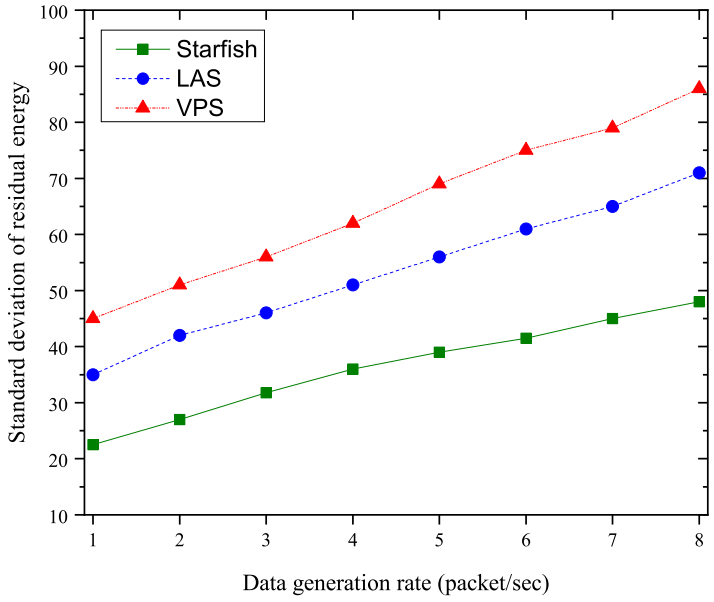

Figure 4.7: Std. dev. of residual energy for varying rates of data generation

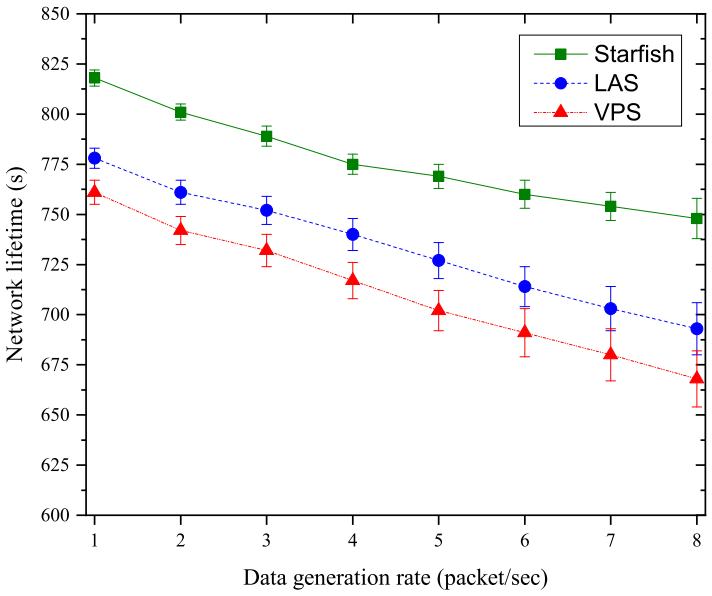

Figure 4.8: Network lifetime for varying rates of data generation

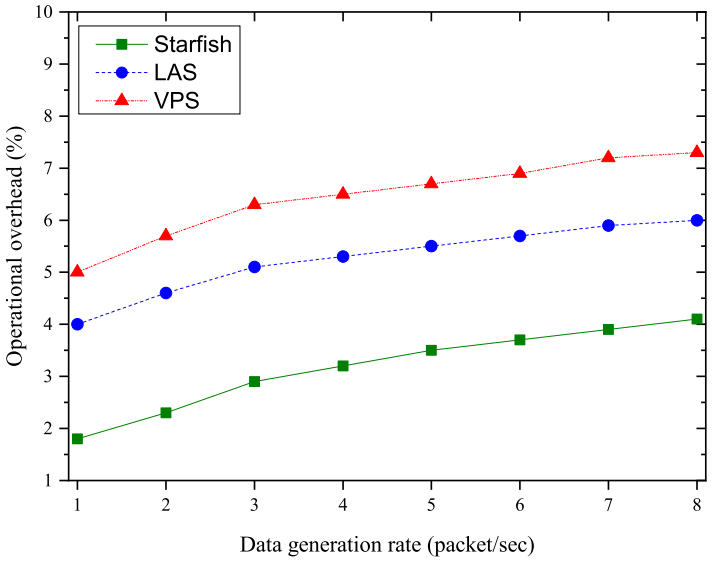

Figure 4.9: Operational overhead for varying rates of data generation

no query requirement for sink's fresh location, and finally, forwarding data over pre-constructed routing backbone in the network.

In the experiments, we also computed the *standard deviation of residual energy* when network lifetime was exhausted. The simulation results show a gradual increase of *standard deviation* for the higher data generation rates, as illustrated in Fig. 4.7, because of fluctuating energy expenditure from the different corners of the network. The proposed *Starfish* data scheduling exhibits the lowest standard deviation of residual energy due to balanced energy consumption over the Starfish backbone nodes while forwarding data to the mobile sink. Here, *Starfish* scheduling finds the optimal path over minor energy-expensive sojourn locations for each cycle. Since energy expenditure and standard deviation of residual energy are increased for higher rates of data generation, as described earlier, the *lifetime of the network* is inherently decreased for the increasing rate of data generation, as depicted in Fig. 4.8. Finally, with the increasing rate of data generation, it requires more control packets to deliver sensed data to the mobile sink. Thus *operational overhead* increases, as shown in Fig. 4.9. In the case of the proposed data collection scheduling, operational overhead is the lowest among the studied works because of forwarding data packets over the preformed Starfish routing backbone in the network.

4.5.3.2 Impacts of varying number of obstacles

Obstacles are an integrated part of a practical network scenario, and thus the efficiency of real-time data collection scheduling in the presence of obstacles should be determined. This section presents the experimental results for the increasing number of obstacles from 10-70, given that obstacles collectively occupied 15 %

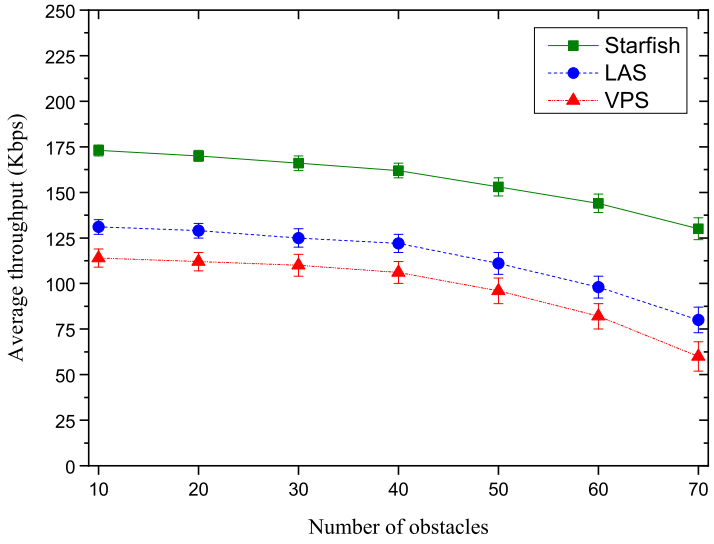

Figure 4.10: Average throughput for varying number of obstacles

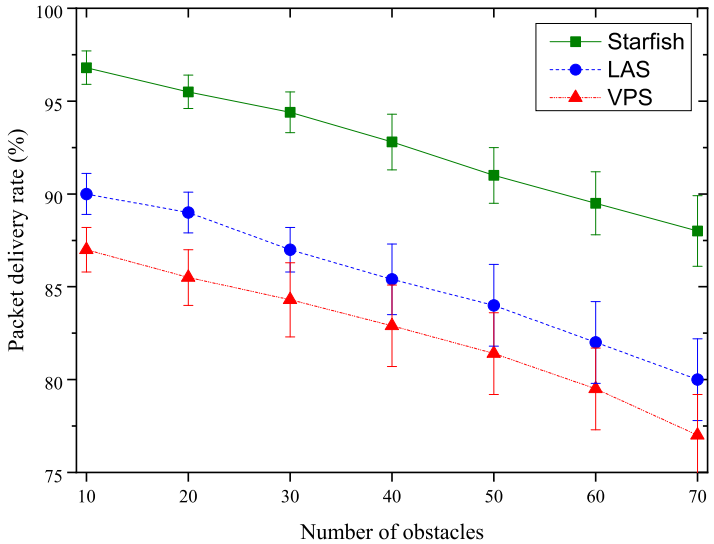

Figure 4.11: Packet delivery ratio for varying number of obstacles

of a network 600×450 m^2. In the experiments, the sink speed was fixed at 6 *meter/second*, and the packet generation rate was fixed at 3 *packets/second*.

The experimental results show that *average data throughput* within delay-deadline decreases sharply with the increasing number of obstacles, as shown in Fig. 4.10. This happens because sink mobility for visiting sojourn locations is hampered due to obstacles, increases path length of the mobile sink, requires more hop distance and increases packet retransmission, etc. These reasons also exhibit decreasing order of *packet delivery ratio (PDR)* within the delay-deadline, as depicted in Fig. 4.11. However, in the case of *Starfish* data collection schedule, the performances of average throughput and PDR outperform over VPS [43], and LAS [44] strategies because of faster and continuous data forwarding over obstacle-aware starfish routing backbone in the network.

On the contrary, Fig. 4.12 illustrates that the *average end-to-end packet delivery delay* sharply increases with a growing number of obstacles. This is mostly due to the increase in the proximity of the mobile sink with the obstacles, consequently increasing the path length and end-to-end packet delivery delay. However, the proposed *Starfish* scheduling performs better compared to VPS [43] and LAS [44] strategies because mobile sink visits sojourn locations based on the corresponding data arrival rate at rendezvous nodes. Moreover, the mobile sink collects data around the ring-canal, and all source nodes forward their data over pre-determined obstacle-aware Starfish routing backbone nodes.

Later, we also evaluated the *standard deviation of residual energy* among backbone nodes for an increasing number of obstacles when the network lifetime was exhausted. The graphs, as presented in Fig. 4.13, illustrate that the deviation of

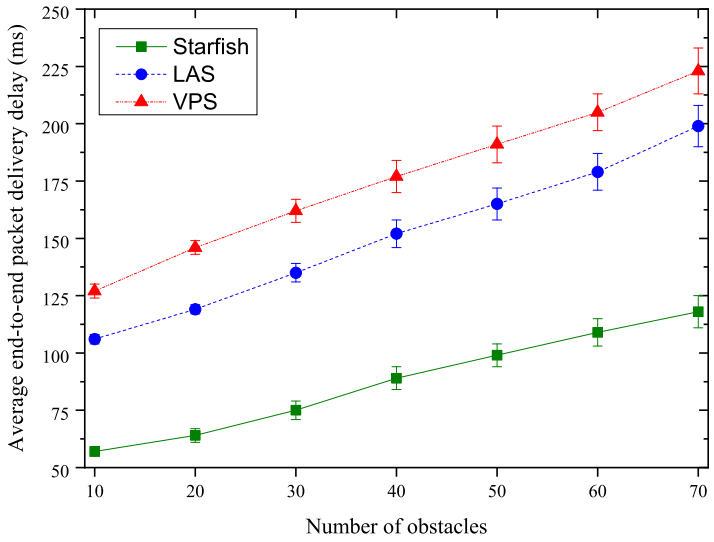

Figure 4.12: End-to-end delay for varying number of obstacles

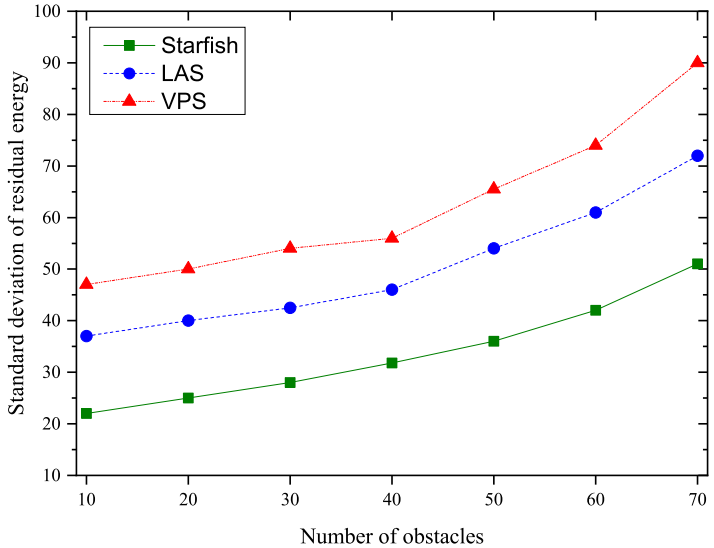

Figure 4.13: Std. dev. of residual energy for varying number of obstacles

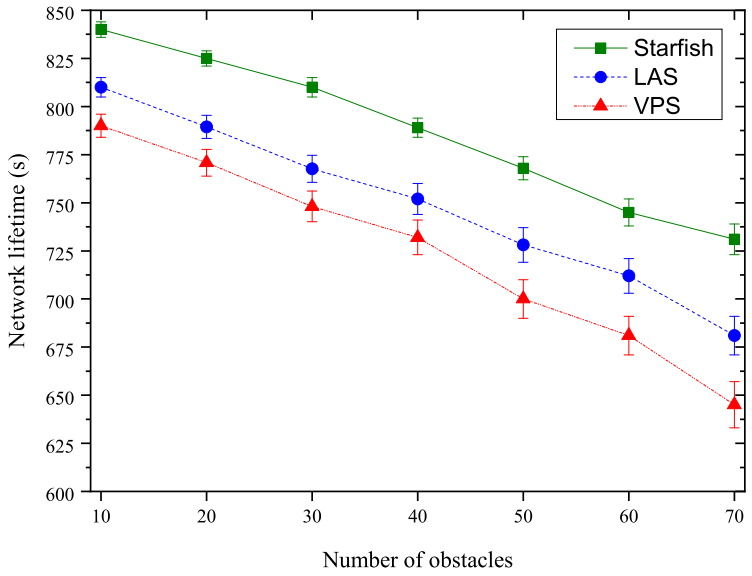

Figure 4.14: Network lifetime for varying number of obstacles

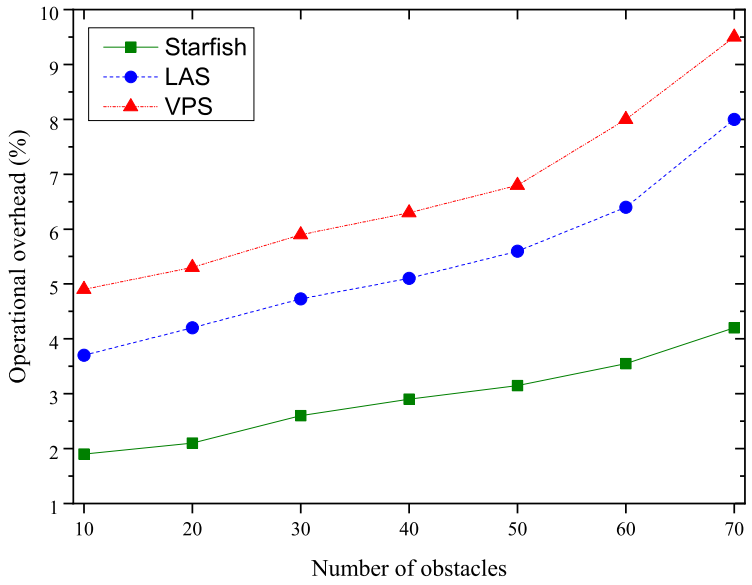

Figure 4.15: Operational overhead for varying number of obstacles

energy sharply expands as the number of obstacles increases. Since obstacles are sporadically distributed in the network and source nodes exhibit fluctuating energy expenditure due to those obstacles, it expands the standard deviation of residual energy. For similar reasons, some of the backbone nodes exhaust earlier, and thus *network lifetime* decreases with an increasing number of obstacles, as depicted in Fig. 4.14.

Finally, with the growing number of obstacles, more control packets are required to forward data avoiding sporadically situated obstacles in the network. Thus it results in increasing *operational overhead*, as shown in Fig. 4.15.

4.5.3.3 Impacts of varying sizes of networks

In a practical WSN application, the network performances and lifetime maximization are not only affected by data generation rate and a number of obstacles but also on the area of a network. Therefore, we evaluated the scalability and efficiency of the proposed *Starfish* scheduling, varying the network sizes from 400×225 m^2 to 900×675 m^2, while data generation rate, sink speed. The number of obstacles is fixed at 3 $packets/second$, 6 $meter/second$, and 40, respectively. In the case of different sizes of networks, we considered sporadic size of 40 obstacles that collectively occupied 15 % area of the corresponding size of the network with specific node density as stated in Section 4.5.1.

The graphs, as shown in Fig. 4.16, depict that *data throughput* within delay-deadline steadily decreases with the larger networks for all studied data collection scheduling. This happens because sink mobility for visiting sojourn locations is hampered due to obstacles, increasing path-length of the mobile sink, requiring more hop distance, increasing retransmission of packets, etc. These reasons also

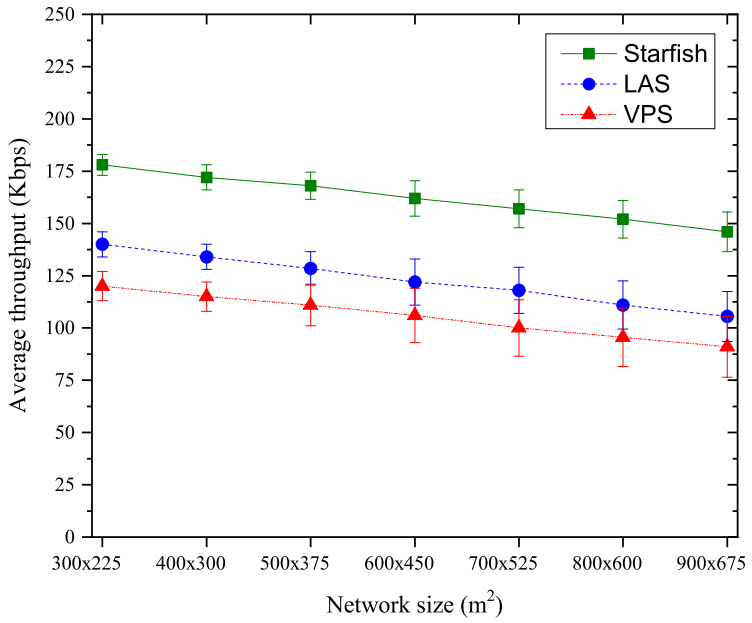

Figure 4.16: Average throughput for varying sizes of networks

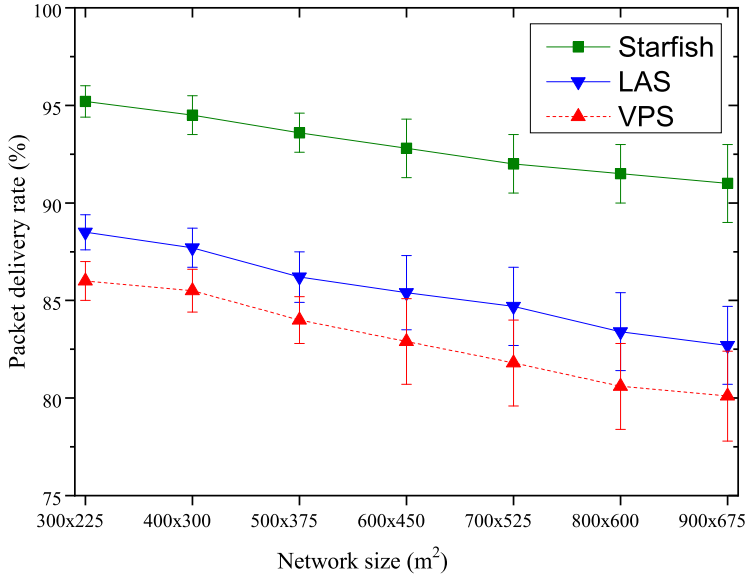

Figure 4.17: Packet delivery ratio for varying sizes of networks

reduce event notification and the reception probability of data packets by the mobile sink. In the case of *Starfish* scheduling, *average data throughput* is higher compared to VPS [43] and LAS [44] strategies because of collecting data over the optimal ring-canal, single hop reachability from any source node and continuous data forwarding over obstacle-aware backbone nodes. For similar reasons, *packet delivery ratio (PDR)* decreases, as shown in Fig. 4.17. The performances of data throughput and PDR prove the suitability and reliability of the *Starfish* data collection schedule for larger networks even though there exist obstacles.

On the contrary, the graphs, as presented in Fig. 4.18, depict that *end-to-end packet delivery delay* within the application delay-deadline is steadily increased for all studied data collection scheduling with increasing network sizes. It is obvious due to the linear increase of hop distance, the larger ring-canal size with obstacles. Moreover, experimental results show that the proposed *Starfish* scheduling outperforms VPS [43], and LAS [44] because of guaranteed single-hop access to at least one backbone node by a source node while forwarding data to the sojourn locations, collecting data over the ring-canal nodes, avoiding (re)tracing the mobile sink, etc. *End-to-end delay* performance of the proposed scheduling proves its suitability for real-time applications maintaining delay-deadline.

In the experiments, we computed the *standard deviation of residual energy*, when the network lifetime was exhausted. Fig. 4.19 shows that it increases monotonically because of fluctuating energy expenditure for increasing sizes of networks. Fluctuating energy expenditure occurs for the existence of obstacles at random locations throughout different areas of the network, larger size of the ring-canal, etc. The proposed *Starfish* data collection scheduling exhibits the lowest deviation of energy among other strategies due to the balanced energy consumption of the

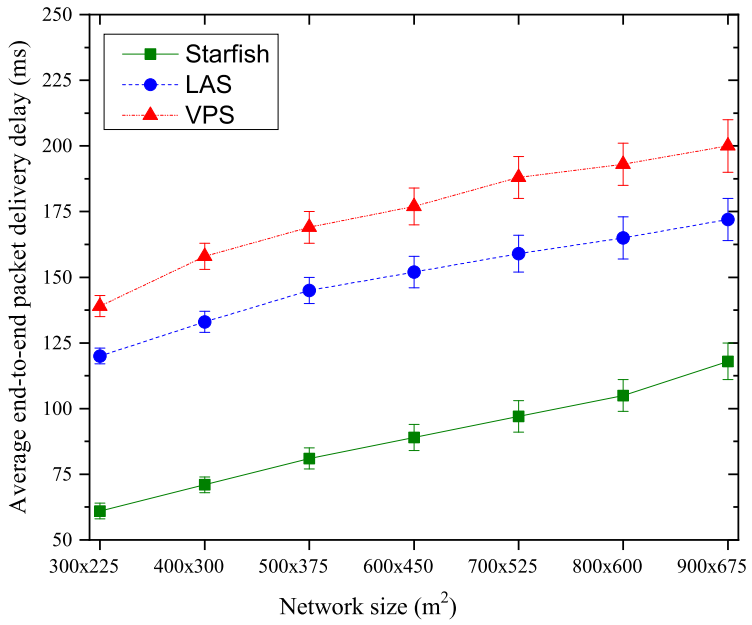

Figure 4.18: End-to-end delay of varying sizes of networks

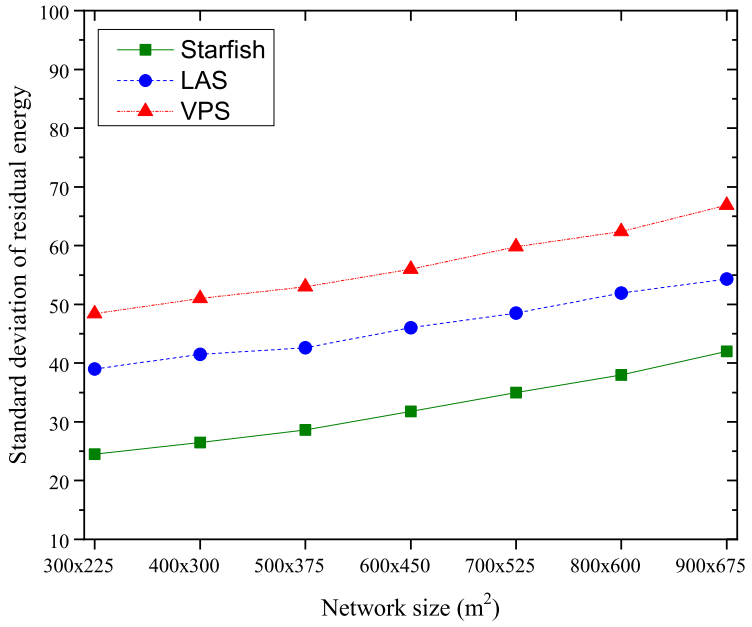

Figure 4.19: Std. dev. of residual energy for varying sizes of networks

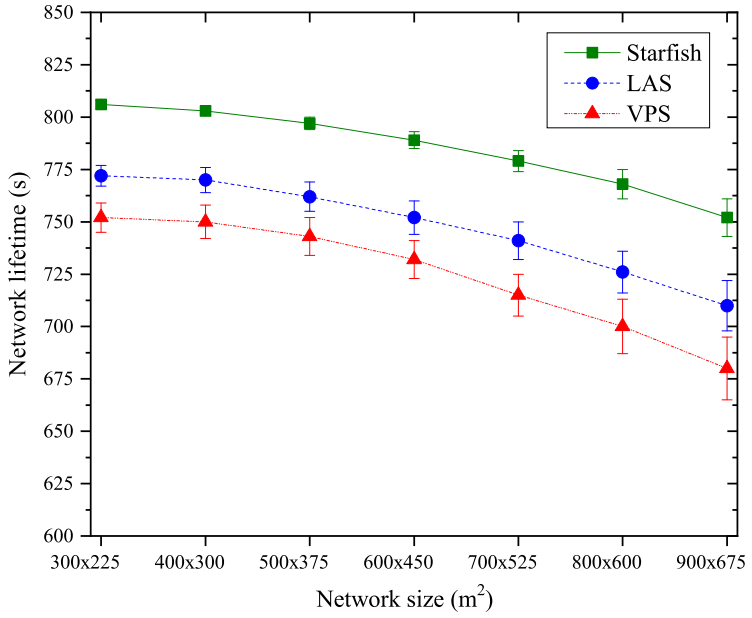

Figure 4.20: Network lifetime for varying sizes of networks

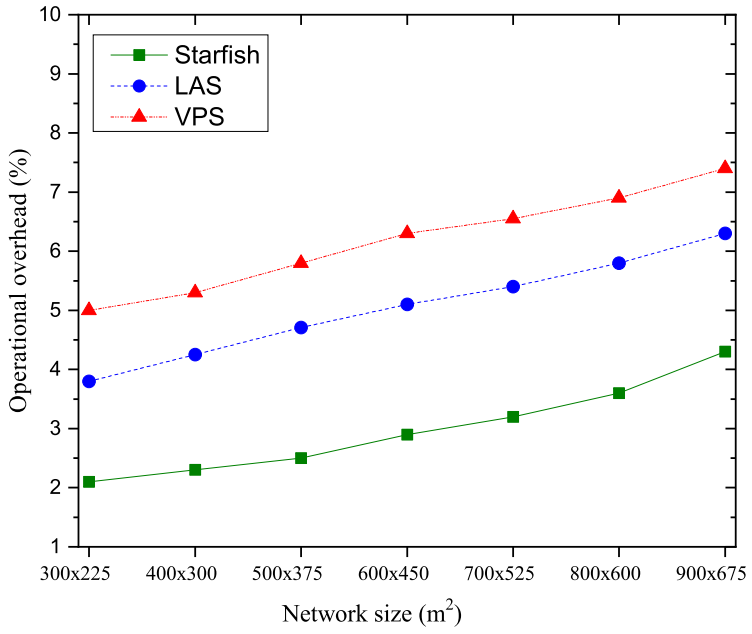

Figure 4.21: Operational overhead for varying sizes of networks

Starfish backbone nodes during forwarding data to the mobile sink. Since energy expenditure and standard deviation of residual energy increase, inherently the *network lifetime* is decreased for an increasing rate of data generation, as depicted in Fig. 4.20. Finally, with the increasing size of networks, it requires more control packets due to longer hop distance to collect data that results in increasing *operational overhead*, as shown in Fig. 4.21.

4.5.3.4 Complexity analysis

In a separate experiment, we compared the complexities of the studied scheduling schemes in NEOS optimization [126] server (2 Intel Xeon E5-2698 @ 2.3GHZ CPU and 192GB RAM) for selecting the optimal set of rendezvous nodes for each cycle. We find those for both viable path scheduling (VPS) [43] and landmark-assisted scheduling (LAS) [44] are $\mathcal{O}(\mathbb{N}^3)$, where $\mathbb{N}$ is the number of nodes. In the case of the Starfish data collection schedule, the mobile sink visits rendezvous nodes that are optimally selected over the ring-canal nodes ($\mathbb{Z}$).

According to the MILP formulation, it determines a set of sojourn locations $\mathbb{M}_n^c \in \mathbb{R}^c$ over the ring-canal nodes, instead of overall sensor nodes or all backbone nodes. The constraint in Eq. (4.7) computes over the power set of the ring canal nodes $\mathbb{Z}$, and finds out the most energy-efficient set of sojourn locations achieving maximum duration. Therefore, the computational complexity of the Starfish scheduling is estimated as $\mathcal{O}(c \times |\mathbb{Z}| \times 2^{|\mathbb{Z}|})$ which is significantly less compared to those of VPS and LAS.

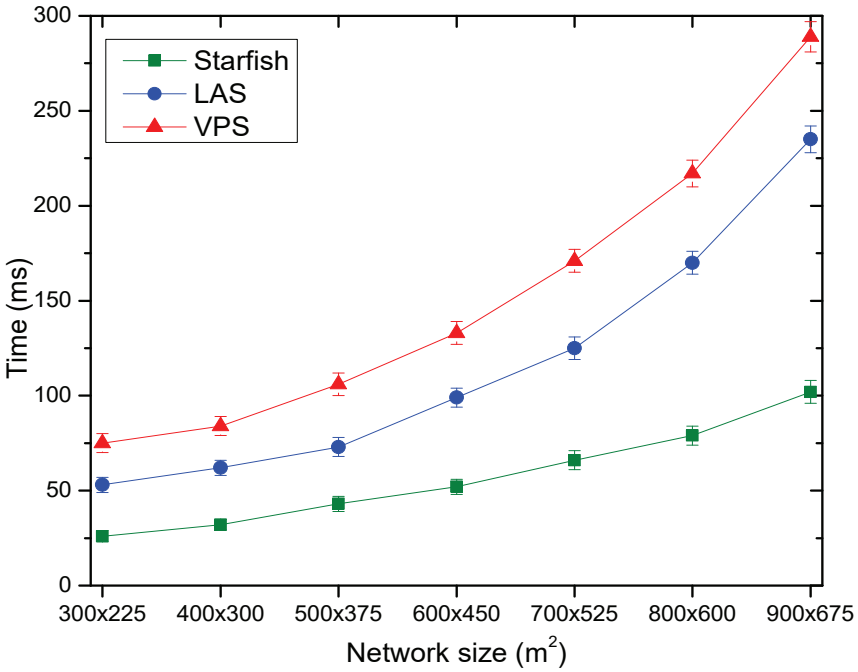

Figure 4.22: Computational complexity

The graphs in Fig. 4.22 show the computation time required for the execution of the studied data collection schedule algorithms for increasing the size of networks from 300 × 225 to 900 × 675. As VPS and LAS strategies explore all nodes in the network to find out data collection schedules, their computation time increase exponentially compared to a linear graph observed for the Starfish schedule. It is obvious since the Starfish schedule explores candidate power sets on the ring canal nodes only. The problem can be grouped as an NP-complete one [127]. However, the constraints in Eq. (6) - Eq. (13) of the MILP formulation facilitate us to significantly reduce the input sets for selecting the optimal number of sojourn locations. Thus the solution is found in polynomial time.

Moreover, for varying sizes of network, time complexity increases monotonically for the Starfish scheduling due to preformed routing-backbone with *ring-* and *radial-canals* and *guaranteed single-hop* access to the backbone. For the LAS and VPS strategies, determining the route throughout the obstructed network exhibits higher overhead and time complexity than the Starfish scheduling.

The above results and discussions conclude that *Starfish* data collection schedule shows its efficiency in terms of computational complexity, data throughput, end-to-end data delivery delay, network lifetime, etc. for real-time applications (within certain delay-deadline) in an obstructed network significantly. Moreover, the proposed Starfish schedule is applicable for an obstacle-free network as well, as was primarily studied in [110].

However, the simulation trace file data shows that when the data generation rate at a particular node on the ring-canal is superabundant compared to other nodes, the sojourn location is discriminatorily selected for consecutive cycles. This exhibits a quicker partition of the routing backbone than the average network lifetime.

Table 4.6: Performance improvements of the proposed SFR backbone over the state-of-the-art works

	LAS [44]			**VPS [43]**		
Control variable	Area	Rate	Obstacle	Area	Rate	Obstacle
Data throughput	+24.71 %	+43.79 %	+39.53 %	+43.28 %	+79.25 %	+65.56 %
Packet delivery ratio	+8.70 %	+8.84 %	+8.50 %	+12.03 %	+13.07 %	+12.22 %
End-to-end delay	-41.16 %	-42.96 %	-42.59 %	-49.71 %	-52.49 %	-50.97 %
Operational overhead	-41.58 %	-38.54 %	-46.09 %	-52.33 %	-49.74 %	-56.66 %
Network lifetime	+5.00 %	+5.93 %	+5.16 %	+8.37 %	+9.21 %	+8.84 %
Stdev. of residual energy	-30.61 %	-32.15 %	-33.81 %	-43.49 %	-44.69 %	-46.59 %

4.6 Summary

This work explored data collection challenges and lifetime maximization strategies for real-time applications in an obstructed sensor network with a mobile sink. For real-time data collection, we considered *Starfish* routing backbone with obstacles, and after that, formulated mixed-integer linear programming to find an optimal set of sojourn locations on its ring-canal nodes for a round, corresponding sojourn duration with data collection scheduling so as to maximize network lifetime.

The simulation results, as summarized in the Table 4.6, clearly indicated that the performance improvements of the proposed *Starfish* data collection scheduling over the state-of-the-art works (e.g., LAS and VPS) based on the evaluation metrics for varying size of networks, data generation rates, and increasing number of obstacles in the network.

Chapter 5

Conclusion

In this chapter, we summarize and discuss the research results presented in the thesis, and state few directions for the future research works.

5.1 Summary of the Research

In this thesis, we developed a novel data routing framework - Starfish routing (SFR) backbone, and a real-time data collection strategy of a mobile sink exploiting the SFR backbone in an obstructed network. The developed framework optimizes network lifetime through uniform energy consumption, balancing data routing load throughout the network, heterogeneous data generation rates, application's delay-deadline, loop-free traveling path in the network.

This thesis also contributed different variants of SFR-backbone architectures to accommodate multiple shape scenarios and to maximize network lifetime for both obstacle-free and obstructed networks. In this work, lifetime maximization was achieved through developing a Starfish-like backbone architecture that offered balanced energy consumption throughout the network. In SFR, the backbone nodes (e.g., *ring-canal* and *radial-canals*) were spread over the different regions in the network in such a way that a source node could access at least one of the

backbone nodes directly. The construction of *ring-* and *radial-canals* on different SFR-architectures was mathematically modeled based on the transmission range of sensor nodes and the size of the network area. Moreover, the scalability of the SFR-backbones was maintained through developing the optimal circular and elliptical ring-canals within rectangular-, square- and circular-shaped networks. Furthermore, statistical analysis for expected end-to-end data delivery delay over the SFR-backbone had been carried out considering both hop distance to the sink and the number of retransmission attempts in the network. As a whole, SFR-architecture acted as a high-speed routing backbone that could simultaneously optimize end-to-end data delivery delay and network lifetime significantly.

Next, we developed an optimal data collection strategy of a mobile sink in an obstructed network. In this regard, we reconstructed the Starfish routing (SFR) backbone in an obstructed network, and developed an optimization framework for maximizing the lifetime of the sensor network. In this work, we found an optimal travel plan for data collection by visiting a set of rendezvous nodes and corresponding sojourn durations that guaranteed loop-free travel schedules over the optimal rendezvous nodes, ensuring balanced energy consumption for a time-constraint application. Theoretical proofs of the desirable properties of the Starfish-schedule were derived to validate the optimization framework.

Finally, the performances of the SFR-backbones, and the Starfish-schedule were carried out in Network Simulator (e.g., NS-2) [48]. The experimental results depicted that the *Starfish data collection scheduling* improved network lifetime and reduced end-to-end data delivery delay. Besides, we observed significant improvements in terms of different QoS and network lifetime metrics for obstacle-free and obstructed networks.

5.2 Discussion

Over the last few years, the usages of IoT devices increased significantly to develop embedded intelligent systems for most industrial and smart-city applications. The efficiency of these applications was highly dependent on data routing and lifetime maximization strategies. Therefore, we explored real-time data collection strategies and key factors to maximize network lifetime. We investigated that the existing routing protocols of sensor networks would not be feasible for the upcoming 5G/6G network services to satisfy minimum QoS requirements of real-time applications. Therefore, we focused on developing a proactive routing-backbone in the network that substantially minimized end-to-end packet delay and extended network lifetime.

My Ph.D. journey started with the aim to work with real-time data collection with a mobile sink in an obstacle-free sensor network. Exploring the state-of-the-art works, we found a promising field of introducing a high-speed routing backbone in sensor networks. From the functional characteristics of those protocols, we identified that not only the energy consumption of individual sensor nodes was important, but also balanced energy consumption among all the sensor nodes was highly expected to maximize network lifetime. Violation of delay-deadline for real-time multimedia applications in the state-of-the-art works forced to develop an efficient data routing backbone in the network. Later, we found that a data collection scheduling of a mobile sink over a backbone architecture became challenging in an obstructed network. Therefore, we concentrated on developing an efficient routing backbone and optimization framework for maximizing the lifetime of a sensor network in an obstructed network.

To find an efficient solution to the problem, we studied the state-of-the-art tools, techniques and acquainted with those. We explored different mobile-sink-based routing strategies and optimization techniques to maximize network lifetime for real-time applications in an obstructed network. After a mathematical formulation, we had to go for simulation to evaluate the performances of the proposed Starfish routing (SFR) backbone in terms of QoS and network lifetime metrics. For this reason, we had to spend a significant amount of time learning network simulators and implementing the proposed SFR protocol for obstacle-free and obstructed networks. For the theoretical models, numerical evaluation, and experimental performances of the SFR backbones, we had to learn NS-2, MATLAB, and Python. Finally, after spending a significant amount of time in the laboratory, we had been able to implement our proposed Starfish routing backbones for obstacle-free and obstructed networks whose performances were compared with a good number of state-of-the-art works.

From the experimental results, it was observed that moderate sink mobility was beneficial for network performances for all studied data collection strategies. However, the SFR outperformed HexDD and Ring backbones due to the fair distribution of data traffic over backbone nodes within the network. The iSFR-elliptical architecture took advantage of the optimal elliptical-shaped ring-canal over its circular and basic SFR variants. Moreover, SFR achieved a higher level of scalability for varying sizes of networks compared to the studied protocols. It was also studied that iSFR-elliptical architectures' energy-deviation outperformed iSFR-circular and bSFR backbones because of developing an optimal elliptical ring-canal in the network. These experimental results strengthened the formation of iSFR-elliptical

backbone in sensor networks. Finally, the results substantiated the efficiency of *Starfish routing backbone* over the state-of-the-art works to achieve extended network lifetime and to provide significant QoS performances.

5.3 Limitations

Though the construction of Starfish routing backbone and development of Starfish data collection schedule showed significant benefits over the state-of-the-art works, we observed difficulties to construct the Starfish routing backbone for an irregular shaped network. Moreover, the simulation trace file data shows that when the data generation rate at a particular node on the ring-canal is superabundant compared to other nodes, the sojourn location is discriminatorily selected for consecutive cycles. In such scenario, the network lifetime performance significantly degraded, and the routing backbone become partitioned earlier than the average network lifetime.

5.4 Future Works

Though the results of the performances are encouraging, there are ample issues and open challenges that require more investigation for further extension of the proposed data collection strategy. As a planned study, in the future, we envision designing distributed and machine-learning-based algorithms for data collection schedules by multiple sinks in a very large-scale network.

This work is motivated from the water vascular system of a sea-fish namely Starfish on which there are few lateral-canals. We may construct efficient lateral-canals (as on the water vascular system of a Starfish) on the SFR backbone through

mathematical analysis. It would be an interesting open research problem for future study. A suitable distributed algorithm would be developed to increase the scalability of the proposed *Starfish routing backbone* in the network.

For the further improvement on network lifetime, multiple sets of connected backbone nodes for SFR backbone would be defined so that these sets could be changed periodically. This strategy can enhance network lifetime multiple times based on the sets of connected backbone nodes. Moreover, local repair strategy for the backbone nodes would reduce the complexity of SFR backbone formation periodically.

Though we achieve higher efficiency through the optimal size of the ring-canal in the network, for a extraordinary large network or irregular shaped network, the efficiency of the Starfish routing backbone would degrade for real-time wireless sensor network applications due to the single ring-canal in the network. Moreover, it is challenging to determine whether it requires multiple ring-canals in the network for the Starfish routing backbone. Therefore, we would study the feasibility of multiple ring-canals for the Starfish routing backbone extraordinary large network or irregular shaped network.

Bibliography

[1] R. Akhter and S. A. Sofi, "Precision agriculture using iot data analytics and machine learning," *Journal of King Saud University-Computer and Information Sciences*, 2021.

[2] B. Rooppur NPP Authority, "Industrial internet-of-things for nuclear power plant," Accessed: 15 Nov 2021. [Online]. Available: http://www.rooppurnpp.gov.bd/

[3] S. Ansari, A. Ayob, M. S. H. Lipu, M. H. M. Saad, and A. Hussain, "A review of monitoring technologies for solar PV systems using data processing modules and transmission protocols: Progress, challenges and prospects," *Sustainability (MDPI)*, vol. 13, no. 15, p. 8120, 2021.

[4] D. mass transit company authority, "Towards the internet of smart mass transit railway (mtr) in bangladesh," Accessed: 15 Nov 2021. [Online]. Available: http://dmtcl.gov.bd/

[5] B. Rashid and M. H. Rehmani, "Applications of wireless sensor networks for urban areas: A survey," *Journal of Network and Computer Applications*, vol. 60, pp. 192–219, 2016.

[6] P. D. of the UN Department of Economic and S. A. U. DESA), "68 percent of the world population projected to live in urban areas by 2050," Accessed: 15 Nov 2021. [Online]. Available: https://www.un.org/development/desa/en/news/population/2018-revision-of-world-urbanization-prospects.html

[7] A. Z. Abbasi, N. Islam, Z. A. Shaikh *et al.*, "A review of wireless sensors and networks' applications in agriculture," *Computer Standards & Interfaces*, vol. 36, no. 2, pp. 263–270, 2014.

[8] T. Adhikary, A. K. Das, M. A. Razzaque, M. E. H. Chowdhury, and S. Parvin, "Test implementation of a sensor device for measuring soil macronutrients," in *Networking Systems and Security (NSysS), 2015 International Conference on*. IEEE, 2015, pp. 1–8.

[9] I. Markit, "IoT connected devices worldwide 2030," Accessed: 15 Nov 2021. [Online]. Available: "https://cdn.ihs.com/www/pdf/IoT_ebook.pdf"

[10] G. Kaur, P. Tomar, and P. Singh, "Design of cloud-based green IoT architecture for smart cities," in *Internet of Things and Big Data Analytics Toward Next-Generation Intelligence*. Springer, 2018, pp. 315–333.

[11] L. D. Xu, E. L. Xu, and L. Li, "Industry 4.0: state of the art and future trends," *International Journal of Production Research*, vol. 56, no. 8, pp. 2941–2962, 2018.

[12] R. Sahal, S. H. Alsamhi, J. G. Breslin, and M. I. Ali, "Industry 4.0 towards forestry 4.0: Fire detection use case," *Sensors*, vol. 21, no. 3, p. 694, 2021.

[13] U. C. R. Service, "Wildfire statistics," Accessed: 15 Nov 2021. [Online]. Available: https://crsreports.congress.gov/

[14] J. Wan, M. A. Al-awlaqi, M. Li, M. OGrady, X. Gu, J. Wang, and N. Cao, "Wearable IoT enabled real-time health monitoring system," *EURASIP Journal on Wireless Communications and Networking*, vol. 2018, no. 1, pp. 1–10, 2018.

[15] M. M. Islam, A. Rahaman, and M. R. Islam, "Development of smart healthcare monitoring system in IoT environment," *SN computer science*, vol. 1, pp. 1–11, 2020.

[16] Q. Shen, X. Liang, X. S. Shen, X. Lin, and H. Y. Luo, "Exploiting geo-distributed clouds for a e-health monitoring system with minimum service delay and privacy preservation," *IEEE journal of biomedical and health informatics*, vol. 18, no. 2, pp. 430–439, 2014.

[17] I. Ahmad, K. Shah, and S. Ullah, "Military applications using wireless sensor networks: A survey," *Int. J. Eng. Sci*, vol. 6, pp. 7039–7043, 2016.

[18] S. Ghafoor, M. H. Rehmani, S. Cho, and S.-H. Park, "An efficient trajectory design for mobile sink in a wireless sensor network," *Computers & Electrical Engineering*, vol. 40, no. 7, pp. 2089–2100, 2014.

[19] N. Ghosh, R. Sett, and I. Banerjee, "An efficient trajectory based routing scheme for delay-sensitive data in wireless sensor network," *Computers & Electrical Engineering*, vol. 64, pp. 288–304, 2017.

[20] S. K. Singh and P. Kumar, "A comprehensive survey on trajectory schemes for data collection using mobile elements in wsns," *Journal of Ambient Intelligence and Humanized Computing*, pp. 1–22, 2019.

[21] X. Ding, Y. Tian, and Y. Yu, "A real-time big data gathering algorithm based on indoor wireless sensor networks for risk analysis of industrial operations," *IEEE transactions on industrial informatics*, vol. 12, no. 3, pp. 1232–1242, 2015.

[22] R. Asorey-Cacheda, A. J. García-Sánchez, F. García-Sánchez, J. García-Haro, and F. J. González-Castano, "On maximizing the lifetime of wireless sensor networks by optimally assigning energy supplies," *Sensors*, vol. 13, no. 8, pp. 10 219–10 244, 2013.

[23] W.-T. Wang and K.-F. Ssu, "Obstacle detection and estimation in wireless sensor networks," *Computer Networks*, vol. 57, no. 4, pp. 858–868, 2013.

[24] A. Das and D. Dutta, "Data acquisition in multiple-sink sensor networks," *ACM SIGMOBILE Mobile Computing and Communications Review*, vol. 9, no. 3, pp. 82–85, 2005.

[25] E. Lee, S. Park, F. Yu, and S.-H. Kim, "Exploiting mobility for efficient data dissemination in wireless sensor networks," *Journal of communications and networks*, vol. 11, no. 4, pp. 337–349, 2009.

[26] M. I. Khan, W. N. Gansterer, and G. Haring, "Static vs. mobile sink: The influence of basic parameters on energy efficiency in wireless sensor networks," *Computer communications*, vol. 36, no. 9, pp. 965–978, 2013.

[27] M. A. Habib and M. S. Hasan, "A performance analysis of backbone structures for static sink based starfish routing in WSN," in *4th International Conference on Networking, Systems and Security (NSysS), Dhaka, Bangladesh.* IEEE, 2017, pp. 1–6.

[28] C.-F. Cheng and C.-F. Yu, "Data gathering in wireless sensor networks: a combine–TSP–reduce approach," *IEEE Transactions on Vehicular Technology*, vol. 65, no. 4, pp. 2309–2324, 2015.

[29] H. Salarian, K.-W. Chin, and F. Naghdy, "An energy-efficient mobile-sink path selection strategy for wireless sensor networks," *IEEE Transactions on vehicular technology*, vol. 63, no. 5, pp. 2407–2419, 2013.

[30] S. Basagni, A. Carosi, E. Melachrinoudis, C. Petrioli, and Z. M. Wang, "Controlled sink mobility for prolonging wireless sensor networks lifetime," *Wireless Networks*, vol. 14, no. 6, pp. 831–858, 2008.

[31] G. Xing, T. Wang, Z. Xie, and W. Jia, "Rendezvous planning in wireless sensor networks with mobile elements," *IEEE Transactions on Mobile Computing*, vol. 7, no. 12, pp. 1430–1443, 2008.

[32] M. A. Razzaque, M. H. U. Ahmed, C. S. Hong, and S. Lee, "QoS-aware distributed adaptive cooperative routing in wireless sensor networks," *Ad Hoc Networks*, vol. 19, pp. 28–42, 2014.

[33] I. Dietrich and F. Dressler, "On the lifetime of wireless sensor networks," *ACM Transactions on Sensor Networks (TOSN)*, vol. 5, no. 1, pp. 1–39, 2009.

[34] H. Yetgin, K. T. K. Cheung, M. El-Hajjar, and L. H. Hanzo, "A survey of network lifetime maximization techniques in wireless sensor networks," *IEEE Communications Surveys & Tutorials*, vol. 19, no. 2, pp. 828–854, 2017.

[35] J. Singh, R. Kaur, and D. Singh, "A survey and taxonomy on energy management schemes in wireless sensor networks," *Journal of Systems Architecture*, vol. 111, p. 101782, 2020.

[36] V. Chamola, V. Hassija, V. Gupta, and M. Guizani, "A comprehensive review of the COVID-19 pandemic and the role of IoT, drones, AI, blockchain, and 5G in managing its impact," *IEEE Access*, vol. 8, pp. 90 225–90 265, 2020.

[37] J.-H. Shin, J. Kim, K. Park, and D. Park, "Railroad: virtual infrastructure for data dissemination in wireless sensor networks," in *2nd ACM international workshop on Performance evaluation of wireless ad hoc, sensor, and ubiquitous networks*. ACM, 2005, pp. 168–174.

[38] E. B. Hamida and G. Chelius, "A line-based data dissemination protocol for wireless sensor networks with mobile sink," in *IEEE International Conference on Communications*. IEEE, 2008, pp. 2201–2205.

[39] A. T. Erman, A. Dilo, and P. Havinga, "A virtual infrastructure based on honeycomb tessellation for data dissemination in multi-sink mobile wireless sensor networks," *EURASIP Journal on Wireless Communications and Networking*, vol. 2012, no. 1, pp. 1–27, 2012.

[40] C. Tunca, S. Isik, M. Y. Donmez, and C. Ersoy, "Ring routing: An energy-efficient routing protocol for wireless sensor networks with a mobile sink," *IEEE Transactions on Mobile Computing*, vol. 14, no. 9, pp. 1947–1960, 2014.

[41] A. V. Sutagundar and S. S. Manvi, "Fish bone structure based data aggregation and routing in wireless sensor network: multi-agent based approach," *Telecommunication Systems*, vol. 56, no. 4, pp. 493–508, 2014.

[42] G. Xie and F. Pan, "Cluster-based routing for the mobile sink in wireless sensor networks with obstacles," *IEEE Access*, vol. 4, pp. 2019–2028, 2016.

[43] H. Huang and A. V. Savkin, "Viable path planning for data collection robots in a sensing field with obstacles," *Computer Communications*, vol. 111, pp. 84–96, 2017.

[44] S. Redhu and R. M. Hegde, "Network lifetime improvement using landmark-assisted mobile sink scheduling for cyber-physical system applications," *Ad Hoc Networks*, vol. 87, pp. 37–48, 2019.

[45] S. Najjar-Ghabel, L. Farzinvash, and S. N. Razavi, "Mobile sink-based data gathering in wireless sensor networks with obstacles using artificial intelligence algorithms," *Ad Hoc Networks*, p. 102243, 2020.

[46] A. Verma, S. Kumar, P. R. Gautam, T. Rashid, and A. Kumar, "Fuzzy logic based effective clustering of homogeneous wireless sensor networks for mobile sink," *IEEE Sensors Journal*, vol. 20, no. 10, pp. 5615–5623, 2020.

[47] L. Villier, "Starfish–biology and ecology of the asteroidea," 2014.

[48] T. Issariyakul and E. Hossain, "Introduction to network simulator 2 (ns2)," in *Introduction to network simulator NS2*. Springer, 2009, pp. 1–18.

[49] T. Adhikary, A. K. Das, M. A. Razzaque, A. Almogren, M. Alrubaian, and M. M. Hassan, "Quality of service aware reliable task scheduling in vehicular cloud computing," *Mobile Networks and Applications*, vol. 21, no. 3, pp. 482–493, 2016.

[50] A. K. Sangaiah, A. S. Rostami, A. A. R. Hosseinabadi, M. B. Shareh, A. Javadpour, S. H. Bargh, and M. M. Hassan, "Energy-aware geographic routing for real-time workforce monitoring in industrial informatics," *IEEE Internet of Things Journal*, vol. 8, no. 12, pp. 9753–9762, 2021.

[51] A. Liu, M. Huang, M. Zhao, and T. Wang, "A smart high-speed backbone path construction approach for energy and delay optimization in wsns," *IEEE Access*, vol. 6, pp. 13 836–13 854, 2018.

[52] P. Roy, A. Tahsin, S. Sarker, T. Adhikary, M. A. Razzaque, and M. M. Hassan, "User mobility and quality-of-experience aware placement of virtual network functions in 5G," *Computer Communications*, vol. 150, pp. 367–377, 2020.

[53] S. Saha, M. A. Habib, T. Adhikary, M. A. Razzaque, M. M. Rahman, M. Altaf, and M. M. Hassan, "Quality-of-experience-aware incentive mechanism for workers in mobile device cloud," *IEEE Access*, vol. 9, pp. 95 162–95 179, 2021.

[54] A. Nayak and I. Stojmenovic, *Wireless sensor and actuator networks: algorithms and protocols for scalable coordination and data communication.* John Wiley & Sons, 2010.

[55] Q. Liu, K. Zhang, J. Shen, Z. Fu, and N. Linge, "GLRM: An improved grid-based load-balanced routing method for wsn with single controlled mobile sink," in *18th International Conference on Advanced Communication Technology (ICACT), South Korea.* IEEE, 2016, pp. 34–38.

[56] I. Al Ajmeh, K. El-Zayyat, and J. Yu, "A hybrid routing protocol for mobile ad hoc and wireless sensor networks," in *4th International Conference on Wireless Communications, Networking and Mobile Computing, China*. IEEE, 2008, pp. 1–5.

[57] Y.-H. Wang, K.-F. Huang, P.-F. Fu, and J.-X. Wang, "Mobile sink routing protocol with registering in cluster-based wireless sensor networks," in *International Conference on Ubiquitous Intelligence and Computing*. Springer, 2008, pp. 352–362.

[58] S. Suraj and D. Suresh, "VGBST: A virtual grid-based backbone structure type scheme for mobile sink based wireless sensor networks," in *International Conference on Advanced Research in Computer Science Engineering & Technology (ICARCSET), India*. ACM, 2015, pp. 1–5.

[59] Q. Wang, W. Liu, T. Wang, M. Zhao, X. Li, M. Xie, M. Ma, G. Zhang, and A. Liu, "Reducing delay and maximizing lifetime for wireless sensor networks with dynamic traffic patterns," *IEEE Access*, vol. 7, pp. 70 212–70 236, 2019.

[60] J. Prakash, R. Kumar, R. K. Gautam, and J. Saini, "Maximizing lifetime of wireless sensor network by sink mobility in a fixed trajectory," in *Next-Generation Networks*. Springer, 2018, pp. 525–536.

[61] T. Hara, V. I. Zadorozhny, and E. Buchmann, *Wireless sensor network technologies for the information explosion era*. Springer, 2010, vol. 278.

[62] A. Z. Prithibi, S. K. Faria, P. Roy, and M. A. Razzaque, "Network lifetime aware routing algorithm for energy harvesting wireless sensor networks," in

2nd International Conference on Sustainable Technologies for Industry 4.0 (STI), Dhaka, Bangladesh. IEEE, 2020, pp. 1–6.

[63] C.-Y. Chang, J.-P. Sheu, Y.-C. Chen, and S.-W. Chang, "An obstacle-free and power-efficient deployment algorithm for wireless sensor networks," *IEEE transactions on systems, man, and cybernetics-part A: systems and humans*, vol. 39, no. 4, pp. 795–806, 2009.

[64] G. Xie and F. Pan, "Cluster-based routing for the mobile sink in wireless sensor networks with obstacles," *IEEE Access*, vol. 4, pp. 2019–2028, 2016.

[65] C. E. Perkins and P. Bhagwat, "Highly dynamic destination-sequenced distance-vector routing (dsdv) for mobile computers," *ACM SIGCOMM computer communication review*, vol. 24, no. 4, pp. 234–244, 1994.

[66] H. Narra, Y. Cheng, E. K. Cetinkaya, J. P. Rohrer, and J. P. Sterbenz, "Destination-sequenced distance vector (dsdv) routing protocol implementation in ns-3," in *Proceedings of the 4th International ICST Conference on Simulation Tools and Techniques*, 2011, pp. 439–446.

[67] P. Jacquet, P. Muhlethaler, T. Clausen, A. Laouiti, A. Qayyum, and L. Viennot, "Optimized link state routing protocol for ad hoc networks," in *Proceedings. IEEE International Multi Topic Conference, 2001. IEEE INMIC 2001. Technology for the 21st Century.* IEEE, 2001, pp. 62–68.

[68] C. E. Perkins and E. M. Royer, "Ad-hoc on-demand distance vector routing," in *Proceedings WMCSA'99. Second IEEE Workshop on Mobile Computing Systems and Applications.* IEEE, 1999, pp. 90–100.

[69] D. B. Johnson, D. A. Maltz, J. Broch *et al.*, "Dsr: The dynamic source routing protocol for multi-hop wireless ad hoc networks," *Ad hoc networking*, vol. 5, no. 1, pp. 139–172, 2001.

[70] L. Yadav and C. Sunitha, "Low energy adaptive clustering hierarchy in wireless sensor network (leach)," *International journal of computer science and information technologies*, vol. 5, no. 3, pp. 4661–4664, 2014.

[71] Y. Xu, J. Heidemann, and D. Estrin, "Geography-informed energy conservation for ad hoc routing," in *Proceedings of the 7th annual international conference on Mobile computing and networking*, 2001, pp. 70–84.

[72] Y. Yu, R. Govindan, and D. Estrin, "Geographical and energy aware routing: A recursive data dissemination protocol for wireless sensor networks," 2001.

[73] J. Kulik, W. Heinzelman, and H. Balakrishnan, "Negotiation-based protocols for disseminating information in wireless sensor networks," *Wireless networks*, vol. 8, no. 2, pp. 169–185, 2002.

[74] D. Xiao, M. Wei, and Y. Zhou, "Secure-spin: Secure sensor protocol for information via negotiation for wireless sensor networks," in *2006 1ST IEEE conference on industrial electronics and applications*. IEEE, 2006, pp. 1–4.

[75] Z. Rehena, S. Roy, and N. Mukherjee, "A modified spin for wireless sensor networks," in *2011 Third International Conference on Communication Systems and Networks (COMSNETS 2011)*. IEEE, 2011, pp. 1–4.

[76] C. Intanagonwiwat, R. Govindan, and D. Estrin, "Directed diffusion: A scalable and robust communication paradigm for sensor networks," in *Proceedings*

of the 6th annual international conference on Mobile computing and networking, 2000, pp. 56–67.

[77] C. Schurgers and M. B. Srivastava, "Energy efficient routing in wireless sensor networks," in *2001 MILCOM Proceedings Communications for Network-Centric Operations: Creating the Information Force (Cat. No. 01CH37277)*, vol. 1. IEEE, 2001, pp. 357–361.

[78] S. Lindsey and C. S. Raghavendra, "Pegasis: Power-efficient gathering in sensor information systems," in *Proceedings, IEEE aerospace conference*, vol. 3. IEEE, 2002, pp. 3–3.

[79] T. He, J. A. Stankovic, C. Lu, and T. Abdelzaher, "Speed: A stateless protocol for real-time communication in sensor networks," in *23rd International Conference on Distributed Computing Systems, 2003. Proceedings.* IEEE, 2003, pp. 46–55.

[80] E. Felemban, C.-G. Lee, and E. Ekici, "Mmspeed: multipath multi-speed protocol for qos guarantee of reliability and. timeliness in wireless sensor networks," *IEEE transactions on mobile computing*, vol. 5, no. 6, pp. 738–754, 2006.

[81] M. A. Razzaque, M. M. Alam, M. Mamun-Or-Rashid, and C. S. Hong, "Multi-constrained qos geographic routing for heterogeneous traffic in sensor networks," *IEICE Transactions on communications*, vol. 91, no. 8, pp. 2589–2601, 2008.

[82] V. Nehra and A. K. Sharma, "Pegasis-e: power efficient gathering in sensor information system extended," *Global Journal of Computer Science and Technology*, 2013.

[83] C. Zhu, G. Han, and H. Zhang, "A honeycomb structure based data gathering scheme with a mobile sink for wireless sensor networks," *Peer-to-Peer Networking and Applications*, pp. 1–16, 2016.

[84] S. Sharma, D. Puthal, S. K. Jena, A. Y. Zomaya, and R. Ranjan, "Rendezvous based routing protocol for wireless sensor networks with mobile sink," *The Journal of Supercomputing*, pp. 1–21, 2016.

[85] J. Zhang, J. Tang, T. Wang, and F. Chen, "Energy-efficient data-gathering rendezvous algorithms with mobile sinks for wireless sensor networks," *International Journal of Sensor Networks*, vol. 23, no. 4, pp. 248–257, 2017.

[86] A. Vajdi, G. Zhang, J. Zhou, T. Wei, Y. Wang, and T. Wang, "A new path-constrained rendezvous planning approach for large-scale event-driven wireless sensor networks," *Sensors (Basel, Switzerland)*, vol. 18, no. 5, 2018.

[87] D. Shang, X. Liu, Y. Yan, C. Li, and B. Zhang, "A ring-based bidirectional routing protocol for wireless sensor network with mobile sinks," in *International Conference on Communications (ICC), Malaysia.* IEEE, 2016, pp. 1–6.

[88] H. A. Oliveira, R. S. Barreto, A. L. Fontao, A. A. Loureiro, and E. F. Nakamura, "A novel greedy forward algorithm for routing data toward a high speed sink in wireless sensor networks," in *19th International Conference on*

Computer Communications and Networks, Switzerland. IEEE, 2010, pp. 1–7.

[89] J. Rezazadeh, M. Moradi, A. S. Ismail, and E. Dutkiewicz, "Superior path planning mechanism for mobile beacon-assisted localization in wireless sensor networks," *IEEE Sensors Journal*, vol. 14, no. 9, pp. 3052–3064, 2014.

[90] C. Zhu, S. Wu, G. Han, L. Shu, and H. Wu, "A tree-cluster-based data-gathering algorithm for industrial wsns with a mobile sink," *IEEE Access*, vol. 3, pp. 381–396, 2015.

[91] S. K. Chaurasiya, J. Mondal, and S. Dutta, "Field-of-view based hierarchical clustering to prolong network lifetime of wmsn with obstacles," in *International Conference on Electronics, Communication and Computational Engineering (ICECCE), India.* IEEE, 2014, pp. 72–77.

[92] Y. Gu, F. Ren, Y. Ji, and J. Li, "The evolution of sink mobility management in wireless sensor networks: A survey," *IEEE Communications Surveys & Tutorials*, vol. 18, no. 1, pp. 507–524, 2015.

[93] L. Cheng, J. Niu, M. Di Francesco, S. K. Das, C. Luo, and Y. Gu, "Seamless streaming data delivery in cluster-based wireless sensor networks with mobile elements," *IEEE Systems Journal*, vol. 10, no. 2, pp. 805–816, 2015.

[94] Z. M. Wang, S. Basagni, E. Melachrinoudis, and C. Petrioli, "Exploiting sink mobility for maximizing sensor networks lifetime," in *38th annual Hawaii international conference on system sciences, USA.* IEEE, 2005, pp. 287a–287a.

[95] N. Gharaei, K. A. Bakar, S. Z. M. Hashim, A. H. Pourasl, and S. A. Butt, "Collaborative mobile sink sojourn time optimization scheme for cluster-based wireless sensor networks," *IEEE Sensors Journal*, vol. 18, no. 16, pp. 6669–6676, 2018.

[96] W. Wen, S. Zhao, C. Shang, and C.-Y. Chang, "EAPC: Energy-aware path construction for data collection using mobile sink in wireless sensor networks," *IEEE Sensors Journal*, vol. 18, no. 2, pp. 890–901, 2017.

[97] Y.-C. Wang and K.-C. Chen, "Efficient path planning for a mobile sink to reliably gather data from sensors with diverse sensing rates and limited buffers," *IEEE Transactions on Mobile Computing*, vol. 18, no. 7, pp. 1527–1540, 2018.

[98] T. Li, W. Liu, T. Wang, Z. Ming, X. Li, and M. Ma, "Trust data collections via vehicles joint with unmanned aerial vehicles in the smart internet of things," *Transactions on Emerging Telecommunications Technologies*, p. e3956, 2020.

[99] B. Jiang, G. Huang, T. Wang, J. Gui, and X. Zhu, "Trust based energy efficient data collection with unmanned aerial vehicle in edge network," *Transactions on Emerging Telecommunications Technologies*, p. e3942, 2020.

[100] N. Gharaei, K. A. Bakar, S. Z. M. Hashim, A. H. Pourasl, and S. A. Butt, "Collaborative mobile sink sojourn time optimization scheme for cluster-based wireless sensor networks," *IEEE Sensors Journal*, vol. 18, no. 16, pp. 6669–6676, 2018.

[101] P. K. Donta, B. S. P. Rao, T. Amgoth, C. S. R. Annavarapu, and S. Swain, "Data collection and path determination strategies for mobile sink in 3D WSNs," *IEEE Sensors Journal*, vol. 20, no. 4, pp. 2224–2233, 2019.

[102] A. Habib, S. Saha, F. N. Nur, A. Razzaque, and M. Mamun-Or-Rashid, "An efficient mobile-sink trajectory to maximize network lifetime in wireless sensor network," in *International Conference on Innovation in Engineering and Technology (ICIET), Dhaka, Bangladesh.* IEEE, 2018, pp. 1–5.

[103] H. Yetgin, K. T. K. Cheung, M. El-Hajjar, and L. H. Hanzo, "A survey of network lifetime maximization techniques in wireless sensor networks," *IEEE Communications Surveys & Tutorials*, vol. 19, no. 2, pp. 828–854, 2017.

[104] S. Sharmin, F. N. Nur, M. A. Razzaque, M. M. Rahman, A. Alelaiwi, M. M. Hassan, and S. M. M. Rahman, "α-overlapping area coverage for clustered directional sensor networks," *Computer Communications*, vol. 109, pp. 89–103, 2017.

[105] W. Liang, J. Luo, and X. Xu, "Prolonging network lifetime via a controlled mobile sink in wireless sensor networks," in *Global Telecommunications Conference (GLOBECOM).* IEEE, 2010, pp. 1–6.

[106] F. N. Nur, S. Sharmin, M. A. Habib, M. A. Razzaque, M. S. Islam, A. Almogren, M. M. Hassan, and A. Alamri, "Collaborative neighbor discovery in directional wireless sensor networks: algorithm and analysis," *EURASIP Journal on Wireless Communications and Networking*, 2017.

[107] D. P. Kumar, T. Amgoth, and C. S. R. Annavarapu, "Machine learning algorithms for wireless sensor networks: A survey," *Information Fusion*, vol. 49, pp. 1–25, 2019.

[108] R. Du, L. Gkatzikis, C. Fischione, and M. Xiao, "On maximizing sensor network lifetime by energy balancing," *IEEE Transactions on Control of Network Systems*, vol. 5, no. 3, pp. 1206–1218, 2018.

[109] W. Wen, C. Shang, C.-Y. Chang, and D. S. Roy, "DEDC: Joint density-aware and energy-limited path construction for data collection using mobile sink in wsns," *IEEE Access*, vol. 8, pp. 78 942–78 955, 2020.

[110] M. A. Habib, S. Saha, M. A. Razzaque, M. Mamun-or Rashid, G. Fortino, and M. M. Hassan, "Starfish routing for sensor networks with mobile sink," *Journal of Network and Computer Applications*, vol. 123, pp. 11–22, 2018.

[111] M. A. Habib, S. Saha, M. A. Razzaque, M. Mamun-Or-Rashid, M. M. Hassan, P. Pace, and G. Fortino, "Lifetime maximization of sensor networks through optimal data collection scheduling of mobile sink," *IEEE Access*, vol. 8, pp. 163 878–163 893, 2020.

[112] S. Saha, M. A. Habib, and M. A. Razzaque, "Compute intensive code offloading in mobile device cloud," in *Region 10 Conference (TENCON)*. IEEE, 2016, pp. 436–440.

[113] S. Saha, M. A. Habib, T. Adhikary, M. A. Razzaque, and M. M. Rahman, "Tradeoff between execution speedup and reliability for compute-intensive code offloading in mobile device cloud," *Multimedia Systems*, vol. 25, no. 5, pp. 577–589, 2019.

[114] M. A. Habib, S. Saha, M. A. Razzaque, and M. Mamun-Or-Rashid, "On the optimal size of ring-canal in starfish routing," in *8th International Conference on Informatics, Electronics & Vision (ICIEV), USA*. IEEE, 2019, pp. 62–66.

[115] S. Lin, D. J. Costello, and M. J. Miller, "Automatic-repeat-request error-control schemes," *IEEE Communications magazine*, vol. 22, no. 12, pp. 5–17, 1984.

[116] F. N. Nur, S. Sharmin, M. A. Razzaque, M. S. Islam, and M. M. Hassan, "A low duty cycle mac protocol for directional wireless sensor networks," *Wireless Personal Communications*, vol. 96, no. 4, pp. 5035–5059, 2017.

[117] F. Gebali, *Analysis of computer and communication networks*. Springer Science & Business Media, 2008.

[118] J. Kurose and K. Ross, "Computer networks: A top down approach featuring the internet," *Peorsoim Addison Wesley*, 2010.

[119] A.-F. Liu, P.-H. Zhang, and Z.-G. Chen, "Theoretical analysis of the lifetime and energy hole in cluster based wireless sensor networks," *Journal of Parallel and Distributed Computing*, vol. 71, no. 10, pp. 1327–1355, 2011.

[120] M. Azharuddin, P. Kuila, and P. K. Jana, "Energy efficient fault tolerant clustering and routing algorithms for wireless sensor networks," *Computers & Electrical Engineering*, vol. 41, pp. 177–190, 2015.

[121] L. A. BARROSO and U. HÖLZLE, "The case for energy-proportional computing," *Computer*, vol. 40, no. 12, pp. 33–37, 2007.

[122] M. Hasan, H. Yu, A. Griffiths, and T. Yang, "Simulation of distributed wireless networked control systems over manet using opnet," in *2007 IEEE International Conference on Networking, Sensing and Control*. IEEE, 2007, pp. 699–704.

[123] M. Cheffena, "Industrial wireless sensor networks: channel modeling and performance evaluation," *EURASIP Journal on Wireless Communications and Networking*, vol. 2012, no. 1, pp. 1–8, 2012.

[124] Y. Luo, Y. Duan, W. Li, P. Pace, and G. Fortino, "Workshop networks integration using mobile intelligence in smart factories," *IEEE Communications Magazine*, vol. 56, no. 2, pp. 68–75, 2018.

[125] P. Pace, G. Fortino, Y. Zhang, and A. Liotta, "Intelligence at the edge of complex networks: The case of cognitive transmission power control," *IEEE Wireless Communications*, vol. 26, no. 3, pp. 97–103, 2019.

[126] J. Czyzyk, M. P. Mesnier, and J. J. Moré, "The NEOS server," *IEEE Computational Science and Engineering*, vol. 5, no. 3, pp. 68–75, 1998.

[127] D. Dereniowski and W. Kubiak, "Shared multi-processor scheduling," *European Journal of Operational Research*, vol. 261, no. 2, pp. 503–514, 2017.

Appendix A

List of Notations

$2a \times 2b$	Area of the network
r	Transmission range of a sensor node
Z	Set of all backbone sensor nodes
Z_a	Set of anchor nodes on network edge
Z_b	Set of radial-canal nodes
Z_c	Set of ring-canal nodes
Z_d	Set of radial-canals on the SFR routing backbone
R	Radius or optimal radius of the ring-canal
m	Major radius of an optimal elliptical ring-canal
n	Minor radius of an optimal elliptical ring-canal
$\Re$	Radius of a circular network model
ϕ	Control variable for ring-canal radius
θ_1, θ_2	Incident angles of radial-canals on principal-axes
E_0	Initial energy of a sensor node in obstacle-free network
E_{res}	Residual energy of a sensor node in obstacle-free network
E_{th}	Energy threshold for backbone nodes
$\mathbb{N}$	Set of all sensor nodes
T	Minimum value of application delay-deadline

C	Set of cycles be completed by mobile sink
D^c	The worst-case end-to-end delay of a packet in a cycle c
σ_m^c	Data arrival rate at sojourn location m in cycle c
S_m^c	Sojourn duration at m in a cycle c
$\mathbb{B}$	Set of nodes on radial-canal in an obstructed-network
$\mathbb{Z}$	Set of nodes on the ring-canal in an obstructed-network
$\mathbb{R}^c$	Power set on ring-canal nodes $\mathbb{Z}$ during cycle c
$\mathbb{M}_n^c$	Set of optimally selected sojourn locations during cycle c
ε_m^0	Initial residual energy of a node in an obstructed-network
e_m^c	Total energy required at m in cycle c
E	Energy expenditure to transmit a bit of data
$\tilde{E}$	Energy expenditure to receive a bit of data
q_m^c	Bit-length of a packet at m in cycle c
A^c	Set of sink's traveling-arcs in cycle c
f_{lm}^c	A variable determining sink from l to m at cycle c
h_m^c	A variable determining sink's sojourn at m in a cycle c
$\overline{\delta}$	The expected end-to-end delay per hop for a packet
H^c	Hop-distance for a packet in a cycle c
$\rho_{H^c}^{z^c}$	Inter-hop transition probability of a packet
μ	Number of nodes willing to transmit
e	Probability that a packet contains one or more bit errors

Appendix B

List of Acronyms

ACM	Association for Computing Machinery
bSFR	basic Starfish Routing Backbone
bSFRc	bSFR Backbone in Circular-shaped network
bSFR-circular	bSFR Backbone with Optimal Circular Ring-canal
bSFR-elliptical	bSFR Backbone with Optimal Elliptical Ring-canal
bSFRs	bSFR Backbone in Square-shaped network
CBR	Constant Bit Rate
CH	Cluster Head
EAPC	Energy Aware Path Construction
FLEC	Fuzzy Logic based Effective Clustering
GPS	Global Positioning System
HexDD	Hexagonal-tiling based Data Dissemination
HSB	High-speed Backbone
IEEE	Institute of Electrical and Electronics Engineers
IoT	Internet of Thing
iSFR	improved Starfish Routing Backbone
iSFRc	iSFR Backbone in Circular-shaped network
iSFRc	iSFR Backbone in Circular-shaped network

iSFR-circular	iSFR Backbone with Optimal Circular Ring-canal
iSFR-elliptical	iSFR Backbone with Optimal Elliptical Ring-canal
iSFRs	iSFR Backbone in Square-shaped network
LAS	Landmark Assisted Scheduling
LBDD	Line-based Data Dissemination protocol
MDC	Mobile Device Cloud
MILP	Mixed Integer Linear Programming
MOLP	Multi-objective Linear Programming
MTR	Mass Transit Railway
NEOS	Network-Enabled Optimization System
NP	Non-deterministic Polynomial-time
NPP	Nuclear Power Plant
NS-2	Network Simulator version-2
PDR	Packet Delivery Ratio
QoE	Quality-of-Experience
QoS	Quality of Service
RN	Rendezvous Node
SCH	Super Cluster Heads
SFR	Starfish Routing
SFRB	Starfish Routing Backbone
TSP	Traveling Salesman Problem
UDP	User Datagram Protocol
VPS	Viable Path Scheduling
WHISPER	Wireless High-Speed Routing
WRP	Weighted Rendezvous Planning

Appendix C
List of Publications

International Journal Papers (SCI-indexed)

1. **M. A. Habib**, S. Saha, M. A. Razzaque, M. M. Rashid, M. M. Hassan, P Pace, G. Fortino, Lifetime Maximization of Sensor Networks Through Optimal Data Collection Scheduling of Mobile Sink, IEEE Access. (2020).

2. **M. A. Habib**, S. Saha, M. A. Razzaque, M. M. Rashid, G. Fortino, and M. M. Hassan. "Starfish routing for sensor networks with mobile sink", Elsevier Journal of Network and Computer Applications. (2018).

3. S. Saha, **M. A. Habib**, T. Adhikary, M. A. Razzaque, M. M. Rahman, M. Altaf, and M. M. Hassan, "Quality-of-Experience-Aware Incentive Mechanism for Workers in Mobile Device Cloud." IEEE Access (2021).

4. S. Saha, **M. A. Habib**, T. Adhikary, M. A. Razzaque, M. M. Rahman, "Tradeoff Between Execution Speedup and Reliability for Compute-Intensive Code Offloading in Mobile Device Cloud", Multimedia Systems Journal (Springer) (2017).

5. F. N. Nur, S. Sharmin, **M. A. Habib**, M. A. Razzaque, M. S. Islam, A. Ahmed, M. M. Hassan, A. Atif, "Collaborative Neighbor Discovery in

Directional Wireless Sensor Networks", Algorithm and Analysis. EURASIP Journal on Wireless Communications and Networking (JWCN) (2017).

International/National Conference Papers

6. **M. A. Habib**, S. Saha, M. A. Razzaque, M. M. Rashid "Starfish Routing Backbone on the Optimal Elliptical Ring-canal in Sensor Networks", 3rd International Conference on Sustainable Technologies for Industry 4.0 (STI 4.0), Dhaka, Bangladesh, 18-19 Dec 2021. (2021). (Submitted)

7. **M. A. Habib**, S. Saha, M. A. Razzaque, M. M. Rashid "Multi-tier Ring-canals for the Starfish Routing Backbone in Wireless Sensor Network", 2020 IEEE Computer Society Bangladesh Chapter Winter Symposium, Dhaka, Bangladesh, 13-14 Nov 2020. (2020)

8. **M. A. Habib**, S. Saha, M. A. Razzaque, M. M. Rashid, "On the Elliptical Ring-canal of Starfish Routing", International Conference on Informatics, Electronics and Vision (ICIEV), 2020, Japan. (2020).

9. **M. A. Habib**, S. Saha, M. A. Razzaque, "Starfish Routing for Sensor Networks with Mobile Sink", 2019 4th Young Scientist Congress, Dhaka, Bangladesh, 13-15 Dec 2019. (2019)

10. **M. A. Habib**, S. Saha, M. A. Razzaque, M. M. Rashid, "On the Optimal Size of Ring-Canal in Starfish Routing." 2019 International Conference on Informatics, Electronics, and Vision (ICIEV), USA, 30 May - 2 June, 2019. (2019)

11. **M. A. Habib**, S. Saha, M. A. Razzaque, M. M. Rashid "An Efficient Mobile-Sink Trajectory to Maximize Network Lifetime in Wireless Sensor Network." 2018 International Conference on Innovation in Engineering and Technology (ICIET). Dhaka, IEEE, (2018).

12. **M. A. Habib** and M. S. Hasan. "A performance analysis of backbone structures for static sink based Starfish routing in WSN." 4th IEEE International Conference on Networking, Systems and Security (NSysS), (2017)

13. **M. A. Habib**, S. Saha, F. N. Nur, M. A. Razzaque, Starfish Routing for Wireless Sensor Networks with a Mobile Sink. IEEE TENCON, Singapore. (2016)

14. S. Saha, **M. A. Habib**, S. Sarkar, M. A. Razzaque, M. M. Rahman, "Minimizing Execution Cost of User Application Codes in Mobile Device Cloud", 2019 International Conference on Sustainable Technologies for Industries 4.0, Dhaka, Bangladesh, 24-25 Dec 2019. (2019).

15. S. Saha, **M. A. Habib**, M. A. Razzaque, M. M. Rahman, "Quality-of-Experience-Aware Incentive Mechanism for Workers in Mobile Device Cloud", 2019 4th Young Scientist Congress, Dhaka, Bangladesh, 13-15 Dec 2019. (2019).

16. F. N. Nur, S. Sharmin, **M. A. Habib**, M. A. Razzaque, M. S. Islam, "Collaborative Neighbor Discovery in Directional Wireless Sensor Networks", IEEE TENCON, Singapore, 22-25 Nov 2016. (2016).

17. S. Saha, **M. A. Habib**, M. A. Razzaque, "Compute Intensive Code Offloading in Mobile Device Cloud", IEEE TENCON, Singapore, 22-25 Nov 2016.